

**Exchanges of Atmospheric CO₂ and ¹³CO₂
with the Terrestrial Biosphere and Oceans from 1978 to 2000.**

I. Global Aspects

Charles D. Keeling¹, Stephen C. Piper¹, Robert B. Bacastow¹, Martin Wahlen¹,
Timothy P. Whorf¹, Martin Heimann², and Harro A. Meijer³

¹Scripps Institution of Oceanography, University of California, San Diego, California

²Max Planck Institute for Biogeochemistry, Jena, Germany

³Centre for Isotope Research, University of Groningen, Groningen, Netherlands

SIO Reference No. 01-06

(Revised from SIO Reference No. 00-21)

June 2001

Table of Contents

Abstract.....	1
Preface.....	2
1. Introduction	2
2. Atmospheric Observations	4
2.1 <i>Data for individual stations</i>	4
2.2 <i>Association of temporal variability of CO₂ with climatic factors</i>	6
2.3 <i>Data globally averaged</i>	8
3. Isotopic Signature of the Seasonal CO ₂ Cycle	8
4. Deconvolution of Global Data.....	10
4.1 <i>General model description</i>	10
4.2 <i>Single deconvolution</i>	11
4.3 <i>Double deconvolution</i>	12
5. Isotopic Discrimination by Terrestrial Vegetation.....	15
5.1 <i>Isotopic fractionation associated with terrestrial photosynthesis</i>	15
5.2 <i>Variability in isotopic discrimination</i>	18
6. Global CO ₂ Fluxes	21
6.1 <i>Deduced by deconvolution calculations</i>	21
6.2 <i>Sensitivity of results to oceanic vertical mixing</i>	24
7. Reliability of Deduced Fluxes	25
7.1 <i>Introduction</i>	25
7.2 <i>Analysis of statistical errors</i>	25
7.3 <i>Analysis of possible systematic errors</i>	25
7.4 <i>Systematic uncertainty in fluxes on short time-scales</i>	27
8. Discussion.....	28
8.1 <i>Introduction</i>	28
8.2 <i>Short-term variability in the global carbon cycle</i>	28
8.3 <i>Ways to reduce uncertainty in estimation of exchange fluxes</i>	30
9. Conclusions	31
Acknowledgments.....	34
Appendix A. Sampling procedures and techniques of measurement.	35
Appendix B. Calibration of concentration data.....	36
Appendix C. Calibration of isotopic data.....	36
Appendix D. Data processing.	37
Appendix E. Auxiliary data.	39
References.....	40
Tables	
Figures	

Abstract

From 1978 through 1999 the global average concentration of atmospheric carbon dioxide increased from 335 ppm to 368 ppm according to measurements of air samples collected at an array of ten stations extending from the Arctic to the South Pole. The global average rate of increase varied widely, however, with highest rates occurring in 1980, 1983, 1987, 1990, 1994, and 1998, all but the first of these calendar years near times of El Niño events. The $^{13}\text{C}/^{12}\text{C}$ isotopic ratio of carbon dioxide, measured on the same air samples, varied in a similarly irregular manner, suggesting that exchange of atmospheric CO_2 with terrestrial plants and soil is the dominant cause of both signals. Quantitative analysis of the data by a procedure called a "double deconvolution" supports this hypothesis but also suggests a variable exchange with the oceans, opposite in phase to the terrestrial exchange. This result may be in error, however, because it depends on an assumption that the global average isotopic discrimination of terrestrial plants has been constant. Allowing for a variation in discrimination of only about 1‰ would eliminate the opposing fluctuations in oceanic flux, if its phasing has been opposite to that of the observed fluctuations in rate of change of CO_2 concentration. In three companion articles that follow, we further deduce regional exchanges of CO_2 , making use of latitudinal gradients computed from the same atmospheric carbon dioxide data used in this global study.

Preface

This is the first of four articles that seeks to characterize sources and sinks of atmospheric carbon dioxide from direct measurements of the concentration and $^{13}\text{C}/^{12}\text{C}$ ratio of atmospheric CO_2 , updating an earlier study by Keeling et al. [1989a]. The articles, organized as though chapters of a single study, are referred to henceforth as Articles I to IV corresponding, respectively, to Keeling et al. [2001], Piper et al. [2001a,b], and Keeling and Piper [2001].

1. Introduction

To establish unequivocally the consequences of human activities on the earth's carbon cycle, direct observations are needed as well as predictions from geophysical and biogeochemical models. During the industrial era, in which the combustion of fossil fuel has contributed to a sharp rise in atmospheric CO_2 (Figure 1), measurements of the concentration and $^{13}\text{C}/^{12}\text{C}$ ratio of atmospheric CO_2 are especially relevant. Ability to predict correctly the time-varying gradients in atmospheric CO_2 that these data establish is an indispensable requirement for trusting models that link the storage of carbon in the atmosphere, terrestrial, and oceanic reservoirs of the carbon cycle to transfers of carbon between these global carbon pools. These transfers, if thus validated, in turn can be compared with integrations of local flux measurements, carried out on land, for example by the Ameriflux and Euroflux eddy-correlation flux networks [Hollinger et al., 2000; Aubinet et al., 2000] and in the oceans, for example by the Joint Global Ocean Fluxes Study [Karl and Michaels, 1996, pp. 127-8], thus combining top-down and bottom-up approaches to assess human impacts on the global carbon cycle.

Figure 1

To acquire an atmospheric CO_2 database adequate to establish human impacts on continental and global scales, it is necessary to sample air world-wide. Because atmospheric turbulence tends to smooth out the effects of local sources and sinks on the atmospheric CO_2 distribution, only a limited number of sampling locations are required, however, provided that they are remote from large local sources and sinks of CO_2 .

In this study we update an early study [Keeling et al., 1989a], in which we depend on data from fewer locations than most other recent global studies, but our more extensive isotopic data compensates to a considerable degree. We have refrained from direct use of atmospheric data measured by other investigators because adequate cross-calibration with our data is still pending, and an analysis based on totally

independent atmospheric measurements should be useful for comparison with the results of other studies.

Our approach here is to calculate a set of regional "source components" that, together, sum to all globally significant transfers of atmospheric CO₂ with the terrestrial and oceanic carbon reservoirs. These components include industrial emissions of CO₂, long term human-induced disturbances to terrestrial vegetation and of soils, and perturbations induced by these disturbances, such as the uptake of CO₂ by the oceans and terrestrial vegetation, and natural CO₂ fluxes. In constructing these components, which portray both sources and sinks of atmospheric CO₂, we make use of *a priori* information as much as possible, including spatially gridded global data sets of observed sea and land surface temperatures and terrestrial photosynthetic activity derived from remote sensing data observed by satellites. For the less reliably known components, we prescribe, *a priori*, only their spatial and temporal structures, adjusting their overall strengths simultaneously to predict optimally our observations of CO₂ concentration and ¹³C/¹²C, taking account of the entire set of component fluxes.

This essentially inverse procedure is carried out in two principal steps. Step 1, to be described here, computes only global average exchanges of atmospheric CO₂. These exchanges, which transfer CO₂ to and from terrestrial vegetation and soils (henceforth, together called the "terrestrial biosphere") and to and from the world oceans (henceforth, "oceans"), are inferred from global averages of time-varying concentration and ¹³C/¹²C ratio determined from our observations. Step 2, to be described in the articles that follow, computes regional fluxes, constrained to agree with the global average fluxes inferred in step 1. This first step employs a global biogeochemical model, consisting of terrestrial and oceanic submodels, that portrays enough of the internal dynamics of the carbon cycle to establish a time-varying global budget of carbon, similar to that employed by Keeling et al. [1989a, pp. 185-193]. In the second step, the global CO₂ fluxes established by this budget are distributed regionally, consistent with boundary conditions specified by regional source components and an atmospheric transport model.

A major challenge is to determine how time-varying sources and sinks of atmospheric CO₂ reflect the interplay of natural processes and human activities, including feedbacks between the earth's carbon cycle and its physical environment. Of paramount interest is that the earth's heat balance is being altered by an enhanced greenhouse effect caused by rising concentrations of CO₂ and other infrared-absorbing gases. Global warming probably is occurring as a consequence, altering the carbon cycle globally [Santer et al., 1995; Crowley, 2000]. The picture is complicated,

however, because natural variations in climate also impact the earth's heat balance [Free and Robock, 1999; Andronova and Schlesinger, 2000] and the carbon cycle [Falkowski et al., 2000].

Although the observations most essential to this study are measurements of CO₂ concentration, valuable information is afforded by its ¹³C/¹²C isotopic ratio, conveniently expressed by the reduced isotopic ratio

$$\delta^{13}C = (^{13}r - ^{13}r_s) / ^{13}r_s \quad (1.1)$$

where ¹³*r* denotes the measured ¹³C/¹²C ratio of a specific sample of CO₂, and ¹³*r_s* a constant reference value defined by an international standard, as noted below. Because the rare stable isotope, carbon-13 (¹³C), during photosynthesis by land plants, is strongly fractionated relative to the more abundant isotope, carbon-12 (¹²C), the terrestrial biosphere alters the δ¹³C of atmospheric CO₂ far more than do the oceans [Keeling et al., 1989a]. Terrestrial and oceanic CO₂ fluxes can thus be distinguished using δ¹³C data, with certain additional information, including variability in the fractionation factor for photosynthesis for different types of plants and under different growing conditions and, on long time-scales, evidence of the degree of vertical mixing of the oceans.

Our analysis of global and regional carbon exchange is presented in the following order. In this first article, Article I, we present our atmospheric CO₂ data followed by a calculation of global average terrestrial and oceanic fluxes based on global averages of our atmospheric CO₂ data. In Article II, we describe a carbon cycle model that enables us to compute regional fluxes under the control of gradients in atmospheric CO₂ concentration and isotopic ratio, deduced from the same atmospheric data used in our global study. In Article III, by sensitivity tests, we assess uncertainties in our estimates of regional fluxes. Article IV describes salient features of our findings and compares them with findings of other investigations.

2. Atmospheric observations

2.1 Data for individual stations

Observations of atmospheric CO₂ concentration and its ¹³C/¹²C ratio, expressed by δ¹³C, were obtained from an array of 10 stations situated along a nearly north-south transect mainly in the Pacific Ocean basin. The stations extend from the Arctic to the

Figure 2
Table 1

South Pole (see Figure 2 and Table 1), at sites on land located as far as possible from biological activity and combustion of fossil fuels. The effects of local interferences were minimized by sampling the air upwind, so that the observations mainly reflect broad-scale CO₂ fluxes. The concentration data set begins in 1957, the isotopic data set in 1977. Data provide complete time-series for all stations of the array from 1986 onward. Here we mainly consider data after 1977.

Each CO₂ concentration record, $C(t)$ was decomposed into a seasonal function, consisting of four harmonics, and a seasonally detrended function, according to the relation

$$C(t) = C_{seas}(t) + C_{annual}(t) \quad (2.1)$$

where

$$C_{seas}(t) = (1 + \gamma t) \sum_{k=1}^m (a_k \sin \omega_k t + b_k \cos \omega_k t) \quad (2.2)$$

In the second expression γ (a "gain factor") and the factors, a_k and b_k , denote constants obtained via a fit to the data; t denotes the time in years; ω_k the angular frequency, equal to $2\pi k$; and m the number of harmonics, chosen to be 4. The seasonally adjusted function, C_{annual} , is expressed by a spline function in which the annual average of the integral of the squared second derivative is set to a predetermined value to provide a nearly uniform degree of smoothing of all of the records. The actual function is established in several steps involving intermediate functions (see Keeling et al. [1989a, p. 167 and pp. 218-227]) to assure stability in the calculation and to determine monthly averages that take into account the actual dates of each observation. The isotopic record, $\delta^{13}C(t)$, is treated similarly.

The CO₂ concentration $C(t)$ is expressed as a mole fraction in parts per million of dry air (ppm), the isotopic data, $\delta^{13}C(t)$, in per mil (‰) departures from the standard PDB [Craig, 1957; Mook and Grootes, 1973]. Methods of sampling, measurements, and calibrations are described in Appendices A, B, and C. Monthly data points and smoothed trends are shown in Figure 3 (the scale of $\delta^{13}C(t)$ inverted). Standard errors of the individual data points to the spline fits for the 10 stations of our array are listed in Tables D3 and D4 and discussed in subsection 7.2, below. Seasonally adjusted trends, C_{annual} and $\delta^{13}C_{annual}$, are summarized in Figure 4 after a linear trend, the same for all stations, has been subtracted to reveal short-term interannual variations. The vertical scales for Figures 3 and 4 are set so that changes in the concentrations and isotopic ratio are in the proportion

Figure 3

Figure 4

$$\Delta\delta^{13}\text{C} / \Delta C = -0.050 \text{‰ ppm}^{-1} \quad (2.3)$$

approximately that expected for seasonal variability in atmospheric CO_2 caused by exchange with the terrestrial biosphere [cf. Keeling et al., 1989a, p. 171].

As indicated in Figure 4, the CO_2 concentration decreases almost monotonically from north to south such that two Arctic stations, Alert and Point Barrow, register concentrations 3 to 5 ppm higher than the most southerly stations, in New Zealand and at the South Pole. The main cause of the southward decrease is the predominance of industrial emissions of CO_2 in the northern hemisphere [Keeling et al., 1989b]. These emissions, in addition, cause $\delta^{13}\text{C}$ of atmospheric CO_2 to increase from north to south, because fossil fuels are strongly depleted in the heavy carbon isotope, carbon-13, relative to atmospheric CO_2 , a reflection of their origins as plant carbon. The explanation for the north-south isotopic gradient in CO_2 is more complicated, however, owing to isotopic fractionation processes not associated with photosynthesis of land plants. Of these processes, the most important is temperature-dependent isotopic fractionation in the air-sea exchange of CO_2 which promotes negative $\delta^{13}\text{C}$ at high latitudes relative to low latitudes, and in the southern hemisphere relative to the northern [Keeling et al., 1989a, p. 323].

Short-term interannual variations in concentration and $\delta^{13}\text{C}$ exhibit similar temporal patterns at individual stations and, to a considerable extent, similar patterns from station to station. Emissions of industrial CO_2 , because they vary only slightly from year to year, contribute little to these temporal patterns. Therefore, because the $\delta^{13}\text{C}$ variations are relatively large, the similarities in patterns implies that terrestrial biospheric fluxes are the dominant cause of short-term variations in CO_2 concentration, as well as in $\delta^{13}\text{C}$.

2.2 Association of temporal variability of CO_2 with climatic factors

To aid in interpreting the interannual patterns seen in Figure 4, and in derived CO_2 fluxes shown later, we identify quasi-periodic variability in atmospheric CO_2 defined by time-intervals during which the seasonally adjusted CO_2 concentration at Mauna Loa Observatory, Hawaii rose more rapidly than a long-term trend line proportional to industrial CO_2 emissions. The Mauna Loa data and the trend line are shown in Figure 5 with vertical gray bars demarking the intervals of rapid rising CO_2 . Data from Mauna Loa Observatory were chosen for this identification because the measurements there are continuous and thus provide a more precisely determined rate of change than any other station in our observing program. Also, the rate observed there

Figure 5

agrees closely with the global average rate estimated from the nearly pole to pole data of Figure 4 (plot not shown).

An association of rapidly rising CO₂ with temperature is seen consistently in the Mauna Loa record since its beginning in 1957 [Keeling et al., 1989a, Figure 63; 1995, Figure 2]. As shown in Figure 5, Panel b, consistent with this association, the gray bars without exception indicate warm periods. As first noted by Bacastow [1976], rapidly rising CO₂ typically occur during El Niño events involving almost global scale changes in climatic factors, especially temperature, and identifiable by a low value of a climatic indicator called the Southern Oscillation Index (SOI) [Rasmusson and Wallace, 1983; Meehl, 1987]. The SOI, also plotted in Figure 5b, indeed, shows low values at times of some of the gray bars, but not all.

The SOI tracks the surface barometric pressure difference across the Pacific Ocean in the tropics. This pressure difference weakens during El Niño events and strengthens during the opposite phase in a so-called El Niño-Southern oscillation (ENSO) cycle. On 3 occasions during the time-period plotted in Figure 5, in 1983, 1987, and 1998, there were pronounced minima in the SOI followed by sharp increases. At these times, very strong El Niño events occurred, accompanied by strong warming and prominent increases in the rate of rise of atmospheric CO₂ [Slingo and Annamalai, 2000]. That the timing of a SOI minimum for these events almost exactly coincides with the commencement of a gray bar suggests a remarkably close phase relation to the rate of CO₂ rise. The SOI-CO₂ relation during a prolonged period of low SOI from 1992 through 1994 is less consistent, indeed, the least consistent for the entire 42 years of the Mauna Loa record. A sharp decrease in rate of rise of CO₂ began immediately after the volcanic eruption of Mt. Pinatubo in 1991 and persisted until 1993. Then CO₂ began to rise in evident association with the dissipation of a volcanic dust veil that had promoted cool temperatures after the eruption. The commencement of a gray bar in late 1993 is evidently not related to the ENSO cycle, although the long duration of the gray bar interval probably marks a return to the SOI-CO₂ association seen in the three prominent events already noted.

The gray bars near 1980 and 1990 are associated with global warming, not evidently correlated with El Niño events. Also, there is no gray bar at the time of a weak El Niño event in 1992, probably because this event was during the period of cooling associated with the Pinatubo eruption. Thus the gray bars of Figure 5 identify times of the ENSO cycle of the past 22 years when it involved strong oscillations in the SOI and was not complicated by a very powerful volcanic eruption, but they also identify times of rapid warming not clearly associated with the ENSO cycle.

2.3 Data globally averaged

From the data described above, we estimated the global average concentration and isotopic ratio, $\delta^{13}\text{C}$, of atmospheric CO_2 from 1978 through 1999 by a procedure described in Appendix D. Data for Mauna Loa Observatory, Hawaii, were not used, as explained in Article II, section 5. The resulting time-series are shown in Figure 6, and their time-derivatives in Figure 7. For modeling purposes, these time-series were extended back to A.D. 1740. The extension of the concentration series, shown in Figure 1, consists of data from air trapped in glacial ice collected at Law Dome, Antarctica, assumed to represent the global average concentration, and after 1955 direct observations, as described in Appendix D. The extension of the $\delta^{13}\text{C}$ series was created by a deconvolution procedure described in section 4, below, making use of the global CO_2 concentration time-series to establish chemical disequilibria of the global carbon cycle, assuming that the atmospheric, terrestrial biospheric, and oceanic carbon reservoirs were at chemical and isotopic equilibria in 1740. The $^{13}\text{C}/^{12}\text{C}$ ratio in 1740 was set so that $\delta^{13}\text{C}$ in 1978 exactly agreed with the value from observations.

Figure 6

Figure 7

3. Isotopic Signature of the Seasonal CO_2 Cycle

The concentration of atmospheric CO_2 and its reduced isotopic ratio, $\delta^{13}\text{C}$, as seen in Figure 3, covary over their seasonal cycles, because the $\delta^{13}\text{C}$ of the carbon of land plants is distinctly more negative than that of atmospheric CO_2 , and seasonality of plant growth and respiration are the dominant causes of seasonality in atmospheric CO_2 . Over the northern hemisphere where this seasonality is a prominent feature of the CO_2 records, the $\delta^{13}\text{C}$ inferred to be exchanged between the terrestrial biosphere and the atmosphere over each annual cycle tends to approach that of CO_2 respired by land plants [Mook et al., 1983, Heimann et al., 1989]. In the southern hemisphere, however, plant activity produces only small seasonal cycles in CO_2 concentration and $\delta^{13}\text{C}$, and, consequently, the average isotopic ratio that explains the covariance of the seasonal cycle there is not precisely established.

The annual average $^{13}\text{C}/^{12}\text{C}$ signature of the seasonal cycle of atmospheric CO_2 , disregarding possible seasonal variability in the signature itself and in any phase difference between oceanic and terrestrial CO_2 exchange, is given by the expression

$$\delta^{13}C_I = \delta^{13}C_o + (\delta^{13}C - \delta^{13}C_o) \mu / (\mu - \mu_o) \quad (3.1)$$

where $\delta^{13}\text{C}$ and μ denote, respectively, the reduced isotopic ratio and mole fraction of any given sample of atmospheric CO_2 , and $\delta^{13}\text{C}_o$ and μ_o are respective reference values. (In this discussion we refer to our measurements of atmospheric CO_2 by the correct term, "mole fraction", although elsewhere, following common practice, we use the less precise term "concentration".) Equation (3.1) follows from the relationship

$$(\delta^{13}\text{C})\mu = (\delta^{13}\text{C}_o)\mu_o + \delta^{13}\text{C}_I(\mu - \mu_o) \quad (3.2)$$

in which the product of $\delta^{13}\text{C}$ and carbon mass (and hence mole fraction, μ) is very nearly additive when two or more samples of CO_2 in a carrier gas, such as air, are mixed [Heimann and Keeling, 1989, pages 261 and 262 after equations (5.11) and (5.17)]. Here we identify a reference sample of air with values $\delta^{13}\text{C}_o$ and μ_o , to which is added $(\mu - \mu_o)$ moles per unit volume of CO_2 gas with an isotopic ratio, $\delta^{13}\text{C}_I$. If, for the reference values, $\delta^{13}\text{C}_o$ and μ_o , we assign annual means appropriate to $\delta^{13}\text{C}$ and μ of atmospheric CO_2 , respectively, the isotopic discrimination term that explains the seasonal covariance of $\delta^{13}\text{C}$ and μ is expressed by

$$^{13}\Delta_{cov} = \delta^{13}\text{C}_I - \delta^{13}\text{C}_o \quad (3.3)$$

For a given location, from a set of paired values of $\delta^{13}\text{C}$ and μ^{-1} , we find, by a linear least squares fit, the intercept, $\delta^{13}\text{C}_I$, and the slope, $(\delta^{13}\text{C}_o - \delta^{13}\text{C}_I)\mu_o$, of the expression

$$\delta^{13}\text{C} = \delta^{13}\text{C}_I + (\delta^{13}\text{C}_o - \delta^{13}\text{C}_I)(\mu_o/\mu) \quad (3.4)$$

derived by solving equation (3.2) for $\delta^{13}\text{C}$ [cf. Keeling, 1961, p. 278]. We afterwards calculate $^{13}\Delta_{cov}$ via equation (3.3).

In our atmospheric records in the northern hemisphere (Figure 8), slight trends can be discerned towards more negative $\delta^{13}\text{C}_I$ (and hence, $^{13}\Delta_{cov}$), from decade to decade, in addition to short-term interannual variability. The decadal trends do not significantly differ, however, from the average $\delta^{13}\text{C}$ trend of atmospheric CO_2 , shown on each plot by a straight line.

Figure 8

Observed short-term interannual variability in $\delta^{13}\text{C}_I$ is typically less after changes in instrumentation and calibrating procedures took place in 1991 (see Appendix C) which resulted in more precise mass spectrometric measurements, as established by replicate analyses. Addressing data only after 1991, the Arctic stations and La Jolla show little interannual variability in $\delta^{13}\text{C}_I$; Mauna Loa and Cape Kumukahi show possibly significant annual variations in the range of 2‰. For these northern stations, where oceanic CO_2 exchange has only a small, or a negligible effect on the seasonal

cycle of atmospheric CO_2 , $^{13}\Delta_{cov}$ is close to the isotopic discrimination for photosynthesis of land plants, suggesting that this discrimination, averaged over large regions, has varied temporally by 1 to 2‰ during the past decade. With respect to latitude, averages of $\delta^{13}C_l$ from 1992-1999, listed in Table 2, show little evidence of variation within either hemisphere, but the hemispheric averages differ sharply: -27.5‰ in the northern, -17.5‰ in the southern. The lower average for $\delta^{13}C_l$ in the southern hemisphere is consistent with a significant contribution to the seasonal cycle of atmospheric CO_2 by oceanic exchange, with its far lower isotopic discrimination than terrestrial exchange. To an indeterminate extent, the lower average may also reflect that a greater part of the vegetation on land in the southern hemisphere utilizes a photosynthetic pathway, C4, with much lower fractionation than the more common pathway, C3 (see section 5, below).

Table 2

4. Deconvolution of Global Data

4.1 General model description

To resolve globally averaged temporal variations in atmospheric CO_2 into terrestrial and oceanic components, we employ an inverse procedure. First, by what we call a "single deconvolution," we deduce the oceanic and terrestrial CO_2 exchange fluxes solely from atmospheric CO_2 concentration data. Then, by a "double deconvolution", we adjust these estimates to be consistent with the $^{13}\text{C}/^{12}\text{C}$ isotopic ratio of atmospheric CO_2 .

In these calculations we identify only the most significant global pools of carbon affecting contemporary atmospheric CO_2 : an oceanic pool consisting mainly of bicarbonate and carbonate salts; a terrestrial biospheric pool consisting of organic carbon stored in living plants, detritus, and soils; and a fossil fuel pool representing the available resource of coal, petroleum, and natural gas, combined. The associated global average exchange fluxes of CO_2 we denote, respectively, by F_{oce} , F_{bio} , and F_{ind} . The industrial flux, F_{ind} , includes a small contribution from the manufacture of cement [Andres et al., 2000], while F_{oce} and F_{bio} represent net fluxes which are the relatively small differences between large one-way fluxes. All fluxes will be expressed here in petagrams of carbon ($\text{PgC} = 10^{12}$ kg of carbon). To a close approximation, the sum of three time-dependent fluxes determine the rate of change of atmospheric CO_2 abundance, N_a , expressed by the mass-conserving global atmospheric carbon cycle budget equation

$$dN_a/dt = F_{ind} + F_{oce} + F_{bio} \quad (4.1)$$

Over the past two decades the average strengths of the terms of equation (4.1) (cf. subsection 6.1, below) are approximately as follows. The concentration of atmospheric CO_2 has risen at about $3\frac{1}{2} \text{ PgC yr}^{-1}$, a little over half the rate of industrial emissions, about 6 PgC yr^{-1} . The atmospheric CO_2 budget is balanced by an oceanic sink of about 2 PgC yr^{-1} and a terrestrial sink of about $\frac{1}{2} \text{ PgC yr}^{-1}$.

To specify this budget in greater detail, we distinguish several different contributions to the net exchange fluxes involving the oceanic and terrestrial biospheric carbon pools [cf. Keeling et al., 1989a, pp.185-193]. We divide the net oceanic exchange flux into two components

$$F_{oce} = F_{ex} + F_{ano,oce} \quad (4.2)$$

where F_{ex} denotes the expected oceanic response to rising atmospheric CO_2 concentration, and $F_{ano,oce}$ an "anomalous" flux representing a remainder not captured by F_{ex} . We divide the net terrestrial biospheric exchange flux into three components

$$F_{bio} = F_{fer} + F_{des} + F_{ano,bio} \quad (4.3)$$

where F_{fer} represents plant growth stimulated ("fertilized") by elevated atmospheric CO_2 concentration relative to the concentration in 1740, and F_{des} represents the release of CO_2 from the terrestrial biosphere owing to biologically destructive human-caused land-use changes, including deforestation and biomass burning. An "anomalous" flux, $F_{ano,bio}$, denotes a remainder not explained by either of the previously identified processes.

4.2 Single deconvolution

In this procedure, beginning with atmospheric CO_2 concentration data for A.D. 1740 [cf. Keeling et al., 1989a, pp. 195-7], we compute the expected oceanic response, F_{ex} , to rising atmospheric CO_2 concentration, using the one-dimensional vertically resolved oceanic box-diffusion model of Siegenthaler and Oeschger [1987]. This oceanic submodel is characterized by a vertical diffusion coefficient, K , and an air-sea CO_2 exchange coefficient, k_{am} [Keeling et al., 1989a, p. 189]; it yields an oceanic sink as a function of atmospheric CO_2 concentration that agrees quite closely with estimates from three-dimensional oceanic circulation models [Keeling et al., 1989a]. We do not regard its temporal variability as a reliable estimate of the true short-term interannual variability in F_{oce} , however. A substantial portion of that variability is found to reside in the anomalous oceanic flux, $F_{ano,oce}$, established later, in the double deconvolution

calculation.

In the single deconvolution, we also compute the expected terrestrial biospheric response, F_{fer} , to rising atmospheric CO_2 , using a terrestrial submodel controlled by a "growth factor." This factor, denoted β_a by Keeling et al. [1989a], expresses the degree to which the increase in atmospheric CO_2 concentration after 1740 caused enhanced plant uptake of CO_2 , expressed as a linear growth response of plants to increasing CO_2 concentration resulting from a stimulation of net primary production (NPP) [Keeling et al. [1989a, p. 188]. For β_a , we have adopted the value 0.41 of Keeling et al., [1989a, p. 193], signifying that the increase in uptake by long-lived biospheric carbon has been 41% of the fractional increase in CO_2 concentration, where the NPP of long-lived carbon in 1740 was calculated to be 24.6 PgC yr^{-1} . (The deconvolution calculations would yield almost the same outputs if, by the inclusion of short-lived biospheric carbon, β_a had been assigned a value of 0.18 with respect to total NPP, the latter calculated to be about 56 PgC yr^{-1} for 1982 [Heimann and Keeling, 1989, p. 262].) The destructive land-use flux, F_{des} , and the anomalous flux, $F_{ano,bio}$, are not determined in this calculation.

4.3 Double deconvolution

The calculations of the single deconvolution are repeated via an iterative scheme that adjusts $F_{ano,oce}$ and the sum $F_{ano,bio} + F_{des}$ at each time step so that both the $^{13}\text{C}/^{12}\text{C}$ ratio and concentration of atmospheric CO_2 agree with observations. This double deconvolution procedure reconciles the global atmospheric CO_2 budget, expressed by equation (4.1) for the sum of the two isotopes, ^{13}C and ^{12}C , and a similar budget equation for the rare isotope, ^{13}C , alone.

The terrestrial biospheric exchange flux, F_{bio} , of equation (4.1), as noted above, represents the difference between two large one-way CO_2 fluxes. These we denote by F_{ab} , an atmospheric CO_2 sink owing to assimilation of CO_2 by plants through photosynthesis, and, F_{ba} , an atmospheric CO_2 source owing to respiratory processes involving decay of vegetative matter. Thus

$$F_{bio} = F_{ba} - F_{ab} \quad (4.4)$$

Both one-way fluxes apply to carbon in general, and thus to the isotopic sum, $^{13}\text{C} + ^{12}\text{C}$. Correspondingly, for ^{13}C the net flux is

$$*F_{bio} = *F_{ba} - *F_{ab} \quad (4.5)$$

where asterisks denote fluxes of ^{13}C alone. The one-way ^{13}C fluxes are related, respectively, to the one-way fluxes for $^{13}\text{C} + ^{12}\text{C}$ by the expressions

$$*F_{ab} = \alpha'_{ab} R_a F_{ab} \quad (4.6)$$

$$*F_{ba} = \alpha'_{ba} R_b F_{ba} \quad (4.7)$$

where R_a and R_b denote, respectively, the ratios $^{13}\text{C}/(^{13}\text{C} + ^{12}\text{C})$ of atmospheric CO_2 and of carbon in the terrestrial biospheric pool, and α'_{ab} and α'_{ba} denote fixed $^{13}\text{C}/(^{13}\text{C} + ^{12}\text{C})$ isotopic fractionation (discrimination) factors. Corresponding factors with respect to $^{13}\text{C}/^{12}\text{C}$ ratios are denoted by α without the prime sign.

We set α_{ab} , which represents an isotopic discrimination of 15.32‰ against ^{13}C associated with photosynthesis (see below), to 0.98468 (i.e., to 1 - 15.32/1000), and we set α_{ba} equal to unity, by assuming, consistent with earlier calculations [Keeling et al., 1989a, Table 8, footnote 13], that no isotopic fractionation accompanies respiration. We then compute their α' equivalents, making use of the relationship [cf. Heimann and Keeling, 1989, pp. 261-264]

$$R_i = r_i (R_s / r_s) \quad (4.8)$$

where R_s and r_s denote, respectively, the $^{13}\text{C}/(^{13}\text{C} + ^{12}\text{C})$ and $^{13}\text{C}/^{12}\text{C}$ ratios of the international standard PDB, and the subscript i refers to any given carbon pool. Equations (4.6) and (4.7) are then rewritten

$$*F_{ab} = \alpha'_{ab} r_a (R_s / r_s) F_{ab} \quad (4.9)$$

$$*F_{ba} = r_b (R_s / r_s) F_{ba} \quad (4.10)$$

where r_a and r_b denote $^{13}\text{C}/^{12}\text{C}$ ratios corresponding respectively to R_a and R_b . Expressions similar to equations (4.4) through (4.10) apply to CO_2 exchange with the oceans, as follows

$$F_{oce} = F_{ma} - F_{am} \quad (4.11)$$

$$*F_{am} = \alpha'_{am} r_a (R_s / r_s) F_{am} \quad (4.12)$$

$$*F_{ma} = \alpha'_{am} \langle \bar{\alpha}'_{eq} \rangle r_m (R_s / r_s) F_{ma} \quad (4.13)$$

where F_{ma} denotes the one-way gross flux of CO_2 from the well-mixed surface layer of the oceans to the atmosphere, F_{am} the reverse flux, and R_m and r_m , respectively, the $^{13}\text{C}/(^{13}\text{C} + ^{12}\text{C})$ and $^{13}\text{C}/^{12}\text{C}$ ratios of the well-mixed surface layer of the ocean. The symbol $\langle \bar{\alpha}'_{eq} \rangle$, equal to $\overline{\alpha'_{ma}/\alpha'_{am}}$, denotes the global annual average $^{13}\text{C}/(^{13}\text{C} + ^{12}\text{C})$ equilibrium factor fractionation for air-sea exchange of CO_2 . (The

simpler symbol, α'_{eq} , is reserved to denote a spatially and temporally variable factor used in Article II). For convenience, we afterwards express most of the results of our double deconvolution calculations as reduced isotopic ratios, defined by equation (1.1), where δ_a , δ_b , and δ_m denote $\delta^{13}\text{C}$ of atmospheric CO_2 , terrestrial carbon, and carbon in surface seawater, respectively. Also, we express isotopic fractionation between carbon pools by fractionation terms with respect to $^{13}\text{C}/^{12}\text{C}$ ratios by the expression

$$\epsilon_{ij} = \alpha_{ij} - 1 \quad (4.14)$$

where i and j denote, respectively, donor and receiver pools. Table 3 lists values of all of the fixed fractionation factors and reduced isotopic ratios used in our calculations. Time-dependent ratios are listed in Table 4.

Table 3

Table 4

In most of the calculations, the $^{13}\text{C}/^{12}\text{C}$ fractionation factor, α_{ab} (equivalently expressed by ϵ_{ab}), is assumed to be constant [cf. Keeling et al. [1989a, Table 8]. However, in section 5, below, we discuss the consequences if this factor, which represents the isotopic discrimination of plants during photosynthesis, is allowed to vary. The factor α_{am} , which represents fractionation attending oceanic uptake, is assumed to be constant. The associated factor α_{ma} , however, is assumed to vary with seasurface temperature, and hence with time, because the equilibrium fractionation, α_{eq} (equal to the quotient α_{ma}/α_{am}), is temperature dependent, as discussed below.

The $^{13}\text{C}/^{12}\text{C}$ isotopic ratio for F_{fer} expressed by annual averages, is set equal to $\alpha_{ab} r_a$, the same ratio as that of CO_2 assimilated by plants during photosynthesis [cf. Heimann and Keeling, 1989, p. 262-263]. The $^{13}\text{C}/^{12}\text{C}$ ratio associated with the sum, $F_{des} + F_{ano,bio}$, is set equal to r_b , computed by taking account of the average storage time of long-lived carbon in the terrestrial pool [Keeling et al., 1989a, p. 229, and Table 8, footnote (3)].

The magnitude of the global average $^{13}\text{C}/^{12}\text{C}$ fractionation factor for CO_2 assimilation during plant growth, α_{ab} , affects the computed values of $\delta^{13}\text{C}$ for all of the biospheric fluxes in the deconvolution calculations [see Heimann and Keeling, 1989, Table 8]. As noted in Table 3 (Footnote (3)), the value that we assign to α_{ab} depends on the relative contributions from two types of plants, C3 and C4, having different photosynthetic pathways. As discussed in subsection 5.1, these pathways have distinctly different degrees of discrimination against ^{13}C , which may vary with time, and also the relative contribution of the two plant types may vary with time. These possible temporal variations are disregarded in our double deconvolution calculations.

The single deconvolution predicts monthly values of all of the exchange CO_2 fluxes defined above, and also the amount and $^{13}\text{C}/^{12}\text{C}$ ratio of carbon in the atmospheric, oceanic, and terrestrial carbon pools. The $^{13}\text{C}/^{12}\text{C}$ ratios for atmospheric CO_2 , so obtained, are then utilized in initializing the double deconvolution calculation in 1978 by setting the value in 1740 such that the predicted annual value agrees with our isotopic observations in 1978, as noted in subsection 2.3, above.

The solubility of CO_2 gas, the dissociation constants K_1 and K_2 of carbonic acid in seawater, and the equilibrium isotopic fractionation factor, α_{eq} , vary as functions of seasurface temperature in our calculations, in the manner described by Keeling et al. [1989a, Table 8, Footnote (11)]. The source of seasurface temperature data is from Jones [1994] (see Appendix E). No account is taken of possible temperature dependence of terrestrial biospheric processes. Further mathematical details are described by Keeling et al. [1989a, Appendix C; 1995] and by Bacastow et al. [2001].

The destructive land-use flux, F_{des} , always positive, is computed only for the time period of the double deconvolution; it is set equal to 2.0 PgC yr^{-1} , the average for 1980-1989 as given by R. A. Houghton [1999] (cf. Article II, subsection A.12). The term, $F_{ano,bio}$, is then calculated by difference, to be consistent with equation (4.3). The relative contributions of F_{fer} , F_{des} , and $F_{ano,bio}$ to the overall net biospheric flux, F_{bio} , though uncertain, only slightly affect the computations of the double deconvolution, because the $^{13}\text{C}/^{12}\text{C}$ ratios for the three fluxes are nearly the same.

5. Isotopic Discrimination by Terrestrial Vegetation

5.1 Isotopic fractionation associated with terrestrial photosynthesis

The C3 photosynthetic pathway of terrestrial plants produces an isotopic discrimination with a typical value of about 18‰ relative to the $^{13}\text{C}/^{12}\text{C}$ ratio of atmospheric CO_2 , and a range for different species of several per mil [Farquhar et al., 1989]. Although C3 plants account for most of net primary production (NPP), plants with the C4 pathway contribute about 20% of global NPP with a discrimination of only about 4‰ [Farquhar et al., 1989]. Consequently, the global average fractionation factor, α_{ab} , defined in section 4, above, is less than for C3 plants alone.

To estimate α_{ab} , as listed in Table 3, we adopted a discrimination for C3 plants of 17.8‰ , and for C4 plants of 3.6‰ , as reported by Lloyd and Farquhar [1994]. We then computed NPP for C3 and C4 plants for selected geographic zones, defined in Article II. We made use of a vegetation map [Hunt et al., 1996] that prescribes types

of biomes at a resolution of 1 degree of latitude and longitude. For each grid point of the map, NPP was computed, as described in Article II, by a method that makes use of remotely sensed radiometric data, from 1982-1990, the only period for which reliable radiometric data were available. Zonal averages are listed in Table 5. The resulting global average fraction of NPP contributed by C4 plants is found to be 17.44%, leading to a global average discrimination for C3 and C4 plants combined of 15.32‰, as indicated in Table 6 and previously quoted after equation (4.7). This calculation of global average discrimination does not take into account subzonal-scale or temporal variability in discrimination of the separate plant types, C3 and C4, issues that we discuss next.

Table 5

Table 6

For the northern hemisphere, discrimination varies in the range from 17.8‰ at high latitudes, to 14.0‰ in the tropics (Table 6), as the C4 fraction of NPP varies from 0 to 27%. For the two extratropical zones, where NPP is mainly owing to C3 plants, discrimination is 1.8‰ less than that inferred from the covariance of atmospheric CO₂ concentration and isotopic ratio, $^{13}\Delta_{cov}$, observed for northern hemisphere stations as listed in Table 2. A 1.3‰ gradient from high to midlatitudes is not observed in the covariance data, however. This lack is probably owing to scatter in $^{13}\Delta_{cov}$ for individual stations and suppression of local variability in covariance by atmospheric mixing.

In the tropics and farther south, the likelihood of substantial oceanic influence on $^{13}\Delta_{cov}$ precludes obtaining reliable estimates of plant discrimination from our station data. It is probably reasonable to assume that the discrimination of C3 plants south of the tropics is nearly the same as north of the tropics, and that the effect of discrimination of C4 plants is too small for neglect of its zonal variability to influence our calculations. The averages quoted in Table 6 for the tropics and mid-southern hemisphere, however, cannot be corroborated by our $^{13}\Delta_{cov}$ data.

Temporal variability in discrimination of C3 plants is more likely to be a serious neglect in our computations than spatial variability. Such variability is expected because the degree of isotopic discrimination varies with stomatal conductance of plant leaves. When stressed by lack of adequate water, plant stomata tend to close, reducing the carbon isotopic fractionation that can occur at the primary sites of CO₂ fixation within the leaves [Lloyd and Farquhar, 1994]. Evidence of interannual variability in C3 plant discrimination is shown in Figure 9, for two sites in conifer forests of western North America, one boreal (53° N.) the other temperate (46° N.). At these sites, which are about 850 km apart, we have determined $\delta^{13}C_l$ in the nocturnal boundary layer over a span of 14 years by measuring CO₂ in our laboratory from flask

Figure 9

samples of air collected repeatedly over the diurnal cycle. The average of $\delta^{13}C_I$ determined in the 1990's for these sites, -25.7‰ , reflects a discrimination of 17.8‰ , in agreement with the global average for C3 plants of Lloyd and Farquhar [1994], suggesting that these sites are representative of extratropical North America. For the more arid southern site (squares in Figure 9), $\delta^{13}C_I$ is less negative on average than for the northern site (circles), with a range of temporal variability over 14 years of about 2.5‰ , suggesting significant and variable water stress, whereas the range for the less stressed northern site is less than 1‰ . Since variable water stress affects much of the world's vegetation, a global average temporal variation of 1‰ or more seems likely on the basis of this limited study.

Time plots of $\delta^{13}C_I$ for our northern atmospheric CO_2 stations (Figure 8), which reflect the seasonal cycle of atmospheric CO_2 averaged over large regions [Kaminski et al., 1996], also suggest significant large scale temporal variability in discrimination, $^{13}\Delta_{cov}$. On the other hand, stations in the far north, which show the greatest seasonality in atmospheric CO_2 concentration, and yield the most precise annual estimates of $^{13}\Delta_{cov}$ (Table 2), show less interannual variability than elsewhere, suggesting that the variability elsewhere may be partly an artifact of statistical error. Also, the average of $^{13}\Delta_{cov}$, 19.6‰ (Table 2), for all stations in the northern hemisphere is statistically significantly greater than the global average of Lloyd and Farquhar [1994] for C3 plants, suggesting a slightly spurious variability from other processes in the determination of $^{13}\Delta_{cov}$, such as an out-of-phase oceanic seasonal signal, or a nearly in-phase seasonality in fossil fuel emissions, for which the CO_2 , on average, has a more negative $\delta^{13}C$ than the average CO_2 from C3 plants.

As discussed in section 4, above, we give greater weight to our calculations of $\delta^{13}C_I$ after 1991 because of lower scatter and standard errors than in earlier data. At the two stations in the far north, Alert and Point Barrow, where the seasonal cycle has high amplitude and is almost exclusively caused by biospheric fluxes, $\delta^{13}C_I$ varies after 1991 by only about 1‰ , little more than the average scatter in the data. At stations farther south that also possess substantial seasonal cycles of CO_2 caused mainly by biological fluxes, La Jolla and Cape Kumukahi show a range in $\delta^{13}C_I$ of about 2‰ , Mauna Loa about 3‰ . In summary, our estimates of the isotopic signature, $\delta^{13}C_I$, in the northern extratropics indicate interannual variability in isotopic discrimination by land plants of the order of 2‰ . Both the diurnal and seasonal cycles of atmospheric CO_2 show some isotopic evidence of an association with variable climate stress, especially in correlation with the El Niño cycle.

Although stations farther south do not add much useful information, we note that $\delta^{13}C_I$ for the South Pole is consistently more negative during El Niño events. This association, although possibly a reflection of variable discrimination by plants, may arise because the very small seasonal signal is difficult to separate from interannual variability that is strongly correlated with El Niño events for both concentration and $^{13}C/^{12}C$ ratio. Failure to distinguish variations correctly on the two time-scales may have produced a false correlation of $\delta^{13}C_I$ with El Niño events.

Because tropical vegetation contributes only slightly to the seasonal cycle of atmospheric CO_2 , our $\delta^{13}C_I$ data mainly reflect the discrimination of C3 plants growing in the temperate and boreal zones. These data suggest that our neglect to consider variable discrimination in these extratropical zones, in computing CO_2 fluxes by double deconvolution, could have led to an underdetermination, rather than an overdetermination, of the amplitude of fluctuations in the global biospheric exchange flux, as discussed in subsection 5.2, below. In the tropics we lack data to determine whether variable discrimination has occurred.

5.2 Variability in isotopic discrimination

To examine how variable discrimination against the rare isotope, ^{13}C , by land plants may affect the net biospheric exchange flux, F_{bio} , as calculated in our double deconvolution procedure, we invoke the isotopic additivity equation (3.2) to establish the shift in $\delta^{13}C$ of atmospheric CO_2 that takes place when atmospheric CO_2 is exchanged with the terrestrial biosphere. We first establish this shift (Case 1) assuming, as in our double deconvolution calculations, that isotopic discrimination attending photosynthesis, α_{ab} , is constant. Then, for comparison (Case 2), we compute the shift if this discrimination varies and there is no net exchange, i.e. the forward and reverse fluxes F_{ab} and F_{ba} of equation (4.4) are equal. Lastly, (Case 3) we compute the shift if the proportions of photosynthesis owing to C3 and C4 plants vary.

As expressed by equations (4.4) to (4.7), the net flux, F_{bio} , and its ^{13}C equivalent, $^*F_{bio}$, denote differences between much larger one-way fluxes, F_{ab} , F_{ba} and $^*F_{ab}$, $^*F_{ba}$, respectively. As previously noted, the respiratory flux, F_{ba} , is assumed to have no fractionation (α'_{ba} of equation (4.7) of unity). Flux F_{ab} , which represents assimilation of CO_2 by plants through photosynthesis, exhibits fractionation, expressed by the factor, α'_{ab} . We now consider the possibility that α'_{ab} varies temporally, either directly, or by varying the proportions of F_{ab} contributed by C3 and C4 plants which have distinctly different degrees of discrimination. We also disregard the small difference between α'_{ab} and α_{ab} [Heimann and Keeling, 1989, p. 263], and adopt the latter

in subsequent expressions.

Substituting in equation (4.5) the relations for $*F_{ab}$ and $*F_{ba}$, as given by equations (4.9) and (4.10), we obtain for the net ^{13}C flux:

$$*F_{bio} = (r_b F_{ba} - \alpha_{ab} r_a F_{ab})(R_s/r_s) \quad (5.1)$$

To proceed we define a hypothetical chemical steady state for the terrestrial biosphere, in which assimilation and respiration balance globally for both ^{12}C and ^{13}C . At this steady state, F_{ba} equals F_{ab} , and F_{bio} and $*F_{bio}$ are both zero. Hence,

$$r_b = \alpha_{ab} r_a \quad (5.2)$$

and therefore the $^{13}\text{C}/^{12}\text{C}$ ratios of F_{ab} and F_{ba} are both equal to the $^{13}\text{C}/^{12}\text{C}$ ratio of the terrestrial biospheric carbon pool, r_b .

Let δ_a and δ_b denote respectively, the reduced isotopic ratios, $\delta^{13}\text{C}$, of atmospheric CO_2 and carbon in the terrestrial biosphere (cf. Table 3). From the definition of $\delta^{13}\text{C}$ (see equation (1.1))

$$r_i = (\delta_i + 1)r_s \quad (5.3)$$

where i stands for either a or b. Replacing r_a and r_b in equation (5.2) according to (5.3), replacing α_{ab} by $\epsilon_{ab} + 1$, according to equation (4.14), and rearranging, the isotopic steady state condition, expressed in per mil notation, is such that

$$\delta_b - \delta_a = \epsilon_{ab} \quad (5.4)$$

(disregarding a product of second order terms, $\epsilon_{ab} \delta_a$).

For each of the three cases under consideration, let us assume that an initial steady state is displaced by an abrupt imbalance either in the one-way fluxes F_{ab} and F_{ba} , which pertain to both isotopes, or only in the one-way ^{13}C fluxes, $*F_{ab}$ and $*F_{ba}$. In each case, for simplicity, we disregard a subsequent approach to a new steady state involving a change in δ_b of the terrestrial biospheric carbon pool. Thus, we compute the maximum possible shift in δ_a in response to a specified displacement from steady state.

Let N_{ao} denote the amount of CO_2 in the atmosphere, and δ_{ao} and δ_{bo} denote δ_a and δ_b , respectively, at the initial steady state. It follows from equation (5.4) that the reduced isotopic ratios of both F_{ab} and F_{ba} are equal to δ_{bo} . We adopt 747.6 PgC for N_{ao} (see Table 3), based on a CO_2 concentration of 352.2 ppm, for 1990 (see Table D.1 in Appendix D), approximately the midpoint of our deconvolution calculations. In

accord with our analysis of global average isotopic discrimination, summarized in Table 6, $\epsilon_{ab} = 15.32\text{‰}$.

Let ΔF_{bio} (cf. equation (4.4)) denote an abrupt departure of either of the one-way fluxes, F_{ba} or F_{ab} , or in both combined, thus

$$\Delta F_{bio} = F_{ba} - F_{ab} \quad (5.5)$$

Both F_{ba} and F_{ab} , as noted above, are assumed initially to have reduced isotopic ratios equal to δ_{bo} . In accord with equation (3.2), and assuming that the departure from steady state has continued for a time-interval, ΔT , too short to cause significant changes in these isotopic ratios

$$N_{ao} \delta_{ao} + \Delta F_{bio} \Delta T \delta_{bo} = (N_{ao} + \Delta F_{bio} \Delta T)(\delta_{ao} + \Delta \delta_a) \quad (5.6)$$

where $\Delta \delta_a$ denotes the shift in the $^{13}\text{C}/^{12}\text{C}$ ratio of atmospheric CO_2 owing to the displacement from steady state. Solving for $\Delta \delta_a$ with $\delta_{bo} - \delta_{ao}$ replaced by ϵ_{ab} , which is time-invariant, according to equation (5.4), and with $\Delta F_{bio} \Delta T \ll N_a$

$$\Delta \delta_a = \epsilon_{ab} \Delta F_{bio} \Delta T / N_{ao} \quad (5.7)$$

$$= (-0.0205 \text{‰}) \Delta F_{bio} \Delta T \quad (5.8)$$

Thus, a 1 PgC yr^{-1} net flux of CO_2 from the biosphere to the atmosphere, acting for one year, ($\Delta F_{bio} \Delta T = 1$) decreases the $\delta^{13}\text{C}$ of atmospheric CO_2 by 0.0205‰ , an opposite flux increases $\delta^{13}\text{C}$ by the same amount. (The product, $\epsilon_{ab} \cdot \Delta F_{bio}$ represents an isotopic flux ("isoflux") between the terrestrial and atmospheric carbon pools, for this example equal to $15.32\text{‰ PgC yr}^{-1}$.)

For Case 2 let $\Delta \epsilon_{ab}$ denote a shift in discrimination for the full one-way flux, F_{ab} , with no change in $\delta^{13}\text{C}$ of the return flux, F_{ba} . Invoking equation (3.2) as in Case 1, but with respect to both addition and subtraction of CO_2 by biospheric exchange:

$$N_{ao} \delta_{ao} + F_{ba} \Delta T \delta_{bo} - F_{ab} \Delta T (\delta_{bo} + \Delta \epsilon_{ab}) = N_{ao} (\delta_{ao} + \Delta \delta_a) \quad (5.9)$$

Solving for $\Delta \delta_a$ with $F_{ab} = F_{ba}$:

$$\Delta \delta_a = -\Delta \epsilon_{ab} F_{ab} \Delta T / N_{ao} \quad (5.10)$$

With F_{ab} set equal to our estimate of global NPP, 61.3 PgC yr^{-1} (see Table 5), and $\Delta \epsilon_{ab}$ set, as an example, to 1‰ , we obtain an isotopic shift, $\Delta \delta_a$, of 0.082‰ in one year, four times that evaluated in Case 1. (The isoflux for this example, $\Delta \epsilon_{ab} \cdot F_{ab}$, is 61.3‰ PgC yr^{-1}). Even if the change in discrimination in Case 2 should occur only in

the tropics, where our regional analysis indicates that most of the correlation of biospheric flux with El Niño events occurs (see Article II), a 1‰ change in discrimination (with respect to an estimated NPP of 32.8 PgC yr⁻¹, see Table 5) would cause a shift of 0.044‰, more than twice that for a transfer of 1 PgC of CO₂ in one year to or from the atmosphere according to Case 1.

For Case 3, a change occurs in the proportion of assimilation by C4 plants, without a change in the fluxes with respect to C3 and C4 plants combined. The disequilibrium flux is equivalent to Case 1 except that it is applied separately for C3 and C4 plants with the added condition that the changes in net biospheric fluxes are equal and opposite for C3 and C4 plants. Denoting the mutual changes by ΔF_b , positive for increasing net C3 flux to the atmosphere (cf. equation (5.7))

$$\Delta\delta_a = ({}^3\epsilon_{ab} - {}^4\epsilon_{ab}) \Delta F_b \Delta T / N_{ao} \quad (5.11)$$

$$= (-0.019\text{‰}) \Delta F_b \Delta T \quad (5.12)$$

where superscripts 3 and 4 distinguish the fractionation factors for C3 and C4 plants, respectively (17.8‰ and 3.6‰, see Table 6). A disequilibrium flux, ΔF_b , of 1 PgC yr⁻¹ causes almost the same isotopic shift, $\Delta\delta_a$, as a 1 PgC yr⁻¹ change in NPP or respiration in Case 1, a result that could be anticipated because the substitution of a C4 flux for a C3 flux has almost the same effect on the ¹³C/¹²C of atmospheric CO₂ as a diminution in the overall net flux, F_{bio} .

Given the relatively small differences in isotopic discrimination by plants that may cause signals in the ¹³C/¹²C ratio of atmospheric CO₂ shown by these calculations, it may be unrealistic to assume in a double deconvolution that these signals are caused solely by variations in biospheric flux with isotopic discrimination fixed. Variations in discrimination of the order of 1‰, either from changes in discrimination or the fraction of NPP owing to C4 plants, can produce signals that are a significant fraction of those from varying net CO₂ exchange. In section 7 below, we discuss the interpretation of our data in the light of these findings.

6. Global CO₂ Fluxes

6.1 Deduced by deconvolution calculations

Plots of the terms of the global atmospheric carbon cycle budget, expressed by equation (4.1), are shown in Figure 10 together with subordinate terms appearing in equations (4.2 and 4.3). In Panel a are shown the rate of industrial CO₂ emissions,

Figure 10

F_{ind} , (upper curve) and the rate of change in atmospheric concentration, dN_a/dt , (middle curve), terms that serve as inputs to the single deconvolution procedure described in subsection 4.2. Their difference, $F_{bio} + F_{oce}$, (lower curve) constitutes a combined terrestrial biospheric and oceanic sink of industrial CO_2 . In Panel b this sink is separated into biospheric and oceanic components, F_{bio} (thick curve), F_{oce} (thin curve), respectively, as determined by the double deconvolution procedure described in section 4.3. In Panel c the biospheric component is shown divided into three fluxes: F_{fer} , a " CO_2 fertilization sink," representing the response of the terrestrial biosphere to increasing atmospheric CO_2 concentration, an assumed constant "land-use source," F_{des} , of 2.0 PgC yr^{-1} representing human-induced release of terrestrial CO_2 , and an "anomalous biospheric flux," $F_{ano,bio}$, that is presumed to result mainly from natural variability in the carbon cycle, although it may also reflect variability in human disturbances not accounted for by F_{fer} and F_{des} . In Panel d the oceanic component is shown divided into an oceanic "uptake sink," a response to increasing atmospheric CO_2 , F_{ex} , and an "anomalous oceanic flux," $F_{ano,oce}$, mainly, or entirely, of natural origin.

We first address the average strengths of these terms of the carbon cycle budget equation. As shown in Table 7, averages of the terms plotted in Panels a and b for the 1980's agree within 0.2 PgC yr^{-1} with corresponding fluxes reported by the Intergovernmental Panel on Climate Change in their Second Assessment Report to the United Nations [IPCC, 1996, Table 2.1, page 79], altered only slightly in a Third Assessment Report [IPCC, 2001, Table 303, P. 208]). Agreement is also close for the 1990's with respect to atmospheric CO_2 increase and emissions of fossil fuel CO_2 , but we find a substantially larger oceanic uptake of atmospheric CO_2 (by 0.7 PgC yr^{-1}) than the IPCC and a smaller biospheric uptake (by 0.6 PgC yr^{-1}). These disagreements are within the range of uncertainty in the absolute magnitude of the IPCC budget estimates when expressed at 90% confidence, but this range is so large that the relative importance of the oceans and terrestrial biosphere in removing industrial CO_2 from the air evidently cannot yet be determined reliably.

The flux estimates just described also reveal variability in the atmospheric CO_2 budget on the decadal time-scale. In agreement with the IPCC we find that atmospheric CO_2 rose at nearly the same rate in the 1980's and 1990's in spite of an increase in CO_2 emissions from fossil fuel combustion of 0.9 PgC yr^{-1} . These changes are well established, because uncertainty in absolute magnitudes, as stated by the IPCC, to a considerable degree reflect biases that don't change appreciably from one decade to the next.

Table 7

Estimates of decadal changes in the oceanic and terrestrial biospheric CO_2 exchange fluxes are less certain. We find an increased oceanic sink by relying on a double deconvolution calculation that takes account of changing $\delta^{13}\text{C}$, based on data acquired using consistent procedures of both sampling and measurement. The calculations are sensitive, however, to model assumptions regarding how global terrestrial biospheric and oceanic reservoirs respond to perturbations induced by changing atmospheric CO_2 . The IPCC in their Third Assessment Report found a reduced oceanic sink by interpreting a shift in the O_2/N_2 ratio in the atmosphere as measured in the 1980's from archived air samples compared with direct measurements in the 1990's. The change in data source from decade to decade contributes uncertainty to some unknown degree, and the results are subject to modeling uncertainty not yet fully established, because of aspects of the oceanic carbon cycle, such as outgassing of oxygen, that are not fully understood. Thus it is not possible with any great confidence to decide whether a diminishing oceanic sink and an increasing terrestrial biospheric sink, as reported by the IPCC, are more likely to be correct than our finding the reverse. An important finding on which the IPCC and we agree qualitatively, however, is that the terrestrial biospheric flux increased from the 1980's to the 1990's.

Shorter term interannual variations in the fluxes of the budget equation (4.1), summarized by the IPCC [2001, pp. 208-210], are a principal interest of our study. Such variations in the rate of change in atmospheric CO_2 concentration, dN_a/dt , and in industrial CO_2 emissions, F_{ind} , shown by the two upper curves of Figure 10, Panel a, are both well determined, the former derived from our atmospheric observations (cf. Figure 7), the latter from Andres et al. [2000], the same international statistical data used by IPCC. Variations in their difference, equal to $F_{oce} + F_{bio}$, are therefore also well determined. (So is their decadal average value, as discussed in subsection 7.3, below). This combined oceanic and terrestrial sink (lower curve in Figure 10, Panel a), indeed, has nearly the same interannual pattern of variability as the change in atmospheric CO_2 concentration, dN_a/dt , because global industrial CO_2 emissions, F_{ind} , vary only slightly from year to year. Most notable are maxima in $F_{oce} + F_{bio}$ close to time-intervals shown by vertical gray bars, suggesting a coupling of both oceanic and terrestrial carbon cycle components with globally average warm periods, often El Niño events, as discussed in section 2.2, above.

The oscillatory pattern of variations in F_{bio} , especially its phasing, is so similar to that of dN_a/dt and $F_{oce} + F_{bio}$, that biospheric exchange, F_{bio} , appears to represent the predominant cause of short-term interannual variability in dN_a/dt . The calculated amplitudes of the prominent fluctuations in F_{bio} , however, substantially exceed those

in dN_a/dt , resulting in opposing patterns in the oceanic and biospheric fluxes.

6.2 Sensitivity of results to oceanic vertical mixing

Double deconvolution computations yield results that differ on long time-scales depending on the degree of vertical mixing specified in the oceanic submodel, because the oceanic exchange of CO_2 with the atmosphere over decades and centuries acts to reduce the air-sea $^{13}\text{C}/^{12}\text{C}$ isotopic disequilibrium at a rate that depends on the degree of vertical mixing [Bacastow et al., 2001]. There is also a dependency of results on the specified rate of air-sea exchange of CO_2 and specified storage time of carbon in the terrestrial biospheric pool, but these last two dependencies are not independent of each other in the double deconvolution, because the sum of the terrestrial biosphere and oceanic fluxes is determined solely by the global budget equation.

Despite the uncertainties associated with these model dependencies on long time-scales, the deconvolution procedure can be shown to be insensitive to uncertainties in the oceanic submodel parameters on short time-scales [Bacastow et al., 2001], as illustrated in Figure 11. Changing the oceanic diffusion coefficient, K , in the double deconvolution (Panel a), causes the oceanic uptake, F_{ex} , to differ approximately as in a single deconvolution computation in which the oceanic submodel uniquely specifies this uptake. In contrast, the anomalous flux, $F_{ano, oce}$, is only affected by a slow increase in discrepancy between sensitivity computations, reflecting the effect of differing degrees of vertical mixing on the isotopic disequilibrium of oceanic carbon with atmospheric CO_2 . Varying the air-sea exchange coefficient within its range of uncertainty has little effect on either F_{ex} or $F_{ano, oce}$ (Panel b).

Figure 11

The insensitivity to submodels on the short-term does not extend, however, appreciably beyond the time-scale of El Niño events. The calculated decadal averages of F_{ex} becomes less negative, and $F_{ano, oce}$ more positive, when K is reduced. For the 1990's their sum, representing the full oceanic CO_2 uptake, diminishes from $-2.36 \text{ PgC yr}^{-1}$ (for K of $7685 \text{ m}^2 \text{ yr}^{-1}$, cf. Table 7), to $-0.82 \text{ PgC yr}^{-1}$ (for K of $2000 \text{ m}^2 \text{ yr}^{-1}$). The calculated oceanic CO_2 uptake, for any value of K that we have considered, increases from the 1980's to the 1990's, but this increase also diminishes as K is reduced: from $0.362 \text{ PgC yr}^{-1}$ for the highest K considered, to $0.001 \text{ PgC yr}^{-1}$ for the lowest. Only about half of the diminution is found by the single deconvolution (a decreased decadal change in F_{ex} from $0.251 \text{ PgC yr}^{-1}$ to $0.113 \text{ PgC yr}^{-1}$), the rest associated with the double deconvolution. This broad range in calculated oceanic uptake, as K varies, reveals the inability of either the single or double deconvolution to prescribe decadal variability independently of a proven oceanic submodel, but does

not support a decreasing sink from the 1980's to the 1990's as reported in the Third Assessment Report of IPCC.

In summary, the decadal averages of F_{bio} and F_{oce} , as listed in Table 7, are dependent on the choice of oceanic submodel used in the deconvolution procedure. The short-term interannual variability in the anomalous fluxes, $F_{ano,bio}$ and $F_{ano,oce}$, however, is closely prescribed by the CO_2 observations, provided that isotopic discrimination is correctly specified, as discussed in section 7, below.

7. Reliability of Deduced Fluxes

7.1 Introduction

Before discussing our findings regarding the global average terrestrial and oceanic fluxes, F_{bio} and F_{oce} , the extent of possible errors in their calculation will be examined. We address uncertainty in our results on several time-scales.

7.2 Analysis of statistical errors

Statistical errors in F_{bio} and F_{oce} , on short time-scales, are contributed by scatter in the data for both concentration and $^{13}C/^{12}C$ ratio, expressed by standard errors of the fit of individual observations to the spline curves shown in Figure 3. These errors range from 0.15 ppm and 0.02‰ at the South Pole to 1.1 ppm and 0.07‰ at Point Barrow, Alaska (see Table D.3), and result in errors of the order of 0.5 PgC yr⁻¹ with respect to F_{bio} and F_{oce} , as discussed in Article II, subsection 6.2. Thus, although significant, these errors are not large enough to challenge our finding of large short-term interannual fluctuations in biospheric and oceanic fluxes (of the order of several PgC yr⁻¹). A more important issue is whether the calculation of these fluxes is affected by systematic errors, which is possible on all time-scales.

7.3 Analysis of possible systematic errors

We first discuss possible errors associated with the double deconvolution procedure which deduces fluxes from simultaneous data for the concentration and $^{13}C/^{12}C$ ratio of atmospheric CO_2 . We thus add to our earlier discussion (subsection 6.2 above) of uncertainties on the decadal-time scale. In the succeeding subsection we discuss errors on the short-term interannual time-scale, approximately that of the ENSO cycle (cf. subsection 2.2 above)

To deduce the relative strengths of F_{bio} and F_{oce} , which include responses to the combustion of fossil fuels, we have made use of the same inverse double deconvolution procedure used previously by Keeling et al. [1989a, 1995]. Previously, however, only anomalous fluxes were calculated, similar to $F_{ano,bio}$ and $F_{ano,oce}$, plotted in Figure 10, Panels c and d. Here, full net fluxes, denoted by F_{bio} and F_{oce} , are also calculated, as plotted in Figure 10, Panel b. As pointed out in subsection 6.2 above, the validity of the deduced average magnitude of these fluxes depends on the correctness of the oceanic submodel used in the deconvolution procedure.

As explained by Bacastow et al. [2001], although it may appear that the double deconvolution should allow the net oceanic flux to be determined correctly on any time-scale [cf. Joos and Bruno, 1998], the calculation, except on short time-scales, is ill-conditioned, as demonstrated by the results shown in Figure 11. Consequently, although our study contributes to an understanding of the short-term interannual variability of the global carbon cycle over two decades, it does not resolve decadal variability and the so-called "missing CO₂ sink" issue [Wigley and Schimel, 2000, p. 47, pp. 54-150] as to whether the terrestrial biosphere is an important global sink for CO₂ produced by the combustion of fossil fuels. Our estimated net biospheric and oceanic fluxes for the 1980's agree with those of the IPCC reported for the 1980's [IPCC, 1996] (see Table 7) because both studies used oceanic submodels that predicted nearly the same oceanic uptake of CO₂ from combustion, by relying on oceanic data of radiocarbon, ¹⁴C, as a constraint on the calculated degree of oceanic uptake of CO₂. Our estimates of these fluxes disagree with those of the IPCC for the 1990's because we use the same isotopic constraint and same oceanic submodel as before, while the IPCC calculation is based on O₂/N₂ data which provide an estimate of the oceanic flux nearly independent of the choice of oceanic submodel [IPCC, 2001, p. 206].

The principal components of the global atmospheric CO₂ budget are known with widely varying uncertainties. As estimated by the IPCC (Table 7) at 90% confidence, the independent errors associated with the rate of increase of atmospheric CO₂ (± 0.20 PgC yr⁻¹) and industrial CO₂ emissions (± 0.50 PgC yr⁻¹) are so small that the error in the combined oceanic-terrestrial biospheric flux, $F_{oce} + F_{bio}$, is uncertain to only ± 0.54 PgC yr⁻¹ (calculated by quadrature). The errors for the separate oceanic and terrestrial biospheric fluxes alone are substantially larger. When determined from separate errors for three components, the error for F_{bio} is ± 1.9 PgC yr⁻¹. Such a large error is not surprising since data must be assembled globally for many diverse pools of carbon. A substantially lower error for F_{bio} , ± 0.9 PgC yr⁻¹, is obtained when determined by subtracting estimates of F_{oce} from the sum $F_{oce} + F_{bio}$, the approach of the

IPCC, underscoring the value in obtaining precise estimates of oceanic uptake of atmospheric CO_2 as an indirect approach to determining the global average of the terrestrial biospheric flux, F_{bio} , as discussed further in subsection 8.3, below.

7.4 Systematic uncertainty in fluxes on short time-scales

Both the terrestrial and oceanic CO_2 fluxes inferred from our atmospheric CO_2 data show a distinct association with fluctuating temperature, most evident during El Niño events when the concentration of atmospheric CO_2 has risen most rapidly. This association with the ENSO cycle is not surprising because these events are attended by pronounced changes in the temperature and circulation of both the atmosphere and the oceans likely to affect the global terrestrial and oceanic carbon pools. Thus the phasing of the large fluctuations seen in our atmospheric data are not difficult to explain, but our finding of large opposing terrestrial releases and oceanic sinks of CO_2 phased with the ENSO cycle has been challenged on the grounds that our $^{13}\text{C}/^{12}\text{C}$ data through 1988 [Keeling et al., 1989a] contain substantial systematic errors, specifically that they do not agree with other measurements showing only small isotopic fluctuations with little association with the strong El Niño events in 1982-3 and 1987-8 [Francey et al., 1995].

Although two succeeding El Niño events, in 1992 and 1994, were not strong enough to substantiate the plausibility of the large fluctuations that our data show for the 1980's, we now possess data for an El Niño event in 1997-8, for which the rate of change in $^{13}\text{C}/^{12}\text{C}$ ratio (see Figure 7) fluctuated with an amplitude as large as for the strong events in 1982-3 and 1987-8. Furthermore, this fluctuation, as were fluctuations for the El Niño events of 1982-3 and 1987-8, is seen separately for every station in our array (see Figure 4). We argue, therefore, that the only circumstance that could lead to erroneous signals for all three of these events would be gross miscalibration of the mass-spectrometers of two laboratories (see Appendix C) that introduced false variations, synchronous with each event.

Although calibrating errors cannot be ruled out, a more likely source of systematic error is some shortcoming in either the terrestrial biospheric or oceanic submodel of the double deconvolution procedure. A likely possibility is our assumption that isotopic discrimination attending photosynthesis on land is constant. As discussed in section 5, above, our calculations of biospheric flux are sensitive to neglect of variations in discrimination as small as 1‰. A decrease of this magnitude for tropical vegetation as a whole during El Niño events would be interpreted by our double deconvolution as a diminution in the fluctuations inferred for the strong events of

1982-3, 1987-8, and 1997-8, sufficient to eliminate the opposing oceanic flux inferred in our calculations. Such a decrease in discrimination is plausible. Tropical drought and heat attending El Niño events are expected to cause stress in plants causing net primary production (NPP) to decrease and atmospheric CO₂ to rise anomalously as observed. Perhaps a decrease in discrimination accompanies this presumed decrease in NPP, such that the two effects cannot be distinguished by their timing.

In Article II we present evidence that most of the association of terrestrial biospheric and oceanic CO₂ fluxes with warming events is produced in the tropical zone. Correlations of these inferred fluctuations with variations in climatic factors therefore should reflect a relation of climate forcing to the metabolic activity of plants in which the phasing is well determined even if the magnitudes of the fluctuations cannot be established from atmospheric data alone. We thus may gain insight into the relationship of the carbon cycle to climate without yet knowing the extent of variable discrimination by tropical plants, as discussed in Article IV.

8. Discussion

8.1 Introduction

We first discuss our results on the ENSO time-scale and then over the full 22 years of our study. We then discuss possible ways to reduce errors in determining exchange fluxes in the future.

8.2 Short-term variability in the global carbon cycle

To compare the magnitude of fluctuations in exchange fluxes with the strength of El Niño events, a useful measure is the southern oscillation index (SOI), which tracks the ENSO cycle as reflected in the surface barometric pressure difference across the central and western Pacific ocean from Tahiti to Darwin, Australia. For the period of our study, 1978-1999, the most pronounced fluctuations in SOI occurred near the times of strong El Niño events of 1982-3, 1987-8 and 1997-8 (henceforth events of "1983," "1987," and "1998"), as shown in Figure 5b. Following sharp minima in the SOI for these three events, high rates of increase in the concentration of atmospheric CO₂ occurred at Mauna Loa, Hawaii, at times shown by gray bars in the figure. We ask, to what degree did extremes seen in the anomalous biospheric and oceanic fluxes, $F_{ano,bio}$ and $F_{ano,oce}$ (Figure 10, Panels c and d) represent responses to climatic variability at these times?

Because the amplitudes of the fluctuations in SOI are nearly equal for these three El Niño events, it is possible that they reflect approximately equal degrees of climatic forcing. Calculated amplitudes of fluctuations in the anomalous biospheric flux, $F_{ano,bio}$ (Figure 10, Panel c) for these events are also nearly equal, based on our observing nearly equal amplitudes of corresponding fluctuations in rate of change of $^{13}\text{C}/^{12}\text{C}$ ratio (Figure 7). The calculated fluctuation in the anomalous oceanic flux, $F_{ano,oce}$ (Figure 10, Panel d), however, is of lesser amplitude for the 1998 event than for either of the two previous events, reflecting a greater fluctuation in the rate of change of atmospheric CO_2 for this event (Figure 7). How can this lesser oceanic fluctuation be explained?

Either the fluctuations in the oceanic flux, indeed, were different in spite of similar signals in the SOI for all three events, or the terrestrial biospheric flux has been incorrectly calculated. We first discuss the likelihood of variable oceanic fluctuations. In a previous double deconvolution calculation with data only through 1988 [Keeling et al. 1989a], variations in $F_{ano,oce}$ showed a correlation with tropical seasurface temperature. A larger sink than otherwise during El Niño events was attributed to reduced upwelling in the tropical oceans, especially in the east Pacific, that caused a decreased source of CO_2 from the tropical oceans to the atmosphere, in spite of a warmer seasurface. As shown in Figure 12, east tropical Pacific seasurface temperature showed greater warming for the 1998 El Niño event than for the events of 1983 and 1987, whereas the oceanic sink was less pronounced. Thus variable fluctuations in tropical seasurface temperature do not explain quantitatively a smaller oceanic fluctuation in 1998.

Figure 12

Alternatively, neglecting to account for temporal variability in isotopic discrimination by plants may have caused errors in the calculated fluxes, as discussed in subsection 5.2. Although the nearly equal amplitudes of fluctuations in the first derivative of $\delta^{13}\text{C}$ of atmospheric CO_2 that we observe in association with El Niño events (see Figure 7), suggest corresponding nearly equal amplitudes in $F_{ano,bio}$, perhaps this is not a correct conclusion. This flux reflects both anomalous assimilation of carbon by net primary production (NPP) and anomalous release of biospheric carbon by respiration. Although, respiration, as well as NPP, generally responds directly to variability in temperature and precipitation, the sensitivities are not necessarily the same. Variations in NPP, respiration, and variable isotopic discrimination could fortuitously lead to our calculating nearly the same amplitudes for fluctuations associated with the three strong El Niño events of 1983, 1987, and 1998 by ignoring variations in discrimination.

Because these fluctuations probably occur mainly in the tropics, as discussed in Article II, we defer further consideration of their causes here. In Article IV, while reviewing the results of our regional calculations by inversion, we reconsider the possible causes of fluctuations in the biospheric and oceanic fluxes. We find some support that much of the variability in these fluxes appears to be real and not an artifact of neglected variable discrimination.

8.3 Ways to reduce uncertainty in estimation of exchange fluxes

Given the present difficulties in inferring CO₂ fluxes from atmospheric CO₂ data as just discussed, several possible improvements come to mind. One that is obvious is to increase the precision and absolute accuracy of time-series data. Better calibrations would almost surely improve the data base for studying fluxes, especially with respect to isotopic data. In particular they would prevent the finding of such large differences in results between laboratories that one laboratory may find a large isotopic El Niño signal while another does not. Most helpful would be the reintroduction of international isotopic standard reference materials, in the range of oceanic and atmospheric CO₂, for systematic long term intercalibration between laboratories.

Uncertainty in establishing the rate of uptake of atmospheric CO₂ by the oceans presently limits our ability to identify which part of the combined oceanic and terrestrial sink of industrial CO₂ is oceanic, because the terrestrial biospheric sink is, and probably will remain, far less well determined than the oceanic sink, as discussed in subsection 7.3, above. Several indirect means to improve knowledge of the oceanic sink have been pursued: studies of the fundamental behavior of the oceanic carbon cycle through oceanic campaigns such as the JGOFS program, investigations of the ocean circulation, such as was pursued by the World Ocean Circulation Experiment, and the use of transient tracers such as chlorofluorocarbons to define better in general the transport of chemical substances in the oceans. The present uncertainty in the oceanic sink quoted in Table 7 takes into account all of these techniques.

Given the dependency of the double deconvolution procedure on the choice of oceanic submodel, as discussed above, there is no means of estimating the correctness of the average magnitudes of net oceanic fluxes from atmospheric CO₂ data alone. The determination of F_{oce} would be better determined if time-series were available adequate to establish the global average of ¹³C/¹²C ratio of dissolved inorganic carbon (DIC) in surface ocean water [Gruber and Keeling, 2001], and still better if adequate subsurface isotopic data were also available [Quay et al., 1992]. However, no indirect method is likely to be as reliable as direct measurements of DIC, such as were pursued

during the World Oceans Circulation Experiment [Needler, 1992]. Such measurements, however, should be carried out repeatedly to establish the rate of change of the inventory of carbon in the world oceans.

Independently establishing the global exchange of atmospheric CO_2 with the terrestrial biosphere, either by direct flux measurements or by measuring the changing inventory of carbon in plants and sinks, is not likely to produce a precise global inventory for terrestrial biospheric carbon because of the great heterogeneity of the reservoir. Thus the extent to which the terrestrial biosphere is a source or sink of atmospheric CO_2 globally will probably be best determined by subtracting from the well established combined sink, $F_{bio} + F_{oce}$, the estimates of the oceanic flux, F_{oce} , based on direct oceanic inventory data. This approach has long-term merit, because the data gain more and more significance as the time-interval of measurements lengthens.

A third approach is to use precise measurements of atmospheric oxygen concentration concurrently with measurements of CO_2 concentration and $^{13}\text{C}/^{12}\text{C}$ ratio, further to constrain the relative magnitudes of the oceanic and terrestrial CO_2 exchange fluxes. Atmospheric oxygen is influenced by exchanges with the land and oceans in different proportions than carbon dioxide, so the combination of atmospheric O_2 and CO_2 measurements can help to resolve the relative proportions of the land and ocean carbon sinks [R. F. Keeling and Shertz, 1992; Battle et al., 2000]. This method, as all other known methods, has complications, but is likely to produce valuable evidence of the time-evolution of oceanic uptake on all time-scales from seasonal to long-term, complementing direct measurements of increasing carbon in sea water that can be made world-wide only at infrequent intervals.

9. Conclusions

Combined measurements of the concentration and $^{13}\text{C}/^{12}\text{C}$ isotopic ratio of atmospheric CO_2 have provided us with a basis for distinguishing terrestrial biospheric and oceanic exchanges of CO_2 , from 1978 through 1999. We find remarkably similar patterns of fluctuations of variations in concentration and isotopic ratio on the time-scale of the El Niño-southern oscillation (ENSO) cycle, from which we infer increased releases of CO_2 by the terrestrial biosphere, partially offset by greater uptake of CO_2 by the oceans during El Niño events and at other times of above average global temperature. Not all details of these correlations are readily explained, however, and our findings need to be viewed with caution.

The best established correlation of our atmospheric CO₂ data with the ENSO cycle pertains to the sum of the global biospheric and oceanic fluxes, established unambiguously by the rate of change in CO₂ concentration. The global average rate of change in ¹³C/¹²C ratio, though less well established, varies closely in phase with the global CO₂ concentration (Figure 6). It follows, therefore, that the global terrestrial biospheric flux, which the isotopic record reflects, almost certainly has correlated with the ENSO cycle. The global oceanic flux probably also correlates because it is determined by subtracting the biospheric flux from the sum of the two fluxes.

The amplitudes of fluctuations in this sum, derived solely from CO₂ concentration data, are also well established, but the amplitudes relating to the separate global biospheric and oceanic fluxes are uncertain, because miscalibration of the isotopic data, and an inability to interpret these data correctly, may have produced errors in calculating amplitudes. With respect to calibrations, concentration and isotopic data match each other more closely after 1991, a circumstance that we attribute to improved precision of our isotopic data after a change in mass spectrometers, and to better and more frequent isotopic standardizations. Our isotopic data may reflect phenomena not all taken into account in our calculations of fluxes, however, in particular, interannual variability in isotopic discrimination by plants. The similarity in phasing of variations in concentration and isotopic ratio, except for the very rare possibility that even this feature could be an artifact of poor data, demands, however, that possible variations in isotopic discrimination by plants, or other neglected phenomena, be phased consistently with fluctuations in the global biospheric flux.

Phasing of variable discrimination closely tied to the ENSO cycle is, indeed, a possibility. As a regional analysis of fluxes discussed in Article II demonstrates, most of the correlation of biospheric flux with the ENSO cycle occurs in the tropics where drought may cause both the net primary production of plants and discrimination to decrease during El Niño events. Also, as shown in section 5, above, the existence of small average variations in tropical discrimination could explain a substantial part of the amplitude in biospheric fluctuations that we infer. However, the anticorrelation of oceanic flux with tropical seasurface temperature that we deduce supports an hypothesis that discrimination by plants may have varied only slightly over the ENSO cycle, or not at all. Such an anticorrelation is consistent with observed decreases in upwelling of cold CO₂-laden subsurface water in the tropics during El Niño events, expected to produce increased seasurface temperature together with a release of CO₂ to the air.

Quantitatively it is difficult to decide which mechanism better explains the observed fluctuations in CO_2 concentration and $^{13}\text{C}/^{12}\text{C}$ ratio. The southern oscillation index (SOI), a measure of the intensity of El Niño events, shifts by nearly the same amount during three major events in 1983, 1987, and 1998 (whose timing is indicated approximately by gray bars in Figure 5). Tropical seasurface temperature also shows nearly equal shifts for these events (Figure 12). Nevertheless, the oceanic flux that we infer shows a substantially lesser fluctuation in 1998 than during the two earlier events, a finding not readily explained. Fluctuations in the rate of change of $^{13}\text{C}/^{12}\text{C}$ ratio for these three events are nearly the same (Figure 7), consistent with nearly equal strengths of the El Niño events as indicated by the southern oscillation index and sea surface temperature data. A reduction in amplitude owing to reduced discrimination is therefore expected to diminish by similar amounts the biospheric signals for all three events. Thus, if our isotopic data are correct, at least one signal, either oceanic or biospheric, must vary in strength between the events of the 1980's and the 1998 event. At present our analysis cannot reconcile these features.

Because so much of the interannual variability in CO_2 exchange deduced in our study is short-term and attributed to a naturally occurring ENSO cycle, we have not dwelt at length on long-term variability in exchange, nor on anthropogenic factors that cause variability. The double deconvolution procedure that we have used takes account of the unquestionably human-caused rise in atmospheric CO_2 resulting from the combustion of fossil fuel, but this combustion process is sufficiently steady on the short-term that it contributes but little to the interannual variability in atmospheric CO_2 on the ENSO time-scale. Short-term variability is likely, however, to be partly of human cause, because of recent changes in land-use that may have increased the sensitivity of the terrestrial biosphere to natural variations in climatic factors, for example, indirectly by human-caused changes in albedo and latent heat exchange, or directly by causing more and greater forest and grass fires during periods of drought.

In summary, our principal finding from a new analysis of atmospheric CO_2 data is that interannual fluctuations in net exchanges of atmospheric CO_2 are of the order several PgC yr^{-1} and correlate with strong El Niño events. The fluctuations clearly involve the terrestrial biosphere, and probably the oceans, but their amplitudes and phasing cannot yet be precisely determined. Calculations of these fluctuations, however, are not sensitive to further uncertainties which still remain in calculating the long-term sequestration of industrial CO_2 by both the terrestrial biosphere and the oceans.

Acknowledgments. Over the more than 10 years during which we carried out the studies leading to the four articles, of which this is the first, we benefitted greatly from advice and assistance of other scientists. We thank John Chin, Roger Francey, Ralph Keeling, Ingeborg Levin, Martin Manning, Pieter Tans, and Neil Trivett, for assistance in field studies as well as advice; Robert Andres, Tom Boden, Antoinette Brenkert, Andrew Dickson, Timothy Lueker, Greg Marland, and Raymond Weiss, regarding fossil fuels and the chemistry of the atmosphere and oceans; Deborah Clark, Jim Ehleringer, Inez Fung, Richard Houghton, Rachel Law, Jerry Melillo, Willem Mook, Ranga Myneni, Jim Randerson, Steven Running, Compton Tucker, Peter Thornton, and Steve Wofsy for advice on understanding and modeling the terrestrial biosphere; Nikolas Gruber, Fortunat Joos, and Peter Niiler, for advice on understanding and modeling the oceans; Daniel Cayan, Mike Changery, Henry Diaz, James Hansen, Philip Jones, Tom Karl, Rachel Pinker, and Thomas Wigley, for data and advice on weather and climate. We also thank Alane Bollenbacher, Peter Guenther, David Moss, Elisabeth Stewart, and David Stow of the Scripps Carbon Dioxide Research Group for measurements, data workup, computer programming, and assistance in preparing these articles. We are also grateful to authors of this first article who contributed to the other articles without being named as authors. Funding for this research was provided by the U.S. National Aeronautics and Space Administration, U.S. National Science Foundation, and U.S. Department of Energy by grants NASA NAG5-3469, NSF ATM 97-11882, NSF OCE 97-25995, and DOE DE-FG03-95ER62075, by the Vetlesen Foundation, the SIO Support Group, and by the Office of the Director of the Scripps Institution of Oceanography.

Appendices

Appendix A. Sampling procedures and techniques of measurement

Measurements of atmospheric CO₂, shown in Figure 3, were made on samples of air collected in 5-liter glass flasks equipped with Apiezon-greased stopcocks. Flasks were pumped to a high vacuum before shipment to sampling sites where each sample was collected by opening the stopcock for approximately 30 seconds. The flasks were returned to SIO where the CO₂ concentration was measured on an aliquot of air from each flask with an Applied Physics Corporation Model 55 nondispersive infrared (NDIR) gas analyzer. The remaining air, about 80% of the original sample, was removed from each flask by slowly pumping through a special concentric double-spherical trap cooled with liquid nitrogen. The trapped CO₂, together with trace amounts of N₂O also present in the original air samples, was then transferred to a storage tube by sublimation using liquid nitrogen. From 1978 to 1982, such tubes were equipped with stopcocks, greased or equipped with O-rings [Mook et al., 1983]. Thereafter, tubes consisted of ordinary 1/4" diameter Pyrex glass tubes into which the CO₂ samples were sublimed, and each tube then sealed with a torch. The stored CO₂ was later transferred to a mass spectrometer where the 45/44 mass ratio was measured, and the ¹³C/¹²C ratio subsequently determined, with a correction applied for the influence of N₂O [Bollenbacher et al., 2001]. From 1978 to 1991, samples were measured at the Centrum voor Isotopen Onderzoek (CIO) of Groningen University, the Netherlands, with a VG Instrument Inc. Sira mass spectrometer; subsequently they were measured at SIO with a VG Prism II mass spectrometer. Measurement techniques, further described by Keeling et al. [1989a, p. 218], have remained the same throughout the study reported here.

In addition, at Mauna Loa Observatory, measurements of CO₂ concentration were made on site with a NDIR gas analyzer, the same model as used at SIO, following techniques described by Keeling et al. [1982]. Monthly averaged, these nearly continuous concentration data are shown in Figure 3. A parallel data set, based on flask samples (having somewhat more scattered data but nearly the same interannual trend), is not shown.

Appendix B. Calibration of concentration data.

Gas mixtures of natural air, stored in high pressure cylinders, after drying to a water vapor concentration of 2.5 ppm or less, and mixtures of CO₂ in nitrogen gas, were used to calibrate the NDIR gas analyzers for CO₂ concentration. Calibration consisted of analyzing air flowed from one or more cylinders into the analyzer cell in alternation with air from flask samples, the latter introduced into the cell using a mercury Toepler pump. A detailed intercomparison of reference gases on 5 successive dates over not more than a few months, was performed approximately every two years, assuring that the reported concentration data are consistent with the mole fractions of CO₂ established for a set of 11 primary CO₂-in-air reference gases. The mole fractions of these primary reference gas mixtures, and a second set of 13 CO₂-in-nitrogen primary reference gases, were checked approximately every three years, with a constant-volume mercury-column manometer, essentially as described by Keeling et al. [1986].

Appendix C. Calibration of isotopic data.

In the Netherlands, at CIO, calibrations were made with a suite of samples of pure CO₂ attributed to international standards [Mook et al., 1983]. Calibrations were made approximately every third day of analysis. From 1989 to the end of the program at CIO, calibrating was less frequent and not reported to SIO until recently. We consider the data for this period to be less reliable than the earlier data. At SIO, since early 1991, we have made use of 3 calibrating standards, consisting of aliquots of CO₂ extracted from gas mixtures of dried natural air stored in high pressure cylinders, the same kind of gas mixtures used as our primary standards for NDIR gas analysis. These aliquots, prepared in the same way as samples of CO₂ from air collected at field stations, and therefore containing N₂O, were introduced into the analysis schedule every day. Data obtained from their use indicate that the VG Prism II mass spectrometer has varied in performance enough to justify daily calibration. Moreover, comparison with pure CO₂ standards indicates that the mass spectrometer calibration for air-derived CO₂ has drifted over time unidirectionally with respect to calibrations of these conventional standards, the trends interrupted from time to time by abrupt changes in the opposite direction, following instrument repairs. We do not know whether the calibration of the mass spectrometer of CIO for air-derived CO₂ also drifted.

To cross-calibrate isotopic data of CIO and SIO near the time when analyses were transferred to SIO, 36 samples of CO₂ extracted from air collected at La Jolla and 18 aliquots each of 3 SIO standards of CO₂, extracted from air, were measured at CIO and the results intercompared with measurements at SIO of 61 extracts of air from La Jolla and approximately 160 extracts from each of the three standard gases. On the assumption that the calibration of the CIO spectrometer remained the same with respect to international standards measured at CIO, and adopting the N₂O correction determined at CIO [Mook and van der Hoek, 1983], we have adjusted all of our data to the average of replicate calibrations made at SIO against the former international standards of pure CO₂, and carbonate standard, NBS-19. Calibration of the SIO mass spectrometer and the cross-calibration between CIO and SIO are described in detail by Bollenbacher et al. [2001] and Guenther et al. [2001].

There are presently no available international isotopic carbonate standards for interlaboratory calibration of CO₂. Until protocols for reliable intercalibration are put into effect internationally, it is prudent to assume that biases as great as 0.15‰ exist when comparing our data with data of other laboratories. Also, still unresolvable biases may exist between the CIO and SIO isotopic data sets for atmospheric CO₂ reported here.

Appendix D. Data processing.

To establish global averages of CO₂ concentration and ¹³C/¹²C after 1978 (the latter expressed by the reduced isotopic ratio, δ¹³C (see equation (1.1)), weighted averages for 9 stations (those listed in Table 1, excepting Mauna Loa) were computed for each month. The weight for a given station was set to the fraction of area of the earth in zones between latitudes, midway in sine of latitude between neighboring stations (or midway to the pole, if there was no poleward station.) For stations whose records began after 1978, prior estimates were made back to the beginning of 1978, based on their differences from Mauna Loa-South Pole averages over the first 4 years of each station's record, except as noted below. The δ¹³C record for Mauna Loa was extrapolated back to 1978 assuming its difference from the neighboring Christmas Island station record to be constant, averaged over the years, 1978 through 1982. Extrapolated and actual records were joined smoothly using a 9-month triangular filter. The Baring Head, New Zealand δ¹³C record was extrapolated back to 1978 by assuming it to be offset from the Mauna Loa-South Pole average by an observed 5-year average difference.

Data from our northernmost station, Alert, having a similar seasonal interannual pattern to our other northern station, Point Barrow, were merged with data from Point Barrow to form a composite in the far north record for both CO₂ and δ¹³C. The average difference over the first 4 years of the Alert record was used to extrapolate the Alert record back to the start of the Point Barrow data. The merged data were then extended back to 1978, as described above. Data for Mauna Loa Observatory, although used in extrapolating other records, as just described, was not included in the weighted global average. Records of CO₂ concentration of the western United States, 1955-1957, and of Mauna Loa and the South Pole, 1957-1977, were used prior to the beginning of isotopic data in 1978, after being adjusted upward by 0.6119, the mean difference between two composite records: 1) the average of the Mauna Loa and South Pole records and 2) the 9-station composite record from 1979 to 1999. Prior to 1955 measurements from an ice core were used [Etheridge et al., 1996] without adjustment.

The monthly data points for concentration and δ¹³C ratio for each station were fit to nodal splines [Reinsch, 1967], as described by Keeling et al. [1989c]. The smoothness of each spline was prescribed to be the same for each station and constituent of CO₂ by adjusting the stiffness of the spline to arrive at a specified integral of the second derivative per year: 30 (ppm yr⁻²)² for concentration, 1.5 (‰ yr⁻²)² for δ¹³C ratio. The splines for concentration and δ¹³C, were then averaged at monthly intervals to produce smooth line-segments. These are shown, above, in Figure 6 (indistinguishable from smooth curves) after subtracting linear trends, as described in the figure caption. Monthly data points of concentration are listed in Table D.1, of δ¹³C in Table D.2. The standard deviations of the data points for CO₂ concentration and δ¹³C, with respect to each spline, are listed in Tables D3 and D4, respectively; The corresponding variances, obtained by squaring, are accepted as measures of random scatter in the data (see Article II, subsection B.1)

Table D.1

Table D.2

Table D.3

Table D.4

Statistical error in our analysis of fluxes was estimated by a method similar to that used by Keeling et al. [1995]. Owing to greater scatter, relative to impact on the calculation of fluxes, the isotopic data contribute most of the error to the determination of fluxes and have been assumed to contribute all of the error in the fluxes. Firstly, annual rates of change in δ¹³C were estimated, fitting the isotopic data points to straight lines over annual segments of the record, and the standard errors of the slopes determined. Because the annual fluxes are proportional to the slopes, the error of the flux is proportional to the found error of the slope. Secondly, the annual biospheric fluxes, found by double deconvolution, were scaled to the magnitudes of the slopes to

express the errors in PgC yr^{-1} . Because the errors in the sum of the terrestrial biospheric and oceanic fluxes are independent of the $\delta^{13}\text{C}$ data, the errors in oceanic flux were assumed to be equal and opposite to those of the biospheric flux.

Appendix E. Auxiliary Data

The oceanic submodel that calculates the oceanic response flux, F_{ex} , (see equation (4.2)) takes account of variations in seasurface temperature based on global average data of Jones [1994, and personal communication], shown in Figure E.1. The double deconvolution makes use of annual data for the production of fossil fuels and cement manufacture as listed in Table E.1.

Figure E.1

Table E.1

References

- Andres, R. J., G. Marland, T. Boden, and S. Bischof, Carbon dioxide emissions from fossil fuel consumption and cement manufacture, 1751-1991 and an estimate of their isotopic composition and latitudinal distribution, in *The Carbon Cycle*, edited by T. M. L. Wigley and D. S. Schimel, pp. 53-62, Cambridge University Press, Cambridge, 2000.
- Andronova, N. G., and M. E. Schlesinger, Causes of global temperature changes during the 19th and 20th centuries, *Geophys. Res. Lett.*, 27 2137-2140, 2000.
- Aubinet, M., A. Grelle, A. Ibrom, C. Rannik, J. Moncrieff, T. Foken, A. S. Kowalski, P. H. Martin, P. Berbigier, Ch. Bernhofer, R. Clement, J. Elbers, A. Granier, T. Grunwald, K. Morgenstern, K. Pilegaard, C. Rebmann, W. Snijders, R. Valentini, T. Vesala, Estimates of the Annual Net Carbon and Water Exchange of Forests: the EUROFLUX Methodology, *Adv. Ecol. Research*, 30, 113-175, 2000.
- Bacastow, R. B., Modulation of atmospheric carbon dioxide by the Southern Oscillation, *Nature*, 261, 116-118, 1976.
- Bacastow, R. B., C. D. Keeling, S. C. Piper, and T. P. Whorf, On the double deconvolution of atmospheric CO₂ data, submitted to *Journal Geophys. Research*, 2001.
- Battle, M., M. L. Bender, P. P. Tans, J. W. C. White, J. T. Ellis, T. Conway, and R. J. Francey, Global carbon sinks and their variability inferred from atmospheric O₂ and $\delta^{13}\text{C}$, *Science*, 287, 2467-2470, 2000.
- Bollenbacher, A. F., P. R. Guenther, C. D. Keeling, E. F. Stewart, M. Wahlen, and T. P. Whorf, Calibration methodology for the Scripps $^{13}\text{C}/^{12}\text{C}$ and $^{18}\text{O}/^{16}\text{O}$ stable isotope program, 1992-1996, SIO Reference Series, No. 01-2, Scripps Institution of Oceanography, 2001.
- Climate Prediction Center, Monthly Atmospheric and SST Indices, website: www.cpc.ncep.noaa.gov/data/indices/
- Craig, H., Isotopic standards for carbon and oxygen and correction factors for mass-spectrometric analysis of carbon dioxide, *Geochimica et Cosmochimica Acta*, v. 12, p. 133-149, 1957.
- Crowley, P. J., Causes of climate change over the past 1000 years, *Science*, 289, 270-277, 2000.
- Danckwerts, P. V., *Gas-liquid reactions*, 276 p., McGraw-Hill, New York, 1970.
- Etheridge, D. M., L. P. Steele, R. L. Langenfelds, R. J. Francey, J. M. Barnola, and V. I. Morgan, Natural and anthropogenic changes in atmospheric CO₂ over the last

- 1000 years from air in Antarctic ice and firn, *Journal Geophys. Research - Atmospheres*, 101(D2), 4115-4128, 1996.
- Falkowski, P., R. J. Scholes, E. Boyle, J. Canadell, D. Canfield, J. Elser, N. Gruber, K. Hibbard, P. Hogberg, S. Linder, F. T. Mackenzie, B. Moore, T. Pedersen, Y. Rosenthal, S. Seitzinger, V. Smetacek, and W. Steffen, The global carbon cycle: a test of our knowledge of earth as a system, *Science*, 290, 291-296, 2000.
- Farquhar, G. D., J. R. Ehleringer, and J. A. Berry, Carbon isotope discrimination and photosynthesis, *Annu. Rev. Plant Physiol. Plant Mol. Biol.* 40, 503-537, 1989.
- Francey, R. J., P. P. Tans, C. E. Allison, I. G. Enting, J. W. C. White, and M. Troler, Changes in oceanic and terrestrial carbon uptake since 1982, *Nature*, 373, 326-330, 1995.
- Free, M., and A. Robock, Global warming in the context of the Little Ice Age, *J. Geophys. Res.*, 104, 19,057-19,070, 1999.
- Gruber, N., and C. D. Keeling, An improved estimate of the isotopic air-sea disequilibrium of CO₂: Implications for the oceanic uptake of anthropogenic CO₂. *Geophysical Research Letters*, in press, 2001.
- Guenther, P. R., A. F. Bollenbacher, C. D. Keeling, E. F. Stewart, and M. Wahlen, Calibration methodology for the Scripps ¹³C/¹²C and ¹⁸O/¹⁶O stable isotope program, 1996-2000, SIO Reference Series, No. 01-3, 2001.
- Heimann, M., and C. D. Keeling, A three-dimensional model of atmospheric CO₂ transport based on observed winds: 2. Model description and simulated tracer experiments, in *Aspects of Climate Variability in the Pacific and the Western Americas, Geophysical Monograph*, vol. 55, edited by D. H. Peterson, pp. 237-275, AGU, Washington, D.C., 1989.
- Heimann, M., C. D. Keeling, and C. J. Tucker, A three-dimensional model of atmospheric CO₂ transport based on observed winds 3. Seasonal cycle and synoptic time scale variations, in *Aspects of Climate Variability in the Pacific and the Western Americas*, edited by D. H. Peterson, this volume, American Geophysical Union, Washington, DC, 1989.
- Hollinger, D. Y., P. M. Anthoni, P. Bakwin, D. D. Baldocchi, B. W. Berger, K. Davis, E. Falge, J. D. Fuentes, B. E. Law, X. Lee, T. P. Meyers, J. W. Munger, R. Staebler, A. E. Suyker, M. H. Unsworth, S. B. Verma, S. Wofsy, and C. Yi, AmeriFlux: Results from a network of long-term CO₂ flux measurement sites, submitted to *Science*, 2000.

- Houghton, J. T., L. G. Meira Filho, B. A. Callander, N. Harris, A. Kattenberg, and K. Maskell, eds., *Climate Change 1995, The Science of Climate Change, Contribution of Working Group I to the Second Assessment Report of the Intergovernmental Panel on Climate Change*, 572 pages, Cambridge University Press, Cambridge, 1996.
- Houghton, R. A., The annual net flux of carbon to the atmosphere from changes in land use 1850-1990, *Tellus*, 51B(2), 298-313, 1999.
- Hunt, E. R., S. C. Piper, R. Nemani, C. D. Keeling, R. D. Otto, and S. W. Running, Global net carbon exchange and intra-annual atmospheric CO₂ concentrations predicted by an ecosystem process model and three-dimensional atmospheric transport model, *Global Biogeochemical Cycles*, 10, 431-456, 1996.
- Jones, P. D., Hemispheric surface air temperature variations: a reanalysis and an update to 1993, *J. Climate*, 7, 1794-1802, 1994.
- Joos, F, and M. Bruno, Long-term variability of the terrestrial and oceanic carbon sinks and the budgets of the carbon isotopes C-13 and C-14, *Global Biogeochemical Cycles*, 12, 277-295, 1998.
- Kaminski, T., R. Giering, and M. Heimann, Sensitivity of the seasonal cycle of CO₂ at remote monitoring stations with respect to seasonal surface exchange fluxes determined with the adjoint of an atmospheric transport model, *Phys. Chem. Earth*, 21, 457-462, 1996.
- Karl, D. M., and A. F. Michaels, Tropical Studies in Oceanography, *Deep-Sea Research*, 43, 127-8, 1996].
- Keeling, C. D., The concentration and isotopic abundances of carbon dioxide in rural and marine air, *Geochimica et Cosmochimica Acta*, 24, p. 277-298, 1961.
- Keeling, C. D., R. B. Bacastow, and T. P. Whorf, Measurements of the concentration of carbon dioxide at Mauna Loa Observatory, Hawaii, in *Carbon Dioxide Review: 1982*, edited by W. C. Clark, p. 377-385, Oxford University Press, 1982.
- Keeling, C. D., P. R. Guenther, and D. J. Moss, Scripps reference gas calibration system for carbon dioxide-in-air standards: Revision of 1985. Report No. 4 of the Environmental Monitoring Programme of the World Meteorological Organization, Geneva, 34 p. and Addendum, 43 p., 1986.
- Keeling, C. D., R. B. Bacastow, A. F. Carter, S. C. Piper, T. P. Whorf, M. Heimann, W. G. Mook, and H. Roeloffzen, A three-dimensional model of atmospheric CO₂ transport based on observed winds: 1. Analysis of Observational Data, in *Aspects*

- of Climate Variability in the Pacific and the Western Americas, Geophysical Monograph, vol. 55*, edited by D. H. Peterson, pp. 165-236, AGU, Washington, D. C., 1989a.
- Keeling, C. D., S. C. Piper, and M. Heimann, A three-dimensional model of atmospheric CO₂ transport based on observed winds: 4. Mean annual gradients and interannual variations, in *Aspects of Climate Variability in the Pacific and the Western Americas, Geophysical Monograph, vol. 55*, edited by D. H. Peterson, pp. 305-363, AGU, Washington, D. C., 1989b.
- Keeling, C. D., P. R. Guenther, and T. P. Whorf, An analysis of the concentration of atmospheric carbon dioxide at fixed land stations, and over the oceans based on discrete samples and daily averaged continuous measurements, 451 p., Scripps Institution of Oceanography, La Jolla, CA, 1989c.
- Keeling, C. D., T. P. Whorf, M. Wahlen, and J. Van der Plicht, Interannual extremes in the rate of rise of atmospheric carbon dioxide since 1980. *Nature*, 375, 666-670, 1995.
- Keeling, C. D., S. C. Piper, R. B. Bacastow, M. Wahlen, T. P. Whorf, M. Heimann, and H. A. Meijer, Exchanges of atmospheric CO₂ and ¹³CO₂ with the terrestrial biosphere and oceans from 1978 to 2000. I. Global aspects, SIO Reference Series, No. 01-06 (Revised from SIO Reference Series, No. 00-21), Scripps Institution of Oceanography, San Diego, 2001.
- Keeling, C. D., and S. C. Piper, Exchanges of atmospheric CO₂ and ¹³CO₂ with the terrestrial biosphere and oceans from 1978 to 2000. IV. Critical overview, SIO Reference Series, No. 01-09 (Revised from SIO Reference Series, No. 00-24), Scripps Institution of Oceanography, San Diego, 2001.
- Keeling, R. F., and S. R. Shertz, Seasonal and interannual variations in atmospheric oxygen and implications for the global carbon cycle, *Nature*, 358, 723-727, 1992.
- Lancaster, J., Carbon-13 fractionation in carbon dioxide emitting diurnally from soils and vegetation at ten sites on the north American continent. Ph.D. dissertation, University of California, San Diego, 184 pages, 1990.
- Lloyd, J., and G. D. Farquhar, C-13 discrimination during CO₂ assimilation by the terrestrial biosphere, *Oecologia*, 99, 201-215, 1994.
- Marland, G., T. Boden, R. J. Andres, and C. Johnston, Estimates of Global, Regional, and National Annual CO₂-Emissions from Fossil-Fuel Burning, Hydraulic Cement Production, and Gas Flaring: 1751-1995, (data file "global95.ems" dated 9 January 1998), Carbon Dioxide Information and Analysis Center, NDP-030/R8,

1998.

- Meehl, G. A., The annual cycle and interannual variability in the tropical Pacific and Indian ocean regions, *Monthly Weather Review*, v. 115, p. 27–50, 1987.
- Mook, W. G., J. C. Bommerson, and W. H. Staverman, Carbon isotope fractionation between dissolved bicarbonate and gaseous carbon dioxide, *Earth and Planetary Science Letters*, 22, 169-176, 1974.
- Mook, W. G., and P. M. Grootes, The measuring procedure and corrections for the high-precision mass-spectrometric analysis of isotopic abundance ratios, especially referring to carbon, oxygen and nitrogen, *International Journal of Mass Spectrometry and Ion Physics*, 12, 273-298, 1973.
- Mook, W. G., and S. Van der Hoek, The N₂O correction in the carbon and oxygen isotopic analysis of atmospheric CO₂, *Isotope Geoscience*, v. 1, p. 237–242, 1983.
- Mook, W. G., M. Koopmans, A. F. Carter, and C. D. Keeling, Seasonal, latitudinal, and secular variations in the abundance and isotopic ratios of atmospheric carbon dioxide: 1. Results from land stations, *Journal of Geophysical Research*, v. 88, p. 10915–10933, 1983.
- Needler, G. T., WOCE - The World Ocean Circulation Experiment, *Oceanus*, 35 74-77, 1992.
- Piper, S. C., C. D. Keeling, M. Heimann, and E. F. Stewart, Exchanges of atmospheric CO₂ and ¹³CO₂ with the terrestrial biosphere and oceans from 1978 to 2000. II. A three-dimensional tracer inversion model to deduce regional fluxes, SIO Reference Series, No. 01-07 (Revised from SIO Reference Series, No. 00-22), Scripps Institution of Oceanography, San Diego, 2001a.
- Piper, S. C., C. D. Keeling, and E. F. Stewart, Exchanges of atmospheric CO₂ and ¹³CO₂ with the terrestrial biosphere and oceans from 1978 to 2000. III. Sensitivity tests, SIO Reference Series, No. 01-08 (Revised from SIO Reference Series, No. 00-23), Scripps Institution of Oceanography, San Diego, 2001b.
- Quay, P. D., B. Tilbrook, C. S. Wong, Oceanic uptake of fossil fuel CO₂: carbon-13 evidence, *Science*, 256, 74-79, 1992.
- Rasmusson, E. M., and J. M. Wallace, Meteorological aspects of the El Niño/Southern Oscillation, *Science*, 222, 1195-1202, 1983.
- Reinsch, C. H., Smoothing by spline functions, *Numerische Mathematik*, v. 10, p. 177–183, 1967.

- Santer, B. D. et al., in *Climate Change 1995: The IPCC Second Assessment*, edited by J. T. Houghton et al., Cambridge University Press, 407-444, 1995.
- Schimel, D. et al., Chapter 2, Radiative Forcing of Climate Change, in *Climate Change 1995, The Science of Climate Change, Contribution of Working Group I to the Second Assessment Report of the Intergovernmental Panel on Climate Change*, Cambridge University Press, Cambridge, pp. 64-131, 1996.
- Siegenthaler, U., Uptake of excess CO₂ by an outcrop-diffusion model of the ocean, *Journal of Geophysical Research*, 88 3599-3608, 1983.
- Siegenthaler, U., and K. O. Münnich, ¹³C/¹²C fractionation during CO₂ transfer from air to sea, in *SCOPE 16: Carbon Cycle Modelling*, edited by B. Bolin, p. 249-257, John Wiley and Sons, Chichester, 1981.
- Siegenthaler, U., and H. Oeschger, Biospheric CO₂ sources emissions during the past 200 years reconstructed by deconvolution of ice core data, *Tellus*, 39B, 140-154, 1987.
- Slingo, J. M. and H. Annamalai, 1997: The El Niño of the century and the response of the Indian summer monsoon, *Monthly Weather Review*, 128,, 1178-1797, 2000.
- Wigley, T. M. L., and D. S. Schimel, editors, *The Carbon Cycle*, Cambridge University Press, New York, 292 p., 2000.

Table 1. Air Sampling Locations and Dates of Sampling

Station	Code Name	Lat. (deg.)	Long. (deg.)	Elevation (m)	Inclusive Dates of Fit ^a	
					CO ₂	δ ¹³ C
Alert, N.W.T., Canada	ALT	82.5°N	62.3°W	210	May 6, 1985 to Jan. 20, 2000	May 6, 1985 to Jan. 20, 2000
Point Barrow, Alaska	PTB	71.3°N	156.6°W	11	Feb. 3, 1974 to Feb. 4, 2000	Apr. 8, 1982 to Feb. 4, 2000
La Jolla, California	LJO	32.9°N	117.3°W	10	Feb. 18, 1969 to Mar. 28, 2000 ^b	Apr. 1, 1978 to Feb. 28, 2000
Mauna Loa, Hawaii ^c	MLO	19.5°N	155.6°W	3397	Mar. 29, 1958 to Mar. 25, 2000 ^d	Jun. 30, 1978 to Feb. 11, 2000
Cape Kumukahi, Hawaii	KUM	19.5°N	154.8°W	3	Mar. 27, 1979 to Feb. 1, 2000	Feb. 4, 1980 to Dec. 28, 1999
Christmas Island, Kiribati	CHR	2.0°N	157.3°W	2	Dec. 10, 1974 to Jan. 9, 2000	Aug. 2, 1977 to Jan. 16, 2000 ^e
Cape Matatula, American Samoa	SAM	14.2°S	170.6°W	30	Sep. 4, 1981 to Feb. 14, 2000	Feb. 24, 1984 to Jan. 3, 2000
Raoul Island, Kermadec Islands	KER	29.2°S	177.9°W	2	Dec. 8, 1982 to Jan. 3, 2000	Dec. 13, 1983 to Nov. 11, 1999
Baring Head, New Zealand	NZD	41.4°S	174.9°E	85	Jul. 4, 1977 to Jan. 10, 2000	May 14, 1985 to Nov. 22, 1999
South Pole	SPO	90.0°S	0.0°	2810	Jun. 17, 1957 to Jan. 23, 2000 ^f	Mar. 15, 1977 to Jan. 23, 2000

^a Flask samples unless otherwise noted.

^b Supplementary continuous measurements from 1972-1975.

^c Provided for reference but not used in the global deconvolution or zonal model inversion.

^d For CO₂, continuous measurements only at this site.

^e Supplementary flask measurements from Fanning Island from 1977-1983 included (see Keeling et al., 1989a, Table A.2).

^f Supplementary continuous measurements from 1960-1963.

Table 2. Apparent Isotopic Composition of CO₂ Added or Removed from Atmosphere at Various Stations Averaged from 1992-1999

Station Name	Latitude	$\delta^{13}C_I$ (‰)	Standard Error ^a	$^{13}\Delta_{cov}$ ^b (‰)
Alert, N.W.T. (ALT)	82.5°N	-27.8	0.38	19.9
Point Barrow, Alaska (PTB)	71.2°N	-26.5	0.39	18.6
La Jolla, California (LJO)	32.9°N	-27.8	0.77	19.9
Mauna Loa, Hawaii (MLO)	19.5°N	-26.8	1.09	18.9
Cape Kumukahi, Hawaii (KUM)	19.5°N	-28.2	1.38	20.3
Christmas Island, Kiribati (CHR)	2.0°N	-27.8	7.19	19.9
Cape Matatula, American Samoa (SAM)	14.2°S	-16.2	3.14	8.3
Raoul Island, Kermadec Isl. (KER)	29.2°S	-18.3	2.80	10.4
Baring Head, New Zealand (NZD)	41.4°S	-19.9	3.22	12.0
South Pole (SPO)	90.0°S	-15.7	2.60	7.8
Average for northern hemisphere stations:		-27.5	1.00 ^{c, d}	19.6
Average for southern hemisphere stations:		-17.5	3.41 ^c	9.6

^a Of the mean of annual values of $\delta^{13}C_I$ for 1992-1999.

^b Obtained by subtracting from $\delta^{13}C_I$ the average of $\delta^{13}C$ of atmospheric CO₂ at the South Pole from 1992 through 1999.

^c By quadrature.

^d Excluding Christmas Island.

**Table 3. Global Parameters to Compute Isotopic Source Components
Used in the Deconvolution Calculations**

Symbol	Definition	Value	Note
Constant parameters			
$N_{a\ ref}$	Carbon in atmosphere as CO ₂ , corresponding to a mixing ratio of 290 ppm relative to dry air and to a CO ₂ partial pressure at sea level of 289.04×10^{-6} atm	615.6 PgC	1
N_{ao}	Amount of carbon in atmospheric CO ₂ in January, 1990.	747.6 PgC	2
α_{ab}	¹³ C/ ¹² C fractionation factor for CO ₂ uptake by the terrestrial biosphere	0.9846800	3
α'_{ab}	Corresponding ¹³ C/(¹³ C+ ¹² C) ratio	0.9847397	3
α_{ba}	¹³ C/ ¹² C fractionation factor for CO ₂ release by the terrestrial biosphere	1.0000000	4
α'_{ba}	Corresponding ¹³ C/(¹³ C+ ¹² C) ratio	1.0000000	4
α_{am}	¹³ C/ ¹² C fractionation factor for CO ₂ uptake by the surface ocean water	0.9982000	5
α'_{am}	Corresponding ¹³ C/(¹³ C+ ¹² C) ratio	0.9982198	5
r_s	¹³ C/ ¹² C ratio of isotopic standard PDB	0.0112372	6
Time-dependent parameters			
$\alpha_{eq}(t)$	Equilibrium fractionation factor of gaseous CO ₂ with respect to total dissolved inorganic carbon	variable	7
$\alpha_{ma}(t)$	¹³ C/ ¹² C fractionation factor for CO ₂ evasion from surface ocean water	variable	8
$\langle \bar{\alpha}_{eq}(t) \rangle$	Annual average of $\alpha_{eq}(t)$	variable	9
$\langle \bar{\alpha}'_{eq}(t) \rangle$	Corresponding ¹³ C/(¹³ C+ ¹² C) ratio	variable	10
$\bar{\delta}_a(t)$	$\delta^{13}\text{C}$ of atmospheric CO ₂	variable	11
$\bar{\delta}_b(t)$	$\delta^{13}\text{C}$ of carbon in the long-lived terrestrial biosphere	variable	12
$\bar{\delta}_m(t)$	$\delta^{13}\text{C}$ of dissolved inorganic carbon in surface ocean water	variable	12
$\bar{\delta}_{IND}(t)$	$\delta^{13}\text{C}$ of fossil fuel carbon	variable	13

(1) From Keeling [1973a, p. 301] based on an estimate of the mass of dry air in the atmosphere of 5.119×10^{18} kg [Verniani, 1966]. The corresponding mixing ratio with respect to moist air is 289.04 ppm assuming, as did Verniani, that the average content of water vapor in the atmosphere is 0.33 percent. Hence the corresponding CO₂ partial pressure existed at sea level is 289.04×10^{-6} atmospheres.

(2) Carbon in atmosphere as CO₂, seasonally adjusted, on January, 1990, based on a CO₂ concentration of 352.2 ppm, as shown in Table E.2. The calculation is based on the value of $N_{a\ ref}$, above.

Table 3 (continued)

(3) Based on a calculation where the discrimination by C4 and C3 plants, 3.6 and 17.8‰, respectively, is taken from Lloyd and Farquhar [1994], and the contribution by C4 plants was assumed to be proportional to the global percentage of NPP attributed to C4 plants, 17.4407%, calculated using the vegetation map of Hunt et al. [1996], and the NPP averaged for 1982 to 1990, as described in Article II. The factor α'_{ab} is computed from α_{ab} by the formula [cf. Keeling et al., [1989a, Table 8, footnote (12)]]

$$\alpha'_{ab} = \alpha_{ab}(1 + 0.993r_s)(1 + 0.975r_s) \quad (\text{T3.1})$$

where r_s is as listed in this table.

(4) Zero fractionation is assumed (cf. Keeling et al. [1989a, Table 8, footnote 13]).

(5) From Siegenthaler and Münnich [1981, p. 255] (their symbol α_{as}) based on the surface renewal gas exchange model of Danckwerts [1970]. Their estimate of 0.2‰ for the contribution to α_{am} from the reaction of CO₂ with hydroxide ion is included, but fractionation related to the hydration of CO₂ is not included. The factor α'_{am} is computed from α_{am} by the formula [cf. Keeling et al., [1989a, Table 8, footnote (14)]]

$$\alpha'_{am} = \alpha_{am}(1 + 0.993r_s)(1 + 0.993\alpha_{am}r_s) \quad (\text{T3.2})$$

where r_s is as listed in this table.

(6) Established by Mook and Grootes [1973, p. 296]. Same as $^{13}r_s$ of main text (cf. Equation (1.1)).

(7) Computed by the equation:

$$\alpha_{eq}(t) = 1.02389 - \frac{9.483}{T(t) + T_o} \quad (\text{T3.3})$$

where t denotes time and $T(t)$, temperature, in degrees Celsius. The equation, from Mook et al. [1974, p. 175, Table 4, (with $T_o = 273.15^\circ$)], specifies the temperature dependence of the per mil difference, at equilibrium, between gaseous CO₂ and an aqueous bicarbonate solution assumed to fractionate to the same extent as ocean water (cf. Keeling et al. [1989a, Table 8, footnote 14]).

(8) Equal to $\alpha_{am} \cdot \alpha_{eq}(t)$. Not used directly in the calculations, nor is $\alpha'_{ma}(t)$.

(9) Set equal to 0.991351 in the deconvolution for all years prior to 1856, assuming a constant global average temperature of 19.129°C. Thereafter, a spline fit to global average area-weighted gridded temperature anomaly data (plotted in Figure E.1) specifies a variable temperature based on departures from that starting value, in turn used to compute $\langle \alpha_{eq}(t) \rangle$. A different constant value, 0.990983, is used in Article II (see subsection A.3 therein).

(10) Computed by the formula [cf. Keeling et al., 1989a, Table 8, footnote (15)],

$$\langle \bar{\alpha}'_{eq}(t) \rangle = \langle \bar{\alpha}_{eq}(t) \rangle (1 + 0.993r_s) / \langle \bar{\alpha}_{eq}(t) \rangle (1 + 0.993r_s) \quad (\text{T3.4})$$

(11) Based on observations, as plotted in Figure 6b (but without removing a linear trend).

(12) Determined by the double deconvolution.

(13) From Andres et al. [1996c, 2000], as described in Article II, subsection A.2.

**Table 4. Reduced Isotopic Ratios, in per mil,
Used in the Zonal Inversion Model^a**

Date	$\bar{\delta}_{IND}(t)$	$\bar{\delta}_a(t)$	$\bar{\delta}_b(t)$	$\bar{\delta}_m(t)$
1978	-28.17	-7.4924	-22.2364	1.7468
1979	-28.19	-7.5143	-22.2483	1.7343
1980	-28.20	-7.5689	-22.2620	1.7189
1981	-28.24	-7.5759	-22.2763	1.7007
1982	-28.21	-7.5777	-22.2904	1.6880
1983	-28.20	-7.6383	-22.3047	1.6745
1984	-28.28	-7.6688	-22.3203	1.6547
1985	-28.24	-7.6450	-22.3358	1.6392
1986	-28.19	-7.6400	-22.3505	1.6278
1987	-28.30	-7.6926	-22.3653	1.6166
1988	-28.31	-7.7722	-22.3815	1.5979
1989	-28.34	-7.8025	-22.3988	1.5755
1990	-28.43	-7.8024	-22.4162	1.5607
1991	-28.46	-7.7940	-22.4332	1.5476
1992	-28.43	-7.8048	-22.4500	1.5328
1993	-28.43	-7.7988	-22.4665	1.5210
1994	-28.43	-7.8335	-22.4829	1.5086
1995	-28.43	-7.8715	-22.5001	1.4942
1996	-28.43	-7.9015	-22.5177	1.4769
1997	-28.43	-7.9204	-22.5356	1.4625
1998	-28.43	-7.9898	-22.5542	1.4470
1999	-28.43	-8.0187	-22.5723	1.4236

^a Subscripts: *IND*, industrial emissions; *a*, atmosphere; *b*, terrestrial biosphere; *m*, mixed layer of oceans. See Table 3.

Table 5. Zonal Average NPP, in PgC yr⁻¹, for C3 and C4 Plants^a

Plant Type:	C3+C4	C3	C4	C4 Percentage
47-90N	11.6	11.6	0.0	0
23.5-47N	11.7	10.6	1.0	9
23.5S-23.5N	32.8	24.0	8.8	27
23.5-47S	5.2	4.3	0.9	17
47-90S	0.1	0.1	0.0	0
Global ^b	61.3	50.6	10.7	17.4

^a Based on a map of biomes [Hunt et al., 1996] and on Pathfinder NDVI data averaged for 1982-1990 (see text). Final column shows percentage of combined C3 and C4 plants.

^b Sum of zonal values do not all add to the global totals owing to rounding errors.

Table 6. Average Isotopic Discrimination in per mil, Associated with Photosynthesis of C3 and C4 Plants Combined, for Zonal Biospheric Sources^a

Zone	Discrimination
47-90°N	17.80
23.5-47°N	16.55
23.5S-23.5°N	14.00
23.5-47°S	15.35
Global	15.32

^a Determined using proportions of NPP derived from C3 and C4 plants in each zone, shown in Table 5. Separate discriminations, $\Delta C4 = 3.6\text{‰}$, $\Delta C3 = 17.8\text{‰}$, are from Lloyd and Farquhar [1994].

Table 7. Global Net Carbon Dioxide Fluxes, in PgC yr⁻¹, Obtained by Double Deconvolution Compared with Fluxes of IPCC Reports^a

Period covered:	1980-1989		1990-1999	
	IPCC	Present Analysis	IPCC	Present Analysis
Atmosphere increase	+3.3 ± 0.2	+3.3	3.2 ± 0.2	+3.3
Emissions from fossil fuel combustion and cement production	+5.5 ± 0.5	+5.44 ^b	6.4 ± 0.8	+6.41 ^b
Net oceanic uptake	-2.0 ± 0.8	-2.0 ^c	1.7 ± 0.5	-2.4 ^c
Net emissions from changes in tropical land-use	+1.6 ± 1.0		insufficient data	
Uptake by Northern Hemisphere forest regrowth	-0.5 ± 0.5		"	
Other terrestrial sinks ^d	-1.3 ± 1.5		"	
Combined terrestrial biospheric flux	-0.2 ± 1.9 ^e	-0.2	-1.4 ± 1.4	-0.8

^a Fluxes are positive into the atmosphere. Fluxes reported by IPCC [1996, 2001] have errors quoted here at 90% confidence ($\pm 2\sigma$). Those for 1990-1999 are doubled from 67% confidence levels quoted by IPCC [2001].

^b The average for 1980-1989 is based on Marland et al. [1998]. The average for 1990-1999 is based on the last 6 annual values (1990-1995) of Marland et al. [1998], on a 1996 value from T. Boden (personal communication), and on 1997-1999 values calculated assuming a 2.5% annual growth rate.

^c Evaluated as the sum, F_{oce} , of the perturbation flux, F_{ex} , and the anomalous flux, $F_{ano, oce}$ (cf. equation (4.2) of the text).

^d In accord with the 1995 IPCC report, "other terrestrial sinks" may include enhanced forest growth due to CO₂ fertilization (0.5 – 2.0 PgC/yr), nitrogen deposition (0.2 – 1.0 PgC/yr), and response to climatic anomalies (0 – 1.0 PgC/yr).

^e The uncertainty was determined by adding the uncertainties of its components in quadrature. When computed from the difference between the sum of the oceanic and biospheric fluxes and the oceanic flux (see subsection 7.3), the uncertainty reduces to 0.9 PgC yr⁻¹ (see subsection 7.3 of text).

Table D.1. Global Average Concentration of Atmospheric CO₂, in ppm

MONTH	YEAR											
	1953	1954	1955	1956	1957	1958	1959	1960	1961	1962	1963	1964
Monthly Values of Direct Measurements, Seasonally Adjusted ^a												
Jan.	312.58	312.97	313.40	313.80	314.01	314.58	315.33	316.17	316.78	317.61	318.23	318.76
Feb.	312.61	313.01	313.44	313.83	314.02	314.65	315.39	316.25	316.84	317.65	318.30	318.80
March	312.64	313.04	313.48	313.86	314.04	314.72	315.45	316.33	316.90	317.69	318.36	318.84
April	312.67	313.08	313.52	313.89	314.07	314.80	315.50	316.41	316.96	317.73	318.41	318.87
May	312.70	313.11	313.55	313.91	314.10	314.87	315.56	316.47	317.04	317.77	318.46	318.91
June	312.73	313.15	313.59	313.93	314.14	314.93	315.63	316.53	317.12	317.81	318.51	318.94
July	312.77	313.18	313.62	313.95	314.19	315.00	315.69	316.57	317.19	317.85	318.54	318.96
Aug.	312.80	313.22	313.65	313.96	314.25	315.06	315.76	316.61	317.27	317.90	318.58	318.99
Sept.	312.83	313.26	313.69	313.97	314.30	315.11	315.84	316.64	317.35	317.96	318.61	319.01
Oct.	312.87	313.29	313.72	313.98	314.37	315.17	315.92	316.67	317.43	318.03	318.65	319.03
Nov.	312.90	313.33	313.75	313.99	314.43	315.22	316.00	316.70	317.49	318.10	318.68	319.05
Dec.	312.94	313.37	313.77	314.00	314.50	315.28	316.08	316.74	317.56	318.16	318.72	319.08
	1965	1966	1967	1968	1969	1970	1971	1972	1973	1974	1975	1976
Jan.	319.11	320.30	321.28	321.89	322.96	324.32	325.25	325.93	327.50	329.04	329.59	330.75
Feb.	319.15	320.43	321.33	321.96	323.09	324.41	325.29	326.00	327.68	329.06	329.68	330.82
March	319.20	320.55	321.37	322.02	323.22	324.49	325.33	326.08	327.87	329.07	329.78	330.89
April	319.26	320.66	321.41	322.08	323.36	324.58	325.37	326.18	328.06	329.09	329.87	330.95
May	319.33	320.76	321.45	322.15	323.49	324.67	325.42	326.28	328.24	329.10	329.96	331.02
June	319.42	320.84	321.49	322.22	323.61	324.76	325.48	326.40	328.42	329.13	330.06	331.09
July	319.52	320.92	321.54	322.30	323.74	324.85	325.54	326.52	328.58	329.16	330.16	331.17
Aug.	319.64	320.99	321.59	322.39	323.85	324.93	325.60	326.67	328.71	329.21	330.26	331.26
Sept.	319.76	321.06	321.65	322.49	323.96	325.01	325.66	326.82	328.82	329.27	330.37	331.37
Oct.	319.89	321.12	321.71	322.60	324.06	325.09	325.73	326.98	328.91	329.34	330.47	331.48
Nov.	320.03	321.18	321.77	322.71	324.15	325.15	325.79	327.15	328.97	329.42	330.57	331.61
Dec.	320.16	321.23	321.83	322.83	324.24	325.20	325.86	327.32	329.01	329.50	330.67	331.74
	1977	1978	1979	1980	1981	1982	1983	1984	1985	1986	1987	1988
Jan.	331.87	333.70	335.14	336.82	338.48	339.56	340.70	342.64	343.91	345.24	346.68	348.95
Feb.	332.02	333.83	335.25	336.98	338.58	339.65	340.86	342.76	344.02	345.36	346.82	349.15
March	332.16	333.96	335.37	337.13	338.68	339.74	341.03	342.88	344.13	345.48	346.98	349.36
April	332.32	334.09	335.50	337.29	338.77	339.83	341.21	343.00	344.25	345.61	347.15	349.56
May	332.48	334.21	335.64	337.44	338.85	339.92	341.40	343.11	344.36	345.73	347.33	349.75
June	332.64	334.34	335.78	337.60	338.94	340.00	341.58	343.21	344.47	345.85	347.52	349.94
July	332.80	334.46	335.92	337.74	339.02	340.08	341.76	343.31	344.58	345.97	347.71	350.12
Aug.	332.96	334.58	336.07	337.89	339.10	340.16	341.92	343.41	344.69	346.09	347.92	350.29
Sept.	333.12	334.69	336.22	338.02	339.19	340.24	342.08	343.51	344.80	346.20	348.12	350.46
Oct.	333.27	334.81	336.37	338.15	339.28	340.34	342.23	343.60	344.90	346.32	348.33	350.61
Nov.	333.42	334.92	336.52	338.27	339.37	340.44	342.37	343.70	345.01	346.43	348.54	350.76
Dec.	333.57	335.03	336.67	338.38	339.46	340.56	342.51	343.81	345.12	346.55	348.74	350.89
	1989	1990	1991	1992	1993	1994	1995	1996	1997	1998	1999	2000
Jan.	351.02	352.23	353.69	354.74	355.52	356.77	358.66	360.61	361.91	363.66	366.42	367.58
Feb.	351.14	352.35	353.81	354.82	355.57	356.92	358.81	360.77	361.98	363.91	366.55	–
March	351.25	352.46	353.92	354.90	355.64	357.07	358.97	360.91	362.06	364.17	366.66	–
April	351.35	352.58	354.03	354.98	355.71	357.23	359.12	361.05	362.14	364.43	366.75	–
May	351.45	352.70	354.13	355.05	355.79	357.38	359.28	361.18	362.24	364.69	366.84	–
June	351.54	352.82	354.22	355.13	355.88	357.54	359.43	361.30	362.35	364.95	366.91	–
July	351.63	352.95	354.30	355.20	355.98	357.69	359.60	361.40	362.48	365.21	366.99	–
Aug.	351.72	353.07	354.38	355.26	356.10	357.86	359.76	361.50	362.63	365.45	367.07	–
Sept.	351.82	353.20	354.45	355.32	356.22	358.02	359.93	361.60	362.80	365.68	367.16	–
Oct.	351.92	353.32	354.53	355.37	356.34	358.18	360.11	361.68	362.99	365.90	367.26	–
Nov.	352.02	353.45	354.60	355.42	356.48	358.34	360.28	361.76	363.19	366.10	367.36	–
Dec.	352.12	353.57	354.67	355.47	356.62	358.50	360.45	361.84	363.42	366.27	367.47	–

^a Derived from the average of spline fits of each of 9 stations, described in text.

Table D.2. Globally Averaged Isotopic Ratio, $\delta^{13}\text{C}$, of Atmospheric CO_2 since 1978, in ‰

MONTH	YEAR											
	1977	1978	1979	1980	1981	1982	1983	1984	1985	1986	1987	1988
Monthly Values of Direct Measurements, Seasonally Adjusted ^a												
Jan.	–	–	–7.497	–7.544	–7.581	–7.569	–7.598	–7.674	–7.652	–7.638	–7.654	–7.735
Feb.	–	–7.492	–7.499	–7.551	–7.581	–7.569	–7.604	–7.678	–7.650	–7.636	–7.659	–7.742
March	–	–7.490	–7.500	–7.557	–7.580	–7.569	–7.611	–7.679	–7.648	–7.635	–7.665	–7.749
April	–	–7.489	–7.502	–7.562	–7.580	–7.569	–7.618	–7.680	–7.648	–7.635	–7.671	–7.756
May	–	–7.489	–7.504	–7.567	–7.579	–7.570	–7.625	–7.679	–7.647	–7.635	–7.677	–7.763
June	–	–7.489	–7.506	–7.570	–7.578	–7.572	–7.632	–7.676	–7.646	–7.635	–7.685	–7.770
July	–	–7.489	–7.510	–7.573	–7.577	–7.574	–7.640	–7.673	–7.646	–7.636	–7.692	–7.776
Aug.	–	–7.490	–7.514	–7.576	–7.575	–7.577	–7.647	–7.668	–7.645	–7.638	–7.699	–7.781
Sept.	–	–7.492	–7.518	–7.577	–7.574	–7.580	–7.653	–7.664	–7.644	–7.640	–7.706	–7.786
Oct.	–	–7.493	–7.524	–7.579	–7.573	–7.584	–7.660	–7.660	–7.642	–7.643	–7.713	–7.790
Nov.	–	–7.495	–7.530	–7.580	–7.571	–7.588	–7.665	–7.657	–7.641	–7.646	–7.720	–7.794
Dec.	–	–7.496	–7.537	–7.580	–7.570	–7.593	–7.670	–7.654	–7.639	–7.649	–7.728	–7.797
	1989	1990	1991	1992	1993	1994	1995	1996	1997	1998	1999	2000
Jan.	–7.799	–7.804	–7.794	–7.801	–7.800	–7.809	–7.855	–7.888	–7.908	–7.948	–8.022	–
Feb.	–7.801	–7.804	–7.793	–7.803	–7.798	–7.813	–7.858	–7.891	–7.908	–7.955	–8.023	–
March	–7.802	–7.805	–7.791	–7.805	–7.797	–7.818	–7.861	–7.894	–7.909	–7.963	–8.023	–
April	–7.803	–7.806	–7.791	–7.806	–7.796	–7.822	–7.863	–7.897	–7.909	–7.971	–8.023	–
May	–7.803	–7.806	–7.791	–7.807	–7.795	–7.826	–7.866	–7.899	–7.910	–7.978	–8.022	–
June	–7.803	–7.806	–7.791	–7.808	–7.794	–7.830	–7.869	–7.902	–7.912	–7.986	–8.021	–
July	–7.803	–7.805	–7.792	–7.808	–7.795	–7.834	–7.871	–7.904	–7.915	–7.993	–8.019	–
Aug.	–7.803	–7.804	–7.793	–7.807	–7.796	–7.838	–7.874	–7.906	–7.919	–8.000	–8.017	–
Sept.	–7.803	–7.802	–7.794	–7.806	–7.797	–7.842	–7.877	–7.907	–7.923	–8.006	–8.016	–
Oct.	–7.803	–7.801	–7.796	–7.805	–7.799	–7.846	–7.880	–7.908	–7.928	–8.011	–8.014	–
Nov.	–7.803	–7.798	–7.797	–7.804	–7.802	–7.849	–7.882	–7.908	–7.934	–8.016	–8.013	–
Dec.	–7.803	–7.796	–7.799	–7.802	–7.806	–7.852	–7.885	–7.908	–7.941	–8.019	–8.012	–

^a Derived from the average of spline fits of each of 9 stations, described in text.

Table D.3. Annual Numbers of Observations of Atmospheric CO₂ Concentration, and Standard Errors of Spline Fits to Observations

Station	Standard Error of Fit ^a (ppm)	Year												
		1977	1978	1979	1980	1981	1982	1983	1984	1985	1986	1987	1988	1989
ALT	0.9716	—	—	—	—	—	—	—	—	17	32	38	29	25
PTB	1.1112	17	8	19	20	33	47	41	40	45	30	33	44	30
LJO	0.8161	6	6	6	5	9	10	19	36	33	26	38	40	43
MLO	0.3598	53	52	52	52	52	52	53	48	51	52	52	53	52
KUM	0.7818	—	—	8	17	24	41	46	46	48	48	49	41	44
CHR	0.4333	24	19	18	8	15	7	9	29	34	33	31	36	39
SAM	0.5201	—	—	—	—	15	41	31	38	28	16	48	47	46
KER	0.3136	—	—	—	—	—	3	7	8	8	5	8	10	11
NZD	0.4305	30	20	22	14	28	31	30	22	33	31	30	30	35
SPO	0.1469	27	22	24	18	23	22	21	20	25	26	24	25	23
		1990	1991	1992	1993	1994	1995	1996	1997	1998	1999			
ALT		41	44	47	42	47	48	40	41	32	41			
PTB		29	42	44	44	43	32	30	35	34	34			
LJO		42	30	39	41	42	33	33	41	33	34			
MLO		52	52	52	52	53	52	52	52	52	52			
KUM		39	45	42	45	42	43	41	34	41	40			
CHR		17	26	26	27	22	17	16	18	21	27			
SAM		48	50	50	44	41	34	41	39	44	44			
KER		12	11	12	10	14	3	9	9	4	10			
NZD		33	31	39	43	24	41	41	40	30	6			
SPO		24	20	24	24	24	24	24	24	24	18			

^a Annual variances used as weights in the regional inverse calculation (see Article II, Appendix B) are obtained by squaring the standard error of fit and dividing by the number of observations for each year listed.

Table D.4. Annual Numbers of Observations of Atmospheric Reduced Isotopic Ratio, $\delta^{13}\text{C}$, and Standard Errors of Spline Fits to Observations

Station	Standard Error of Fit ^a (ppm)	Year												
		1977	1978	1979	1980	1981	1982	1983	1984	1985	1986	1987	1988	1989
ALT	0.0651	—	—	—	—	—	—	—	—	16	31	37	21	25
PTB	0.0693	—	—	—	—	—	29	38	28	44	25	32	29	22
LJO	0.0517	—	5	5	4	9	9	12	23	21	14	20	20	16
MLO	0.0474	—	—	—	16	18	32	39	35	40	49	47	44	40
KUM	0.0573	—	—	—	16	23	29	42	42	45	46	45	33	37
CHR	0.0438	9	14	20	16	17	14	23	25	36	33	32	29	26
SAM	0.0363	—	—	—	—	—	—	—	28	30	24	46	39	35
KER	0.0336	—	—	—	—	—	—	—	8	9	11	10	12	12
NZD	0.0386	—	—	—	—	—	—	—	—	5	6	17	15	9
SPO	0.0235	7	14	15	15	21	21	20	14	19	26	22	22	16
		1990	1991	1992	1993	1994	1995	1996	1997	1998	1999			
ALT		39	42	47	44	48	49	39	37	32	41			
PTB		23	35	43	41	39	34	28	32	31	31			
LJO		25	22	33	24	26	23	24	29	28	29			
MLO		27	40	49	49	48	42	44	42	53	50			
KUM		34	43	41	45	41	42	40	32	38	43			
CHR		20	35	33	36	28	22	23	25	28	46			
SAM		44	47	49	44	40	33	37	37	44	45			
KER		11	10	12	13	15	1	12	10	7	10			
NZD		13	16	18	21	14	15	15	7	12	10			
SPO		19	18	24	24	23	23	23	25	24	23			

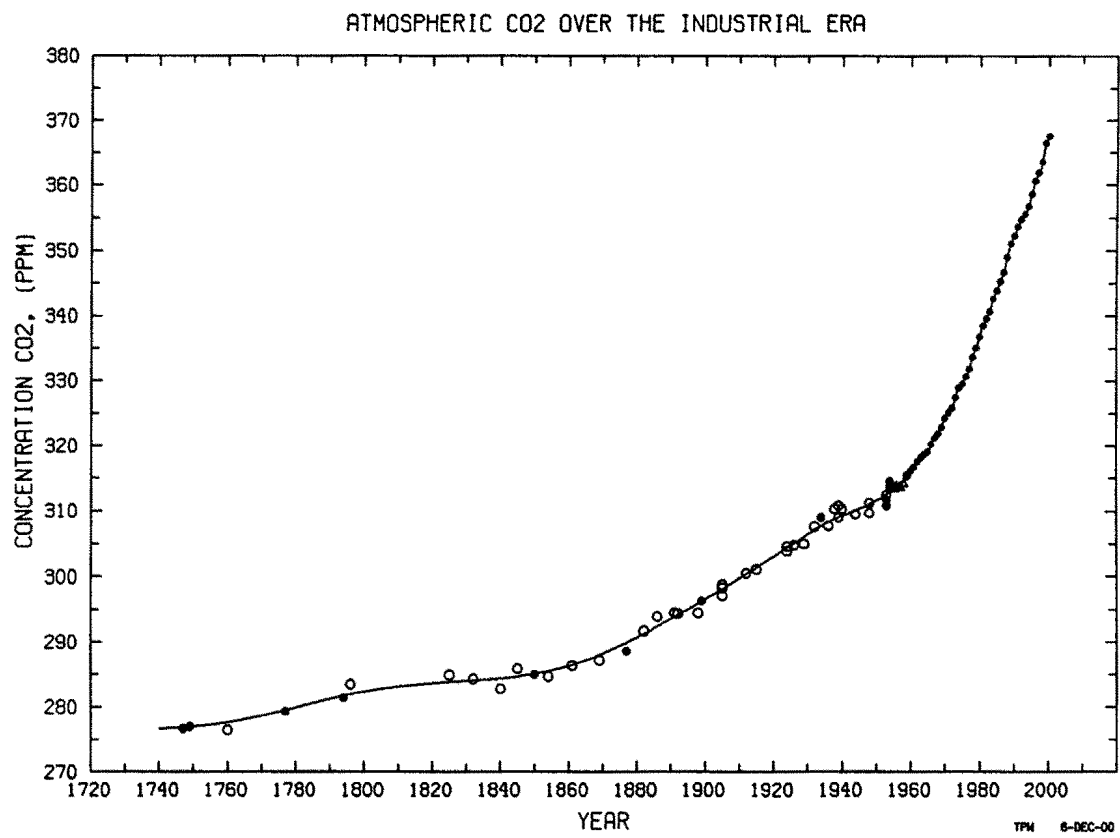
^a Annual variances used as weights in the regional inverse calculation (see Article II, Appendix B) are obtained by squaring the standard error of fit and dividing by the number of observations for each year listed.

Table E.1. Annual Production and Isotopic Ratio, $\delta^{13}\text{C}$, of CO_2 from Fossil Fuel Combustion and Cement Manufacture

Decade	Year of Decade:									
	(0)	(1)	(2)	(3)	(4)	(5)	(6)	(7)	(8)	(9)
<u>Carbon Production (in $\text{kgC} \times 10^9$)</u>										
1860	91.29	98.62	98.47	105.88	115.09	121.89	128.76	137.79	136.91	141.79
1870	145.22	161.90	176.10	188.44	184.05	189.21	191.77	196.12	196.75	207.82
1880	227.36	244.71	262.84	280.24	282.39	276.71	279.13	298.17	322.31	329.19
1890	350.32	366.03	369.29	362.64	377.88	399.41	412.69	432.39	455.88	498.16
1900	526.27	541.49	554.89	607.42	615.69	648.11	698.57	772.30	739.89	771.22
1910	807.30	824.69	869.90	931.26	842.90	834.50	898.64	950.06	934.87	837.02
1920	961.50	836.78	897.64	1012.85	1007.76	1014.64	1016.64	1106.40	1103.91	1182.78
1930	1090.73	980.01	886.81	932.10	1010.20	1047.86	1163.26	1243.69	1181.76	1252.35
1940	1321.57	1357.88	1355.86	1387.32	1375.99	1232.39	1299.68	1454.23	1552.04	1505.94
1950	1637.61	1774.35	1803.78	1847.00	1872.31	2049.16	2185.28	2277.57	2338.56	2471.04
1960	2585.17	2602.81	2707.72	2855.18	3015.64	3154.54	3313.26	3420.60	3595.60	3809.80
1970	4083.00	4235.20	4404.10	4639.70	4648.50	4624.10	4887.70	5026.90	5079.10	5355.10
1980	5276.60	5105.90	5066.90	5059.20	5225.20	5402.60	5589.00	5719.30	5940.10	6047.90
1990	6104.00	6180.70	6095.40	6072.50	6221.00	6407.30	6518.70	6680.60 ^a	6848.60	7018.19
<u>$\delta^{13}\text{C}$ (in ‰)</u>										
1860	-24.10	-24.10	-24.11	-24.11	-24.10	-24.11	-24.11	-24.11	-24.11	-24.11
1870	-24.11	-24.11	-24.11	-24.12	-24.12	-24.11	-24.12	-24.12	-24.12	-24.13
1880	-24.13	-24.15	-24.16	-24.16	-24.17	-24.19	-24.21	-24.23	-24.23	-24.25
1890	-24.27	-24.27	-24.28	-24.29	-24.28	-24.29	-24.30	-24.31	-24.31	-24.31
1900	-24.31	-24.33	-24.34	-24.34	-24.35	-24.36	-24.35	-24.35	-24.37	-24.39
1910	-24.40	-24.40	-24.41	-24.40	-24.44	-24.47	-24.49	-24.50	-24.48	-24.55
1920	-24.55	-24.59	-24.62	-24.67	-24.72	-24.75	-24.79	-24.81	-24.87	-24.94
1930	-24.96	-25.03	-25.07	-25.06	-25.08	-25.09	-25.10	-25.15	-25.17	-25.17
1940	-25.17	-25.16	-25.20	-25.30	-25.43	-25.71	-25.71	-25.69	-25.78	-25.90
1950	-25.86	-26.00	-26.11	-26.16	-26.21	-26.24	-26.29	-26.37	-26.42	-26.51
1960	-26.61	-26.79	-26.91	-27.00	-27.12	-27.23	-27.35	-27.55	-27.70	-27.85
1970	-27.89	-28.01	-28.07	-28.13	-28.16	-28.12	-28.16	-28.09	-28.17	-28.19
1980	-28.20	-28.24	-28.21	-28.20	-28.28	-28.24	-28.19	-28.30	-28.31	-28.34
1990	-28.43	-28.46	-28.43	-28.43 ^b	-28.43	-28.43	-28.43	-28.43	-28.43	-28.43

^a Assumed an annual growth rate of 2.5 percent after 1996.^b Assumed constant after 1992.

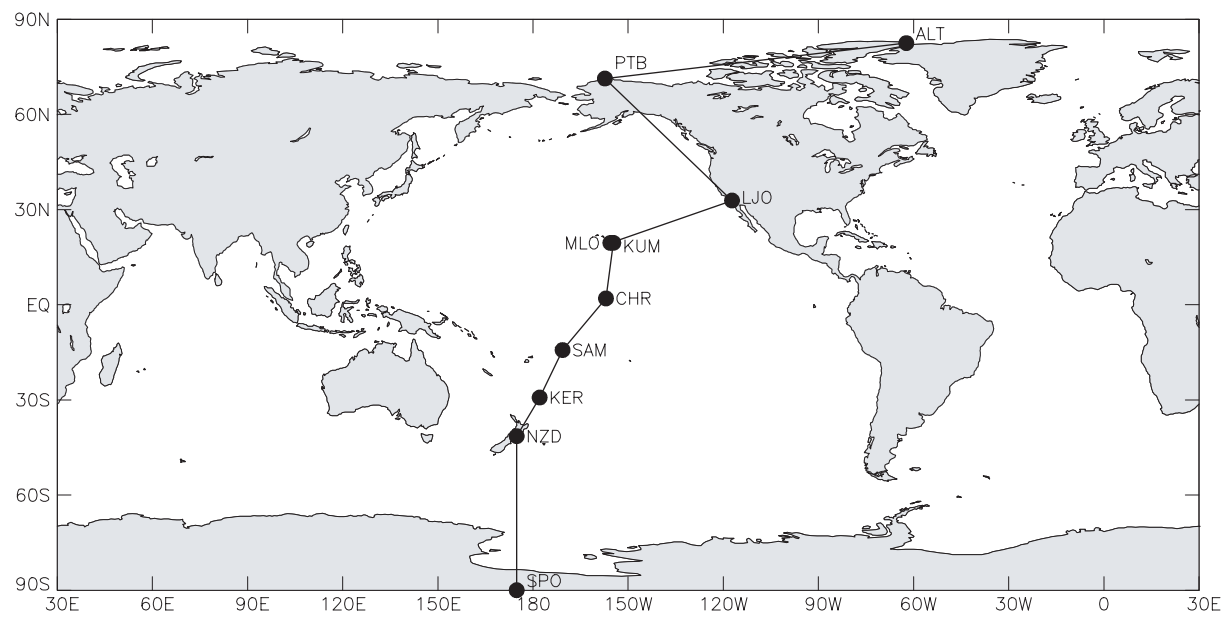
Figure 1. Time trend in the concentration of atmospheric CO₂, in ppm, from A. D. 1740 to 2000. As discussed in Appendix D, data before 1955 are proxies from measurements in air extracted from ice cores at Law Dome, Antarctica (open circles, Francey et al., 1995; closed circles, Etheridge et al., 1996). Data from mid-1955 to the beginning of 1958 are derived from measurements in western United States (open triangles) and from 1957 to 1978 are averages of measurements from the South Pole and Mauna Loa Observatory. Data from 1978 on are averages of direct measurements of air collected from 6 to 9 locations (dots). The curve is a spline function which combines separate fits to the proxy and direct data as described by Keeling et al. [1989a, page 196].



I, Fig. 1

Figure 2. Locations of carbon dioxide sampling stations that furnish data for this study. Station symbols: ALT=Alert; PTB=Point Barrow; LJO= La Jolla; KUM=Cape Kumukahi; MLO=Mauna Loa Observatory; CHR=Christmas Island; SAM=Samoa; KER=Kermadec; NZD=New Zealand; SPO=South Pole. Further information is listed in Table 1. A transect connecting the stations is shown.

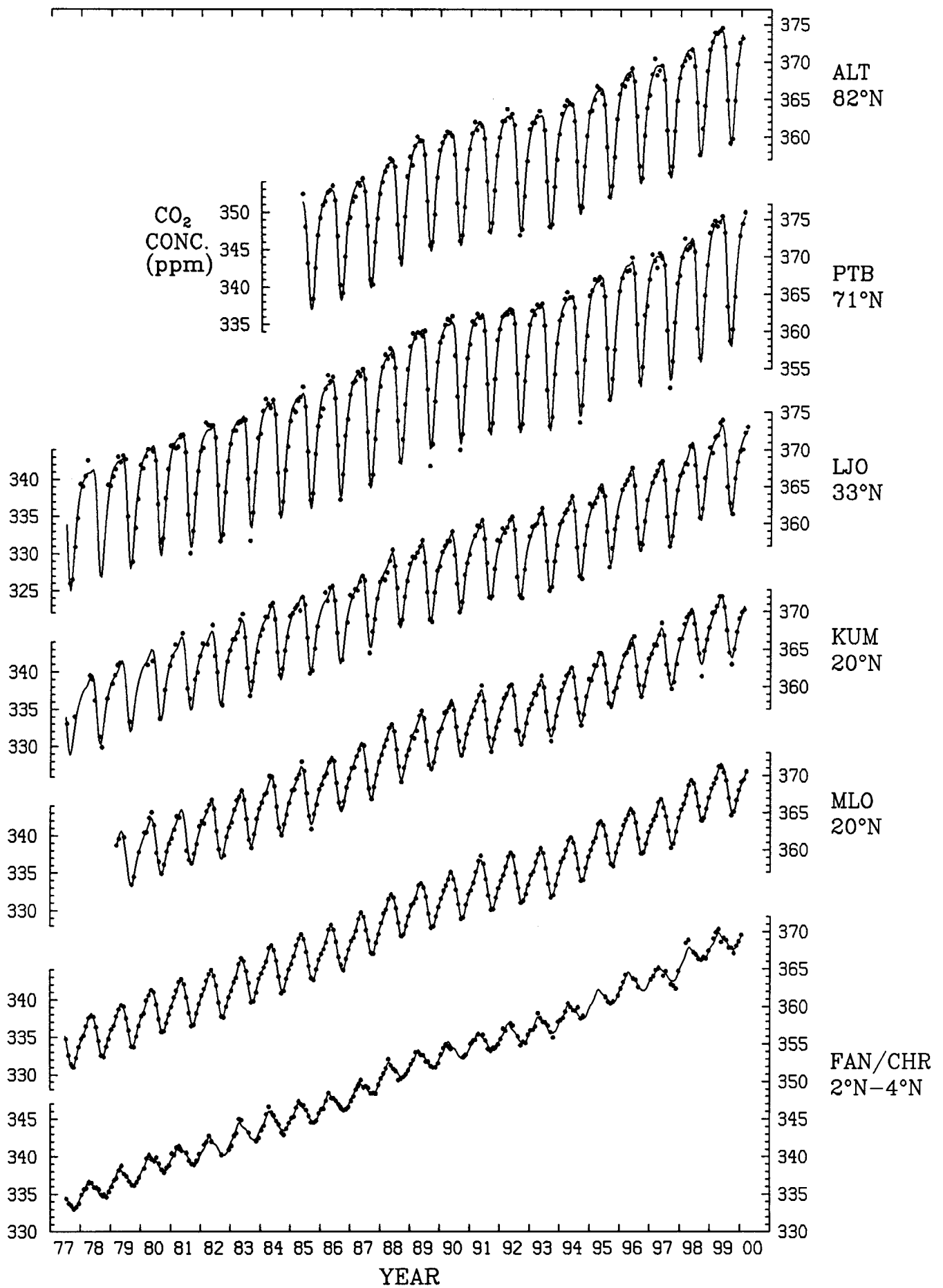
Station Array for Atmospheric CO₂



I, Fig. 2

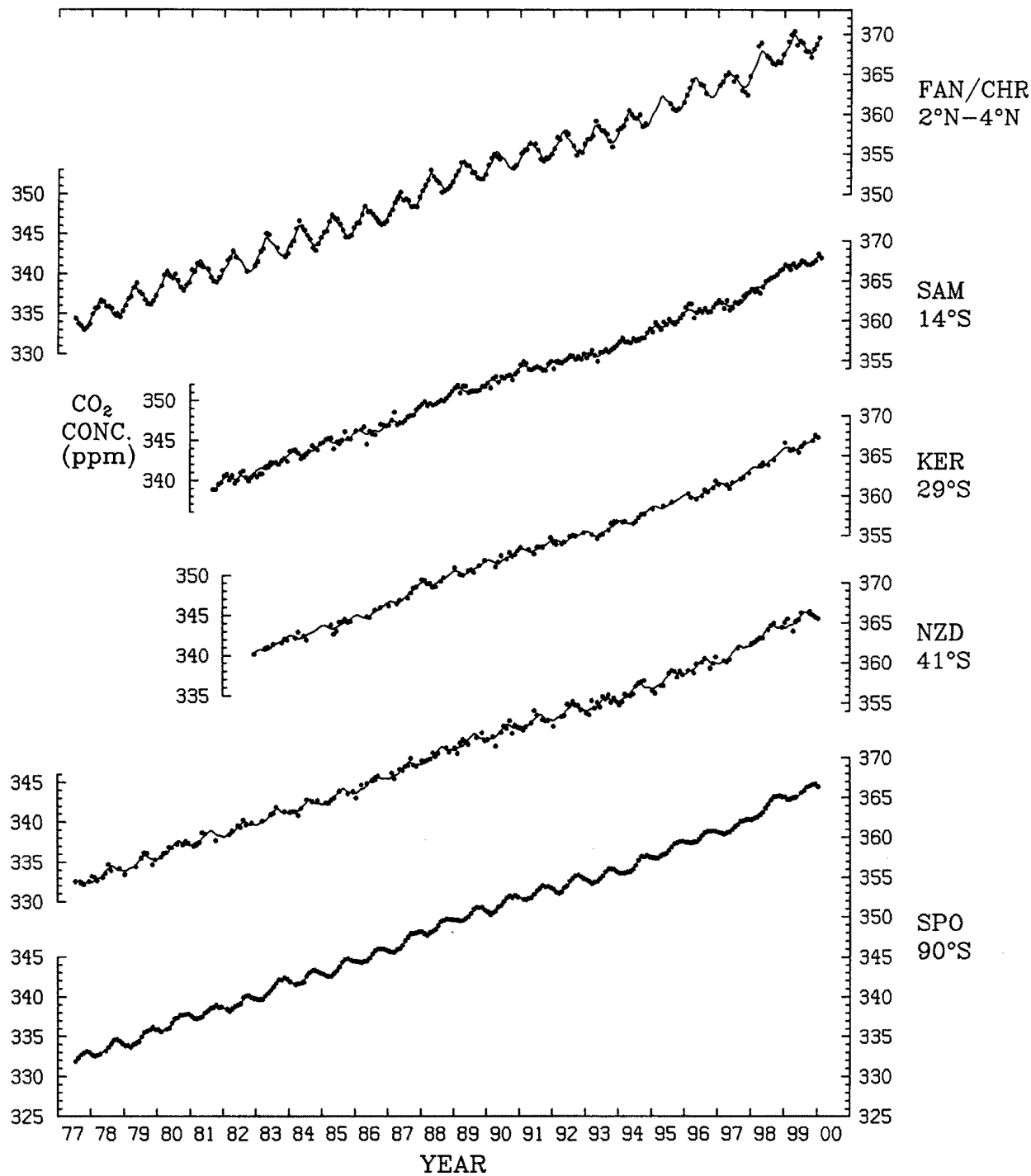
Figure 3. Trends in the measured atmospheric CO₂ concentration and its reduced isotopic ratio, $\delta^{13}\text{C}$. **Panels a and b:** Concentration, in ppm, in the northern and southern hemisphere, respectively, shown by monthly averages (dots) and by a smooth curve consisting of the sum of 4 seasonal harmonics and a spline function (solid lines, see text). The seasonal harmonics include a linear gain factor, to represent increasing amplitude with time. **Panels c and d:** Same, respectively, for reduced isotopic ratio, $\delta^{13}\text{C}$, in ‰. Seasonally adjusted data of concentration and $\delta^{13}\text{C}$ for individual days are plotted in Article IV, Figure 2. Station code names are as defined in Figure 2. FAN/CHR refers to data for Fanning and Christmas Islands, combined (see Table 1, footnote e). The scale of $\delta^{13}\text{C}$ is inverted so that seasonal patterns of concentration and $\delta^{13}\text{C}$ appear with the same phasing.

CO2 CONCENTRATION TRENDS-NORTHERN HEMISPHERE



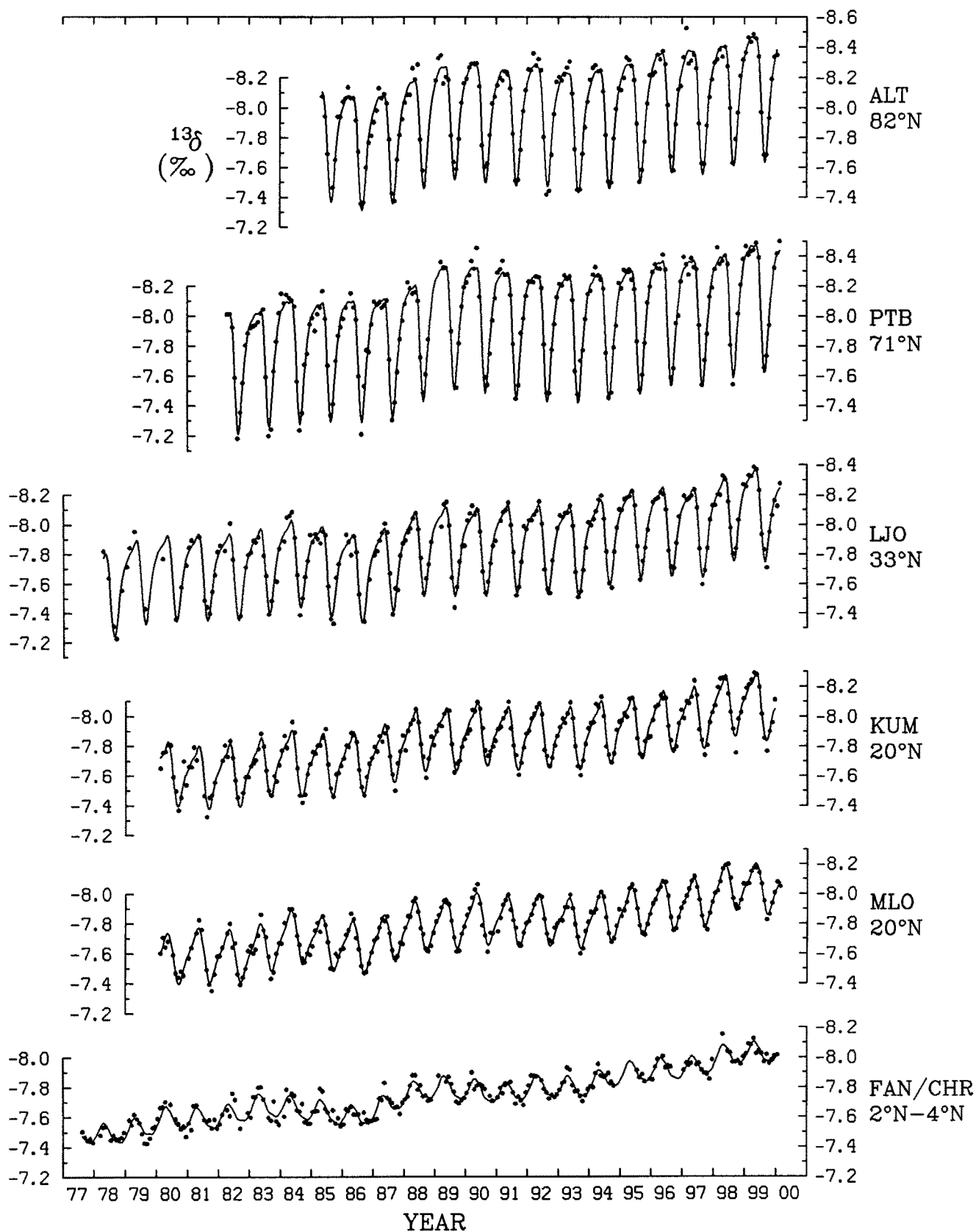
I, Fig. 3a

CO2 CONCENTRATION TRENDS-SOUTHERN HEMISPHERE



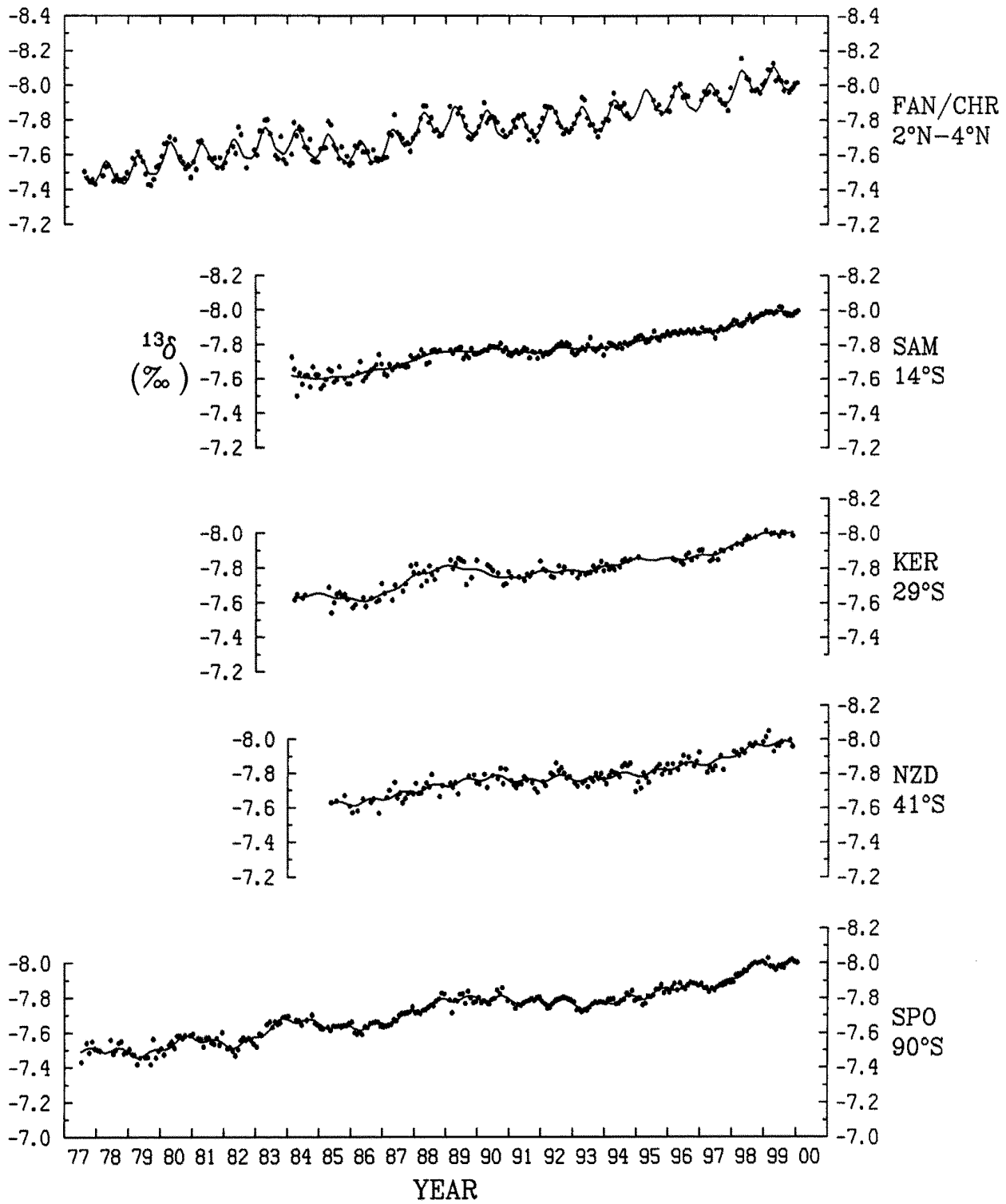
I, Fig. 3b

CO2 ISOTOPIC TRENDS-NORTHERN HEMISPHERE



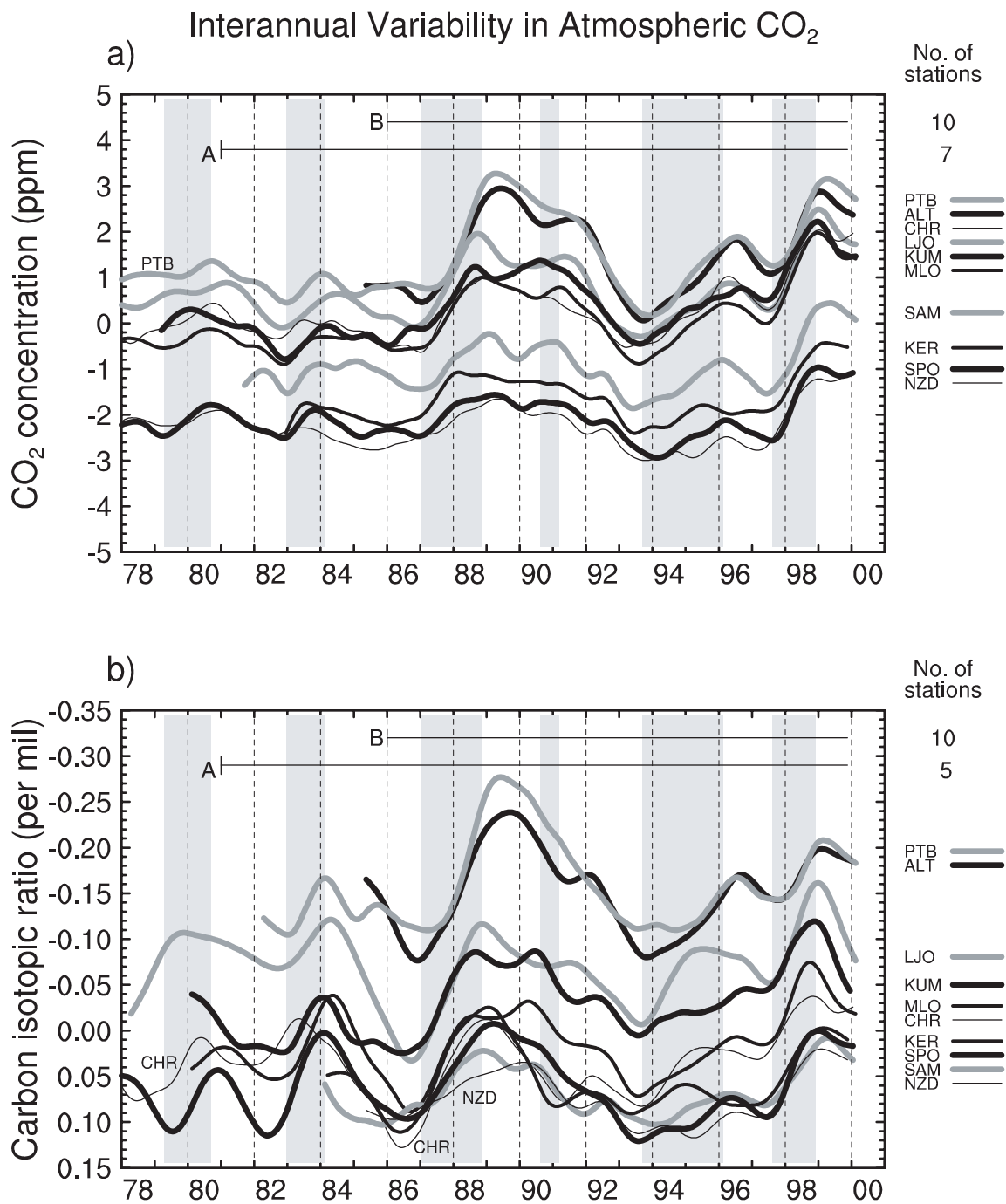
I, Fig. 3c

CO2 ISOTOPIC TRENDS—SOUTHERN HEMISPHERE



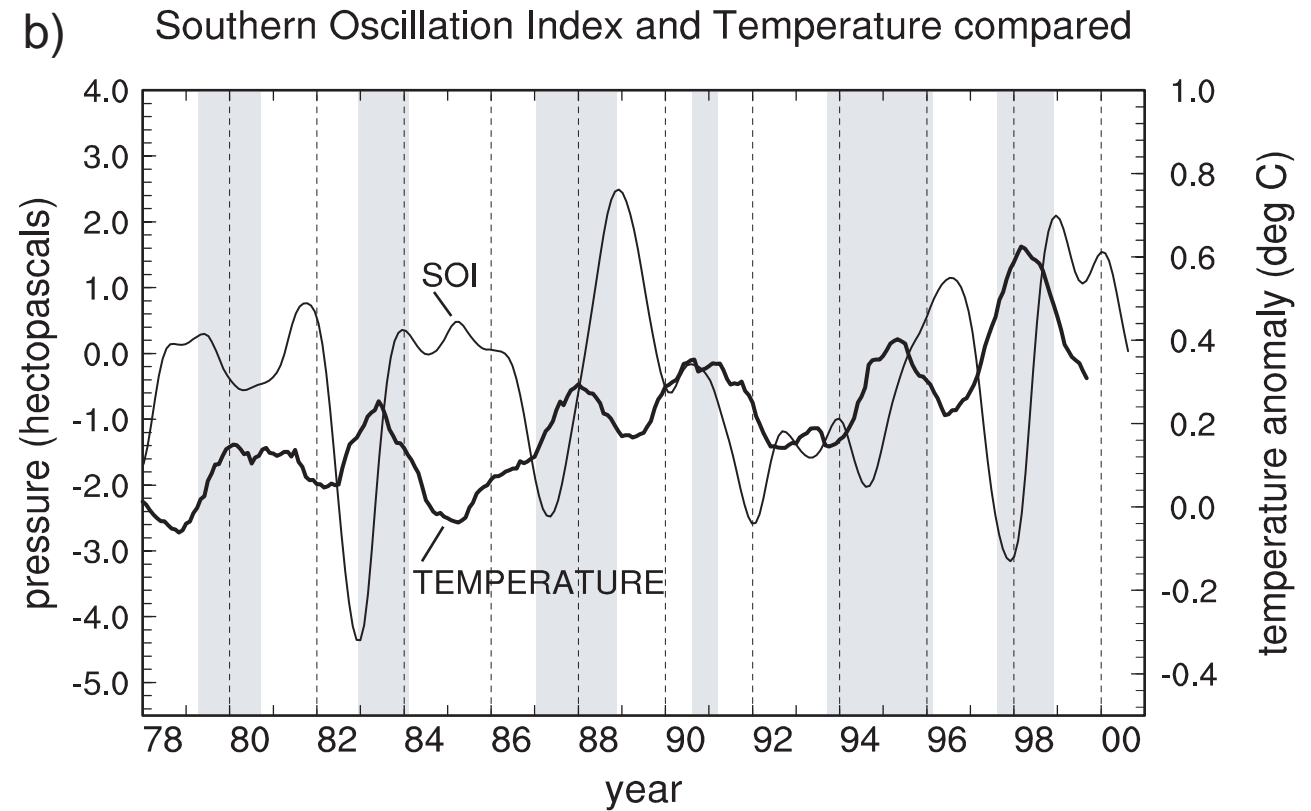
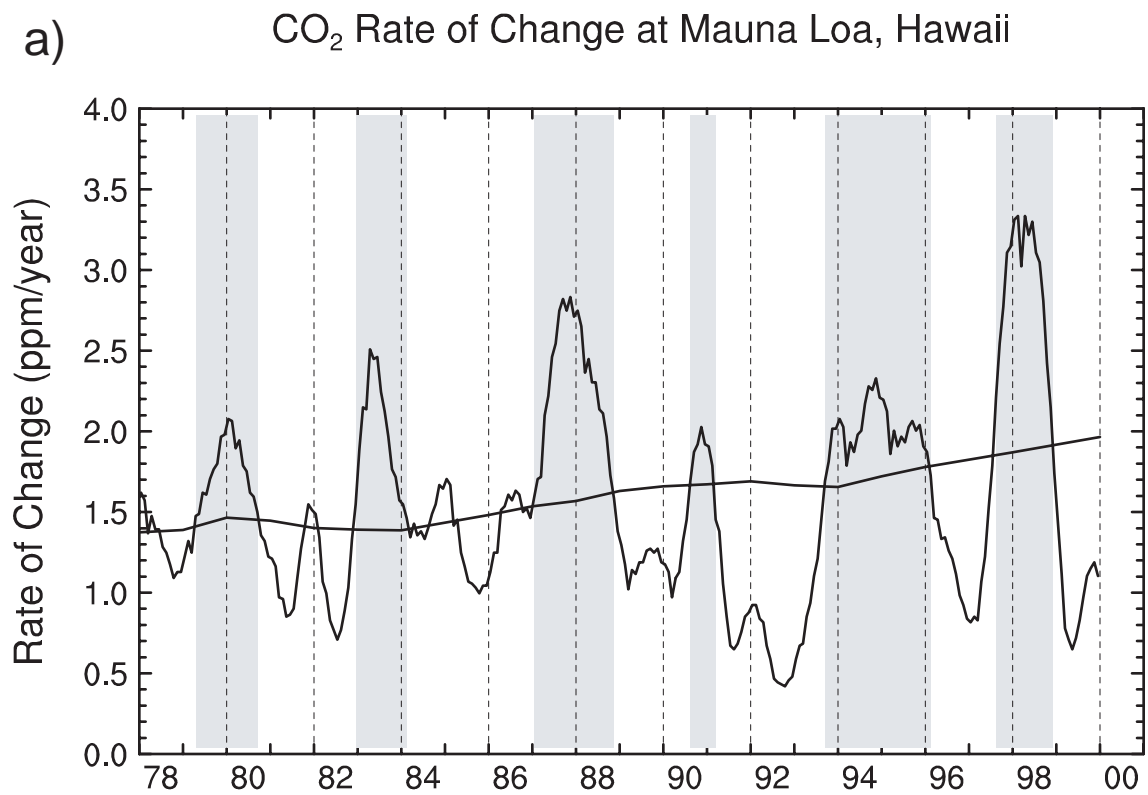
I, Fig. 3d

Figure 4. Seasonally adjusted atmospheric CO₂ concentration and its reduced isotopic ratio, $\delta^{13}\text{C}$, from 1978 through 1999. Station code names are listed in descending order of plotted data on the right side of each panel, as defined in Table 1. The significance of vertical gray bars is explained in Figure 5. **Panel a:** Seasonally adjusted concentration, in ppm, after removing a linear trend (1978 intercept, 335 ppm; slope 1.474 ppm yr⁻¹). Straight line, A, denotes the interval of calculations of regional fluxes, described in Article II; line B, the interval of complete concentration and isotopic data for all stations. **Panel b:** Same as Panel a, except for $\delta^{13}\text{C}$, in ‰, after removal of a linear trend (1978 intercept, -7.440‰ slope -0.0203‰ yr⁻¹). The scale is inverted so that variations are plotted in the same vertical direction as those of CO₂ concentration. Data for Mauna Loa are not included in the global averages shown in Figures 6 and 7.



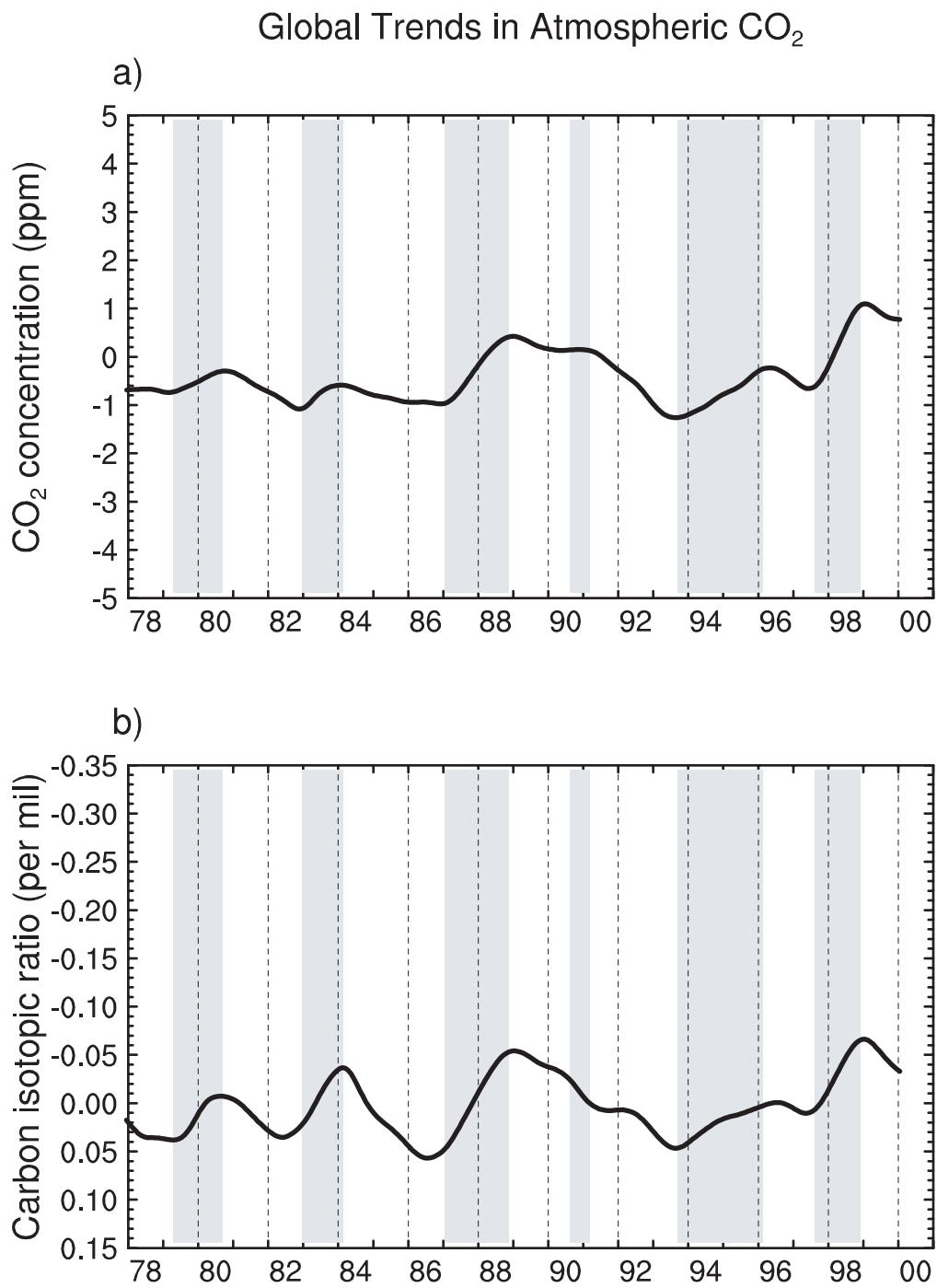
I, Fig. 4

Figure 5. Comparison of quantities that vary with the El Niño-Southern Oscillation (ENSO) Cycle. **Panel a:** Rate of change of atmospheric CO₂ concentration, in ppm yr⁻¹, at Mauna Loa Observatory, Hawaii (strongly fluctuating curve), plotted together with the industrial CO₂ release (slowly rising curve). The latter trend is defined as the average fraction of emissions of industrial CO₂ that remained airborne as determined by Keeling et al. [1995] to be 58.1%. **Panel b:** The Southern Oscillation Index (SOI, thin line), determined as the barometric pressure difference of Tahiti minus Darwin, Australia, in hPa, and global average temperature anomaly (thicker line). The SOI data were derived from Climate Prediction Center [2000], the temperature data from Jones [1994, and personal communication]. Vertical gray bars in both panels indicate time-intervals during which the rate of change of atmospheric CO₂ at Mauna Loa exceeded the industrial CO₂ trend rate (see text).



I, Fig. 5

Figure 6. Global average of seasonally adjusted atmospheric CO₂, shown as spline curves. The averages are derived from the smoothed curves for the individual stations shown in Figure 3, with linear trends removed. The method of computation is described in Appendix D. **Panel a:** concentration, in ppm. **Panel b:** $\delta^{13}\text{C}$, in ‰. Gray bars are as in Figure 5.



I, Fig. 6

Figure 7. Rates of change of globally averaged atmospheric CO₂ concentration, in ppm (thick line), and $\delta^{13}\text{C}$, in ‰ (thin line), computed from the time-trends shown in Figure 6, but without linear trends removed. Gray bars are as in Figure 5.

Global Rates of Change in Atmospheric CO₂

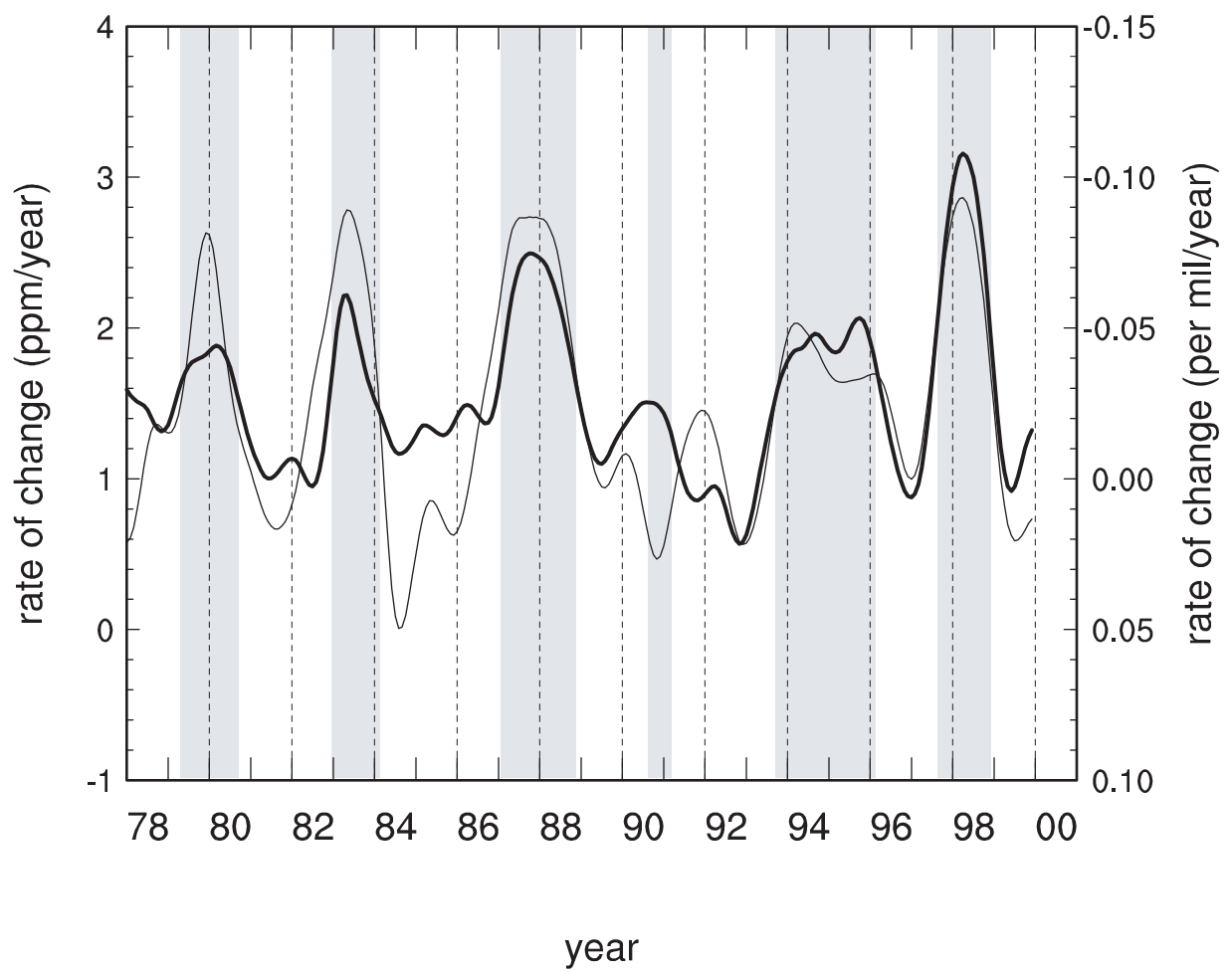
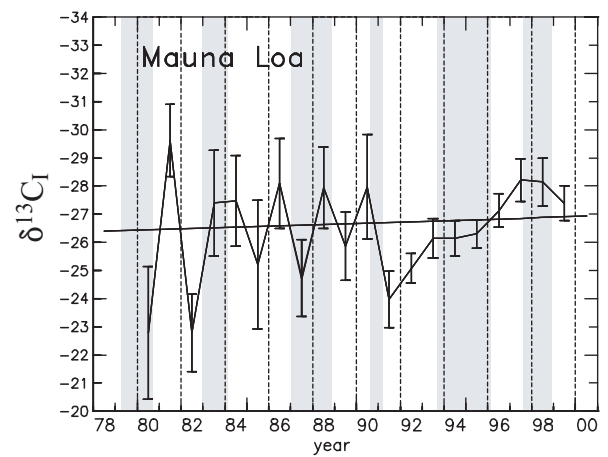
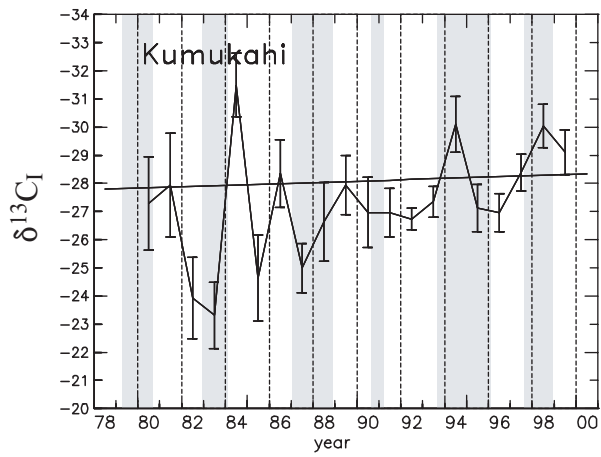
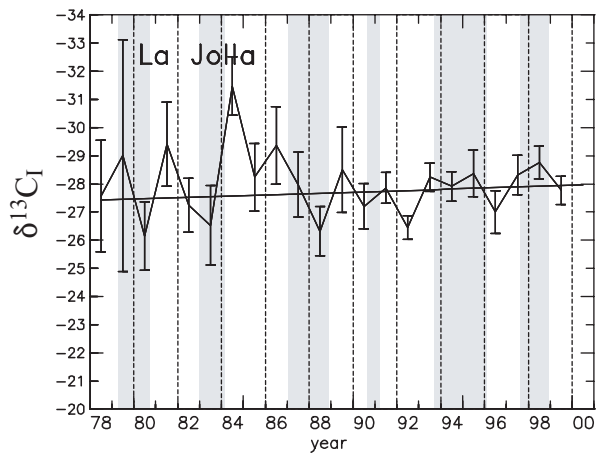
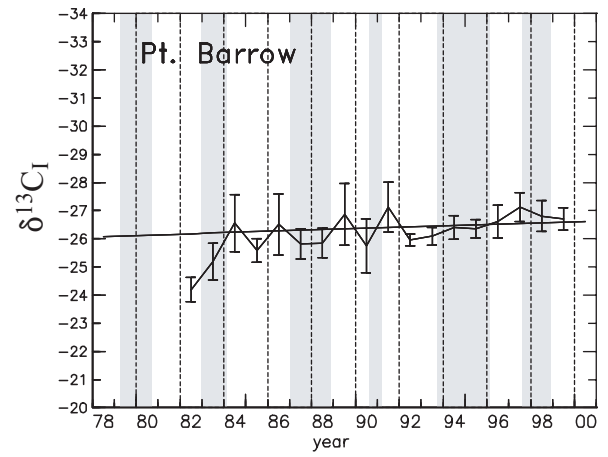
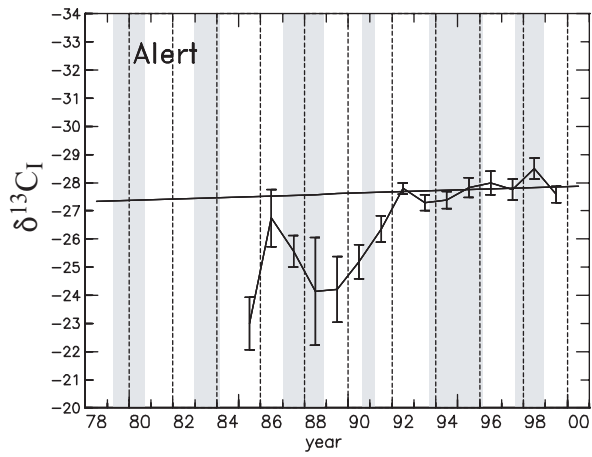


Figure 8. Reduced isotopic ratio, $\delta^{13}\text{C}_I$, in ‰, that explains the covariation of $\delta^{13}\text{C}$ of atmospheric CO_2 with CO_2 concentration over successive annual cycles, computed from pairs of measurements for separate calendar years of observations at stations shown in Figure 2. Vertical bars indicate standard errors of fit (1σ), determined by regressing $\delta^{13}\text{C}$ versus the reciprocal of CO_2 concentration (see text). Sloping straight lines indicate rate of change in $\delta^{13}\text{C}$ of atmospheric CO_2 at Mauna Loa Observatory, Hawaii. Gray bars are as in Figure 5.

Seasonal Isotopic CO₂ Signatures



I, Fig. 8

Seasonal Isotopic CO₂ Signatures (continued)

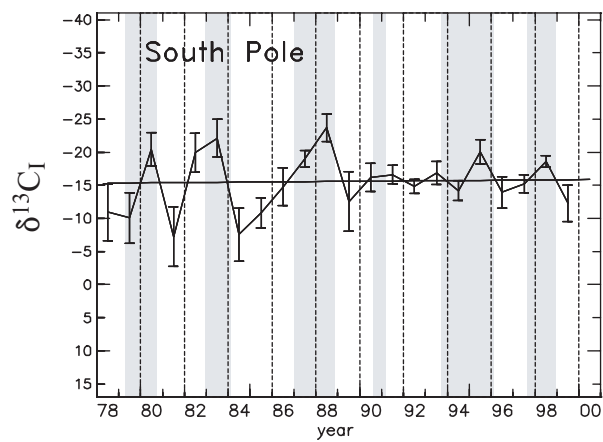
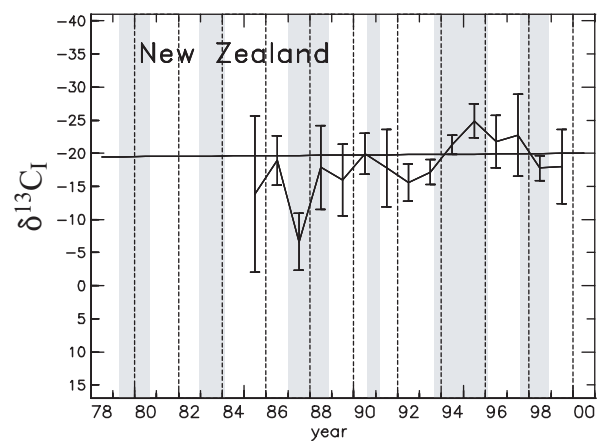
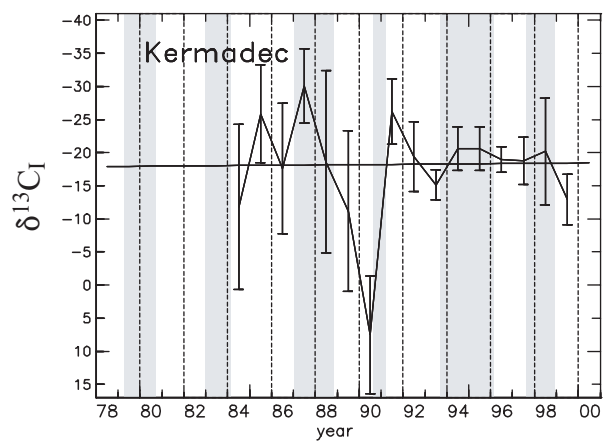
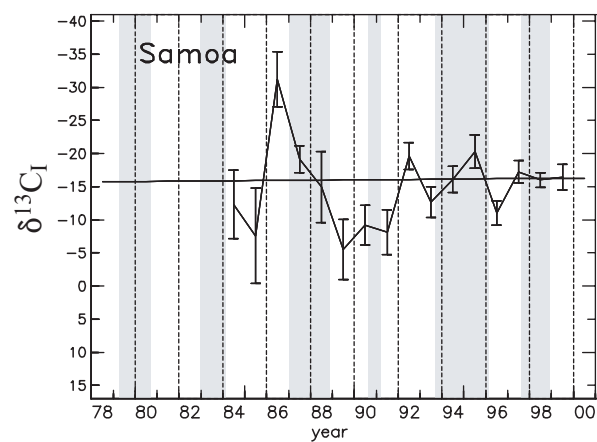
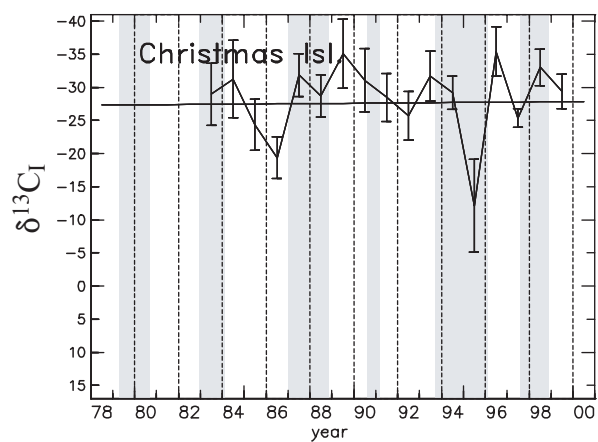
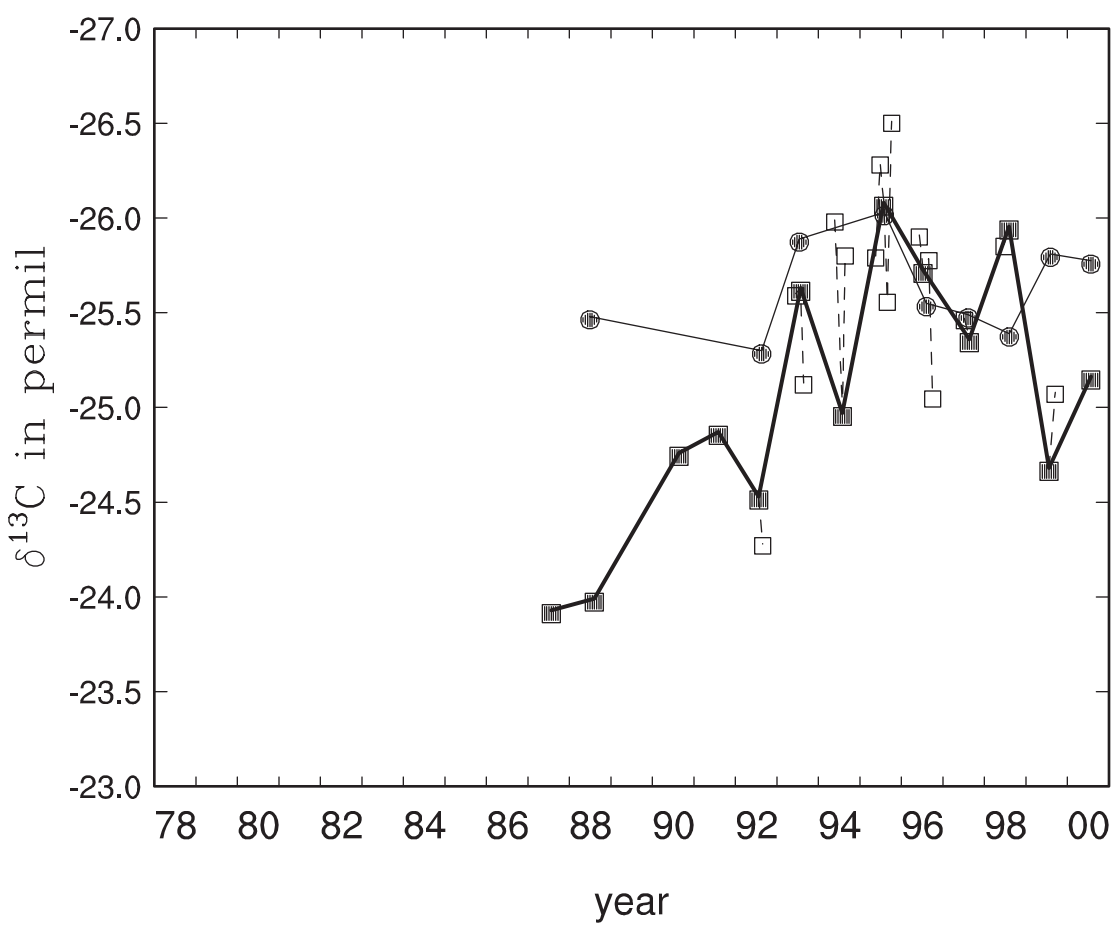


Figure 9. Reduced isotopic ratio, $\delta^{13}C_I$, in ‰, that explains the diurnal variation in $\delta^{13}C$ of CO_2 in the ambient air for two northern conifer forests, computed from pairs of measurements, as in Figure 8 but over 24 hour periods. Squares denote measurements made near Hamilton, Montana (46.3°N, 114.2°W), circles near Rock Lake, Alberta (53.5°N, 118.3°W). Hamilton samples, taken close to 1 August of each year, are shown as solid squares, others as open squares. Sites and experimental methods are described by Lancaster [1990]. Straight line segments between points near 1 August of each year, for each station, are to reveal interannual trends.

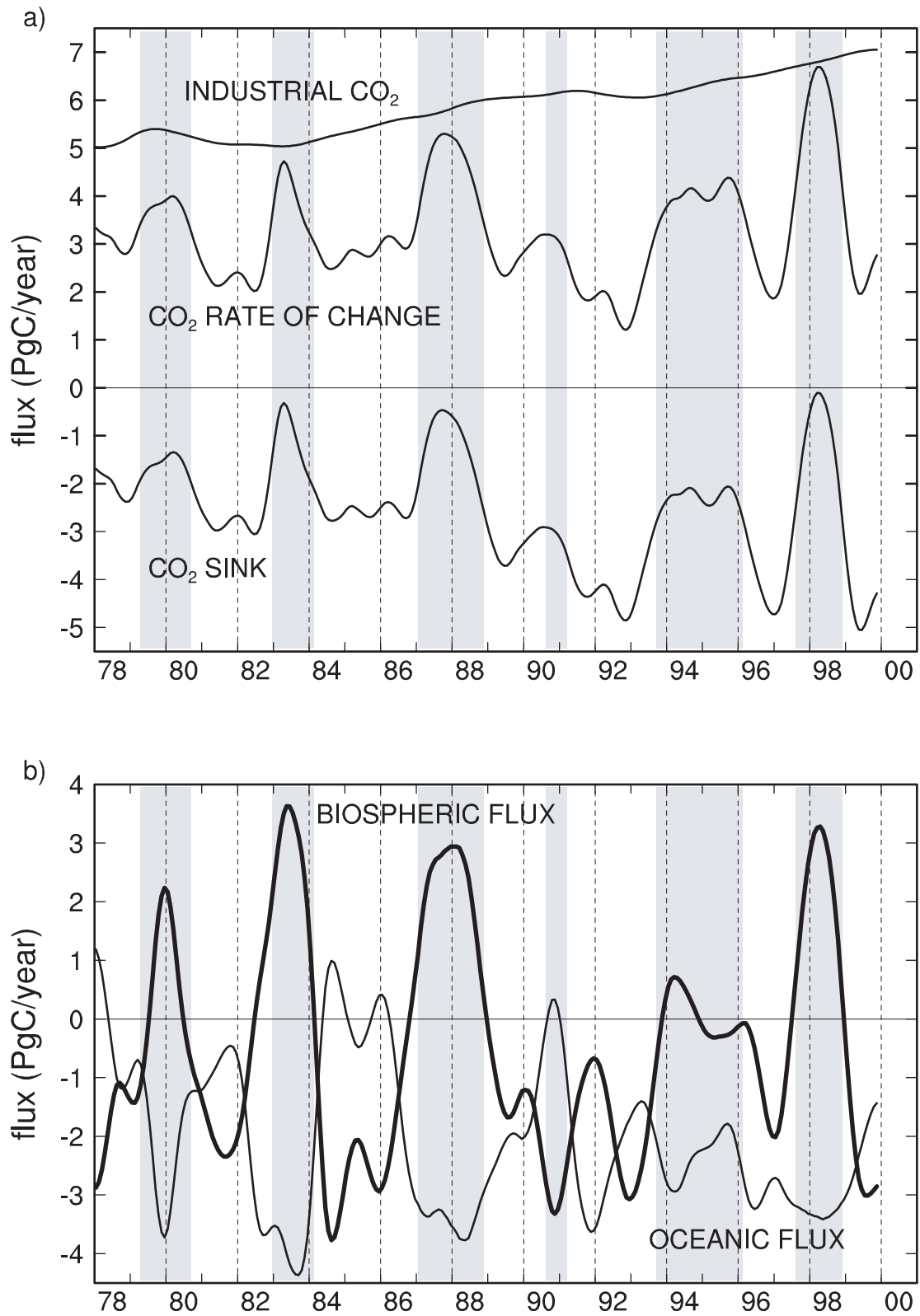
Diurnal Isotopic CO₂ Signatures



I, Fig. 9

Figure 10. Time-varying global CO₂ fluxes, in PgC yr⁻¹, as labeled, positive to the atmosphere, shown as spline fits to monthly data. Gray bars are as in Figure 5. **Panel a:** Industrial CO₂ emissions, rate of change of CO₂ abundance, and an inferred atmospheric CO₂ sink, defined as the difference between emissions and abundance change. **Panel b:** Net terrestrial biospheric and oceanic CO₂ exchange fluxes with the atmosphere (thick and thin lines, respectively), computed by double deconvolution as described in the text, assuming constant isotopic discrimination for C3 and C4 plants. **Panel c:** The terrestrial biospheric exchange flux, shown in Panel b, divided into a contribution related to rising atmospheric CO₂ concentration, F_{fer} , ("CO₂ fertilization flux," lower curve), a constant "land-use source", F_{des} (straight line), and an anomalous flux, $F_{ano,bio}$, as defined in the text. **Panel d:** Oceanic exchange flux of Panel b, divided into an oceanic uptake flux (F_{ex} , lower curve) and an anomalous flux, $F_{ano,oce}$, as defined in the text.

Observed and Simulated Global CO₂ Fluxes



Observed and Simulated Global CO₂ Fluxes (continued)

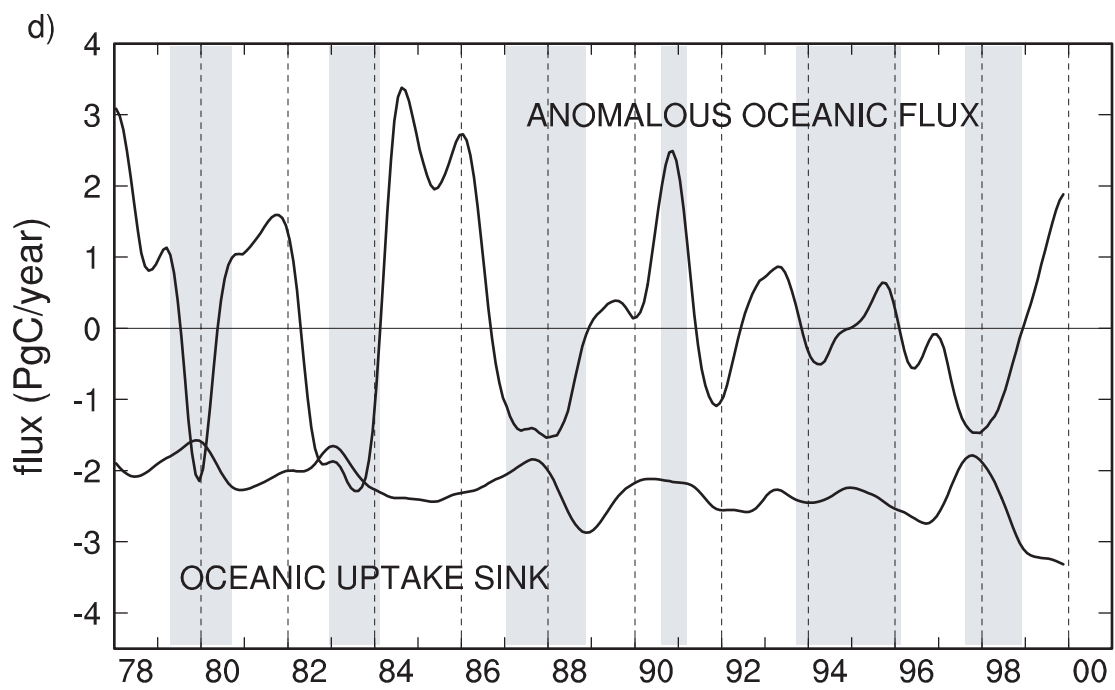
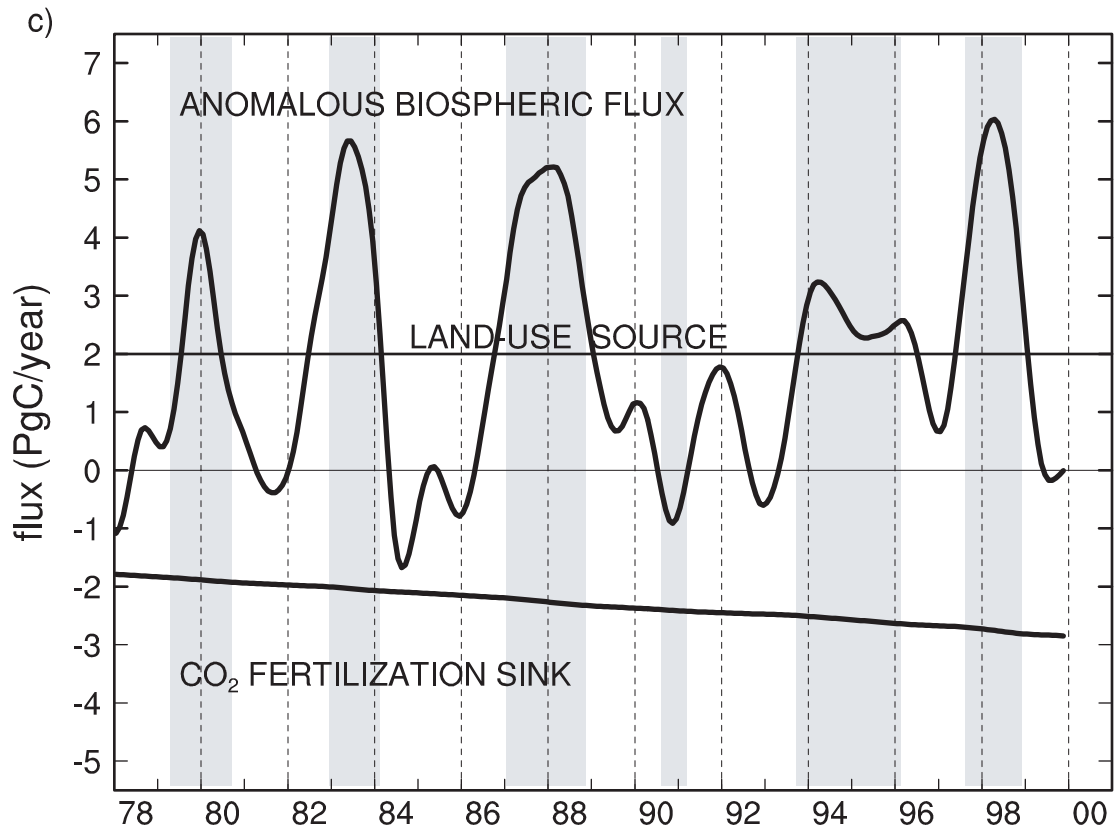


Figure 11. Sensitivity of computed oceanic exchange fluxes (cf. Figure 10d) to parameters of the oceanic carbon cycle model. For each test case the computed oceanic uptake sink, F_{ex} , owing to rising CO_2 , is plotted separately below that of the anomalous oceanic flux. **Panel a:** The oceanic vertical diffusion coefficient, K , successively reduced from $7685 \text{ m}^2 \text{ yr}^{-1}$ (solid line) to 4005 and $2000 \text{ m}^2 \text{ yr}^{-1}$ (successive dashed lines). **Panel b:** The air-sea exchange coefficient, k_{am} , increased from 6.88 yr^{-1} (solid line) to 7.87 yr^{-1} (dashed line). For definitions of K and k_{am} , see Siegenthaler [1983] and Keeling et al. [1989a, Table 8]. Gray bars are as in Figure 5.

Model-Dependence of Oceanic CO₂ Fluxes

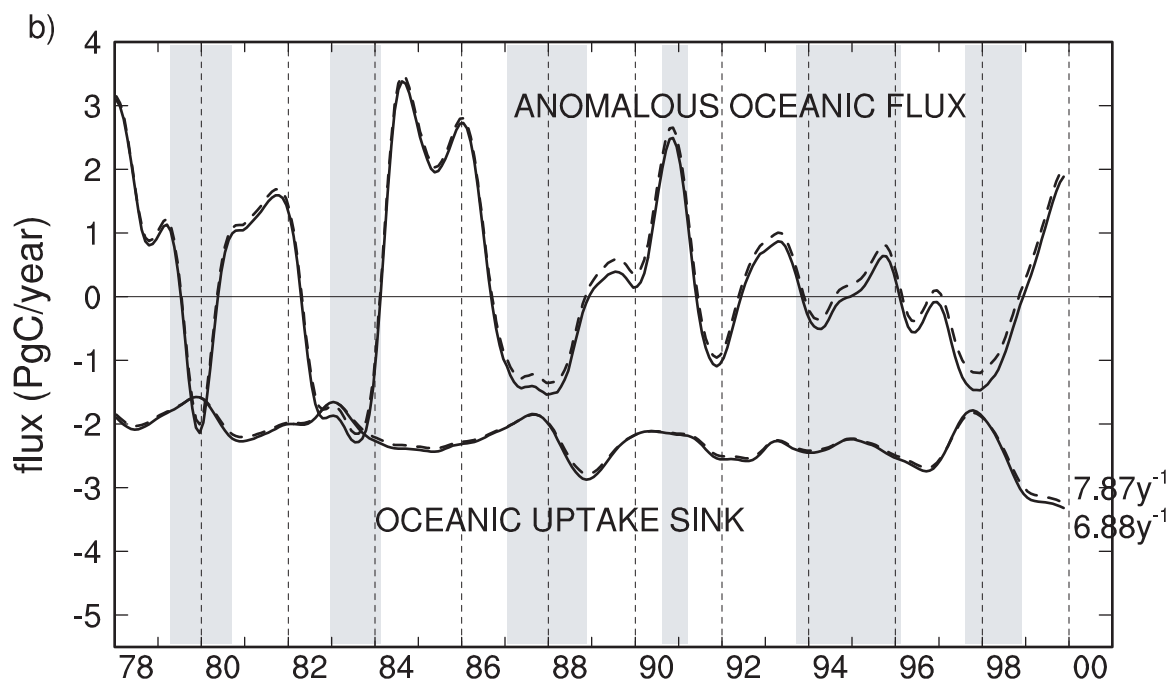
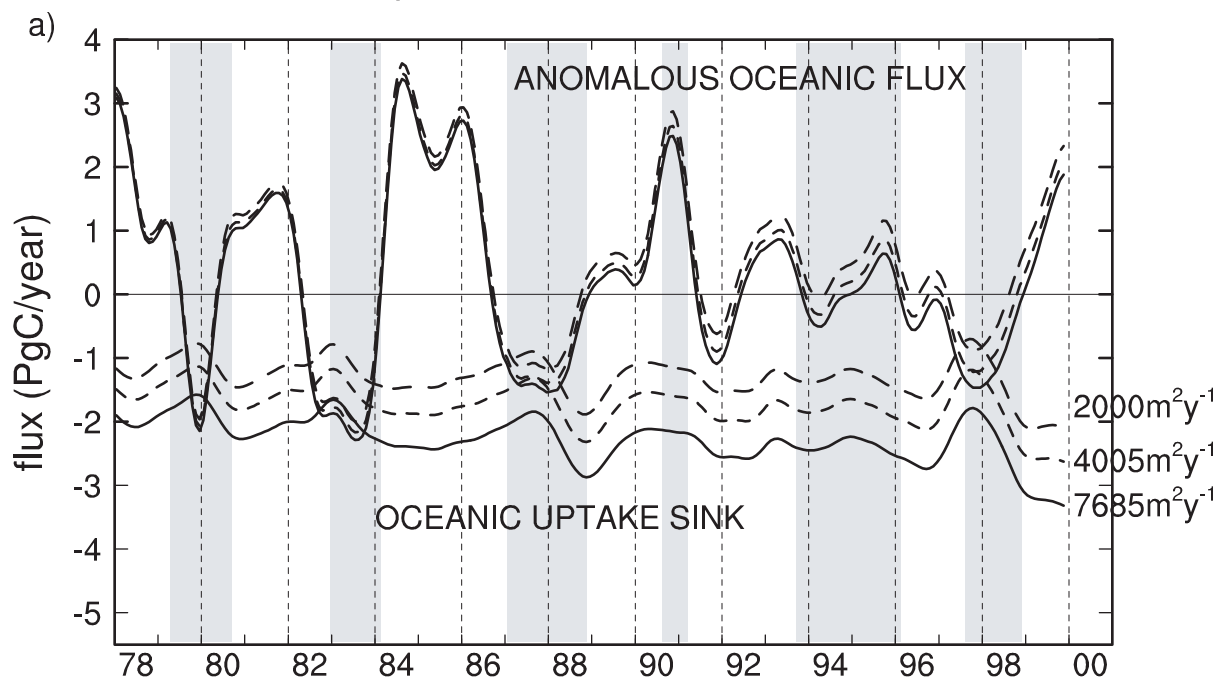
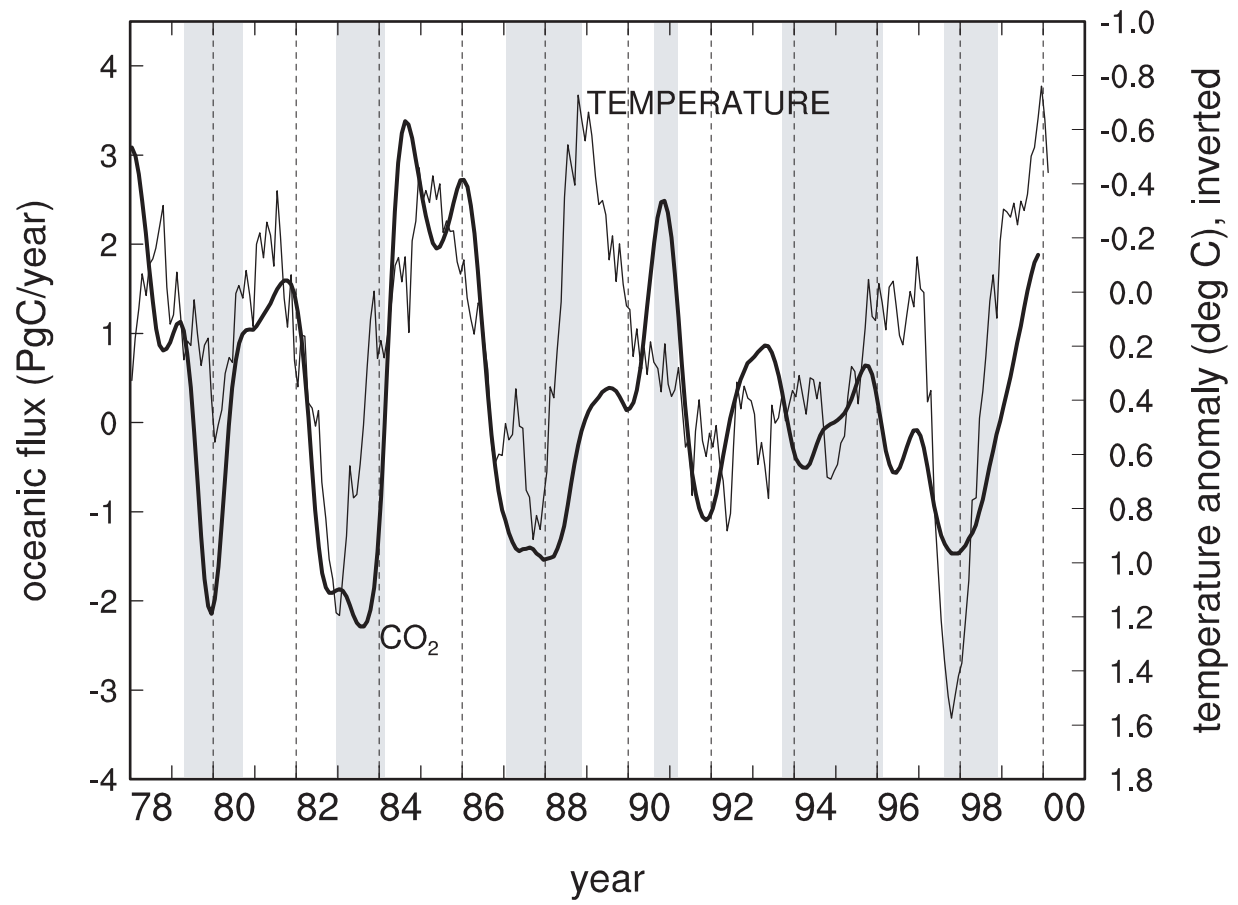


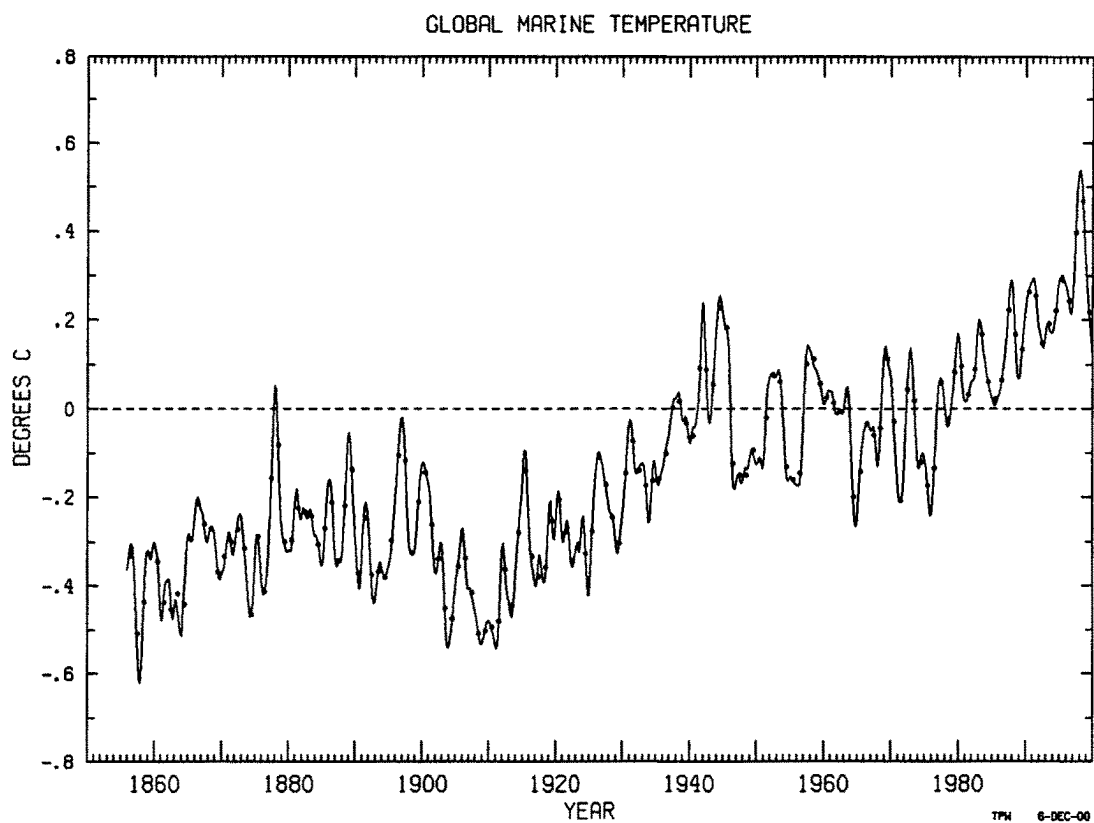
Figure 12. Comparison of the anomalous oceanic flux, $F_{ano, oce}$, (thick line), as plotted in Figure 10, Panel d, with seasurface temperature, (thin line) in °C, in the eastern Pacific Ocean, averaged from 180°W to 80°W longitude, 20°N to 20°S latitude [Jones, 1994, and personal communication]. Gray bars are as in Figure 5.

Oceanic CO₂ Exchange and Temperature Compared



I, Fig. 12

Figure E.1. Global temperature anomaly of surface ocean water, in °C, from 1856 through 1999 [Jones, 1994, and personal communication]. Annual data are shown as dots. The solid line is a spline fit [Reinsch, 1967] to monthly data with a standard error, σ , of 0.058°C.



I, Fig. E1